DEVELOPMENT OF RESIDUAL STRESSES DURING ELECTRON BEAM PROCESSING

By

Przemyslaw Paździor

Department of Mechanical Engineering, McGill University, Montreal

A Thesis Submitted to McGill University in Partial Fulfillment of The Requirements for the Degree of

Master of Science in Engineering

McGill University September 2005

© Przemyslaw Paździor 2005



Library and Archives Canada

Branch

Published Heritage

395 Wellington Street Ottawa ON K1A 0N4 Canada Bibliothèque et Archives Canada

Direction du Patrimoine de l'édition

395, rue Wellington Ottawa ON K1A 0N4 Canada

> Your file Votre référence ISBN: 978-0-494-22661-2 Our file Notre référence ISBN: 978-0-494-22661-2

NOTICE:

The author has granted a non-exclusive license allowing Library and Archives Canada to reproduce, publish, archive, preserve, conserve, communicate to the public by telecommunication or on the Internet, loan, distribute and sell theses worldwide, for commercial or non-commercial purposes, in microform, paper, electronic and/or any other formats.

The author retains copyright ownership and moral rights in this thesis. Neither the thesis nor substantial extracts from it may be printed or otherwise reproduced without the author's permission.

AVIS:

L'auteur a accordé une licence non exclusive permettant à la Bibliothèque et Archives Canada de reproduire, publier, archiver, sauvegarder, conserver, transmettre au public par télécommunication ou par l'Internet, prêter, distribuer et vendre des thèses partout dans le monde, à des fins commerciales ou autres, sur support microforme, papier, électronique et/ou autres formats.

L'auteur conserve la propriété du droit d'auteur et des droits moraux qui protège cette thèse. Ni la thèse ni des extraits substantiels de celle-ci ne doivent être imprimés ou autrement reproduits sans son autorisation.

In compliance with the Canadian Privacy Act some supporting forms may have been removed from this thesis.

While these forms may be included in the document page count, their removal does not represent any loss of content from the thesis.

Conformément à la loi canadienne sur la protection de la vie privée, quelques formulaires secondaires ont été enlevés de cette thèse.

Bien que ces formulaires aient inclus dans la pagination, il n'y aura aucun contenu manquant.



DEDICATION

I would like to dedicate this work to my father M. Henryk Pazdzior.

Dad, you are my true inspiration!

ABSTRACT

In order to further the comprehension of the electron beam (EB) processing of polymers and composites, it is necessary to better understand the development of residual stresses during processing. *In-situ* measurement of stress development during EB irradiation is a challenging task. The instrumentation has to be adequately shielded from the highenergy electron beam. In this work, a special fixture was designed specifically to measure the warpage of a specimen throughout the EB curing process. The specimen consisted of a thin layer of epoxy resin (Tactix 123 or CAT B) embedded in a layer of glass scrim cloth, sandwiched between layers of steel and aluminum plates and also antisymmetric unidirectional carbon-epoxy laminates. The warpage of the specimens was monitored during and after irradiation at different constant dose rates. The results confirmed that the experimental instrumentation was not affected by the EB exposure and that it was possible to monitor the specimen warpage during the EB process. The results show that the EB cured specimens have lower stress-free temperature compared to equivalent thermally cured specimens. It was also shown that an increase in dose rate increased the level of residual stresses. Furthermore, the results suggest that there is a direct relation between the stress free temperature (T_{SF}) and the temperature of the specimen at gelation (T_{GEI}). Also, the stress free temperatures for CAT B specimens were 5°C higher than the Tactix 123 specimens cured under the same curing conditions. Finally, a cure kinetics model for Tactix 123 was used to predict the degree of cure (~0.32) at onset of residual stress development and the results proved to be valid when compared to parallel plate rheology results.

RÉSUMÉ

Afin de bien comprendre le processus de polymérisation des résines à l'aide d'un faisceau d'électrons, il est nécessaire de bien saisir le développement des contraintes résiduelles durant le processus même. Recueillir des données concernant le développement des contraintes durant l'irradiation reste un défi de taille. L'instrumentation électronique doit être adéquatement protégée des bombardements d'électrons à de très haut niveau d'énergie. Dans ce travail, un montage d'essais a été développé afin de pouvoir mesurer le gauchissement, d'un échantillon pendant la polymérisation. Cet échantillon est composé d'une mince couche de résine époxy (Tactix 123 ou CAT B) couvrant un tissu de fibre de verre, le tout placé entre une plaque d'acier et d'aluminium ou encore entre deux laminés de matériau composite (fibre de carbone, résine d'époxy) unidirectionnel, non symétriques. Le gauchissement de l'échantillon a été mesuré pendant et après l'irradiation et ce à des niveaux de flux d'électrons variés. Les résultats ont confirmé que l'instrumentation n'a pas été affectée par le bombardement d'électrons et qu'il est tout à fait possible de mesurer adéquatement le gauchissement de l'échantillon durant la polymérisation. Les résultats expérimentaux ont démontré que les échantillons polymérisés par faisceau d'électrons avaient une température de contrainte nulle considérablement plus basse que les échantillons polymérisés dans un four thermique. De plus, une augmentation du flux d'électrons provoque une augmentation du niveau de contraintes résiduelles dans la structure polymérisée. Aussi, il existe une relation directe entre la température de contrainte nulle et la température de gélification d'une résine. En plus, la température de contrainte nulle pour la résine CAT B est environ 5°C plus élevé que celle de la Tactix 123. Finalement, en se servant d'un modèle de cinétique de la polymérisation, le degré de polymérisation au point de gélification (~0.32), de la résine Tactix 123, a été prédit et confirmé à l'aide de résultats de tests rhéologique avec viscosimètre à plaques parallèles.

ACKNOWLEDGMENTS

First and foremost, I would like to extend my warmest thanks to my supervisor Prof.

Pascal Hubert, from whom I learned the solid basics of experimental research and experimentation techniques. His presence, patience, understanding and implication were greatly appreciated during the good time and especially the harder ones.

I would like to acknowledge the contribution of the National Research Council of Canada in Ottawa. Especially the guidance of Dr. Andrew Johnston, without whom, my understanding of Electron Beam curing would have been greatly diminished and this work probably impossible. I would also like to thank Mr. Drazen Djokic for his hard work and greatly valuable advice in composite making and test preparation. Thanks Drazen, all your work and friendship was welcome and considerably appreciated. I would also like to thank Mr. Eric St-Amant for all his manufacturing skills and his constant good ideas.

I would like to acknowledge the contributions of Dr. Donald Klosterman of the University of Dayton Research Institute for irradiation of the specimens. Financial support for this work was provided in part by McGill University Office of the Vice Principal Fund and EMS Technologies Inc.

Lastly, I would like to say a big "Merci" to my lovely wife Karine Bonenfant for her support, sense of humour, hard work and encouragements all throughout this journey.

TABLE OF CONTENT

DEI	DICAT]	iONi	i
ABS	STRAC	Tii	i
RÉS	SUMÉ.	i	7
ACI	KNOW	LEDGMENTSv	i
LIS	T OF F	IGURESiz	K.
LIS	T OF T	'ABLES xiv	7
1	INTR	RODUCTION AND LITERATURE REVIEW	l
1	.1	MOTIVATION FOR RESEARCH WORK	l
	1.1.1	Space composites	3
	1.1.2	Resin polymerization process	5
	1.1.3	Polymerization techniques	7
	1.1.4	Thermal distortions and residual stresses	9
1	.2	LITERATURE REVIEW	1
	1.2.1	Electron beam overview	1
	1.2.2	Thermal cure residual stress overview	2
1	.3	RESEARCH OBJECTIVES	4
2	EXP	ERIMENTAL PLAN 1:	5
2	2.1	TEST APPARATUS	5
2	2.2	SPECIMEN PREPARATION	7
	2.2.1	Metallic specimen	7
	2.2.2	Composite specimen 1	9
	2.2.3	Resin coupons	1
2	2.3	TEST CONDITIONS	2
	2.3.1	E-Beam cure	2

	2.3.2	Thermal cure	. 29
	2.4	DATA REDUCTION	. 29
3	EXP	ERIMENTAL RESULTS	. 33
	3.1	E-BEAM CURED SPECIMENS	. 33
	3.1.1	Metallic specimens	. <i>33</i>
	3.1.2	Thermal post-cure effects	. 41
	3.1.3	Composite specimens	. 43
	3.2	THERMAL CURED SPECIMENS	. 54
4	MOI	DELING AND DISCUSSION	. 55
5	CON	NCLUSIONS	. 63
6	REC	COMMENDATION FOR FUTURE WORK	. 65
A l	PPENDI	IX A- DOSE RATE VS TIME RESULTS	. 68
A l	PPENDI	IX B - TEMPERATURE AND WARPAGE VS PREDICTED DEGREE OF CURE	
R	ESULTS	5	. 75
A]	PPENDI	IX C – TEMPERATURE, WARPAGE AND DOSE VS TIME OF CURE RESULTS	. 81

LIST OF FIGURES

Figure 1: a) RF component support structure; b) Satellite in testing	2
Figure 2: Printed circuit board	2
Figure 3: Honeycomb panel assembly	3
Figure 4: Laminate sheet fabrication	4
Figure 5: Polymerization steps	6
Figure 6: a) Microcraking of composites; b) Spring In of structure	10
Figure 7: Schematic of the test fixture	17
Figure 8: Metallic specimen components	18
Figure 9: Metallic specimen vacuum bag assembly	19
Figure 10: Composite specimen components	20
Figure 11: Composite specimen vacuum bag assembly	20
Figure 12: Resin coupon fabrication	21
Figure 13: a) Photograph of the test setup, b) Close up showing the specimen	and vacuum
bag	23
Figure 14: Test setup schematic	23
Figure 15: Dose rate measurement.	25
Figure 16: Composite dose rate measurement.	28
Figure 17: Specimen energy balance	30
Figure 18: Beam instability for RS11 (75 s ⁻¹)	35

Figure 19 Calculated EB dose and measured temperature for tests RS09 and RS12. Note
that RS12 was exposed for a total dose of 96 kGy; the third EB irradiation is not
shown
Figure 20: Measured warpage and temperature during EB curing for test RS12 38
Figure 21 Measured warpage during EB curing as function of specimen temperature for
all tests
Figure 22: Measured warpage during post-cure. Note that data above 90°C is not shown
on figure
Figure 23: Calculated dose rate vs time for RS13. The measured average dose rate was
6.86 kGy/min
Figure 24: Dose rate vs measured DOC for Tactix 123 and CAT B specimens
Figure 25: a) Calculated EB dose and b) Measured temperature for specimens RS13,
RS21 and RS25
Figure 26: Maximum temperature comparison between fan and no fan test setup 47
Figure 27: Stress free temperature comparison between with fan and no fan test setup 47
Figure 28: Measured warpage and temperature for a 25 s ⁻¹ irradiation for a) metallic
specimen (RS12), b) composite specimen (RS13)
Figure 29: Measured warpage during EB curing as function of specimen temperature for
Tactix 123 specimens
Figure 30: Measured warpage during EB curing as function of specimen temperature for
CAT B specimens
Figure 31: Specimen warpage at 28°C vs stress free temperature (T _{SF})

Figure 32: Comparison of RS12 EB cure and post-cure response with a specimen cure	d
thermally at 160°C	4
Figure 33: Predicted DOC for Tactix 123 metallic specimens	6
Figure 34: Predicted DOC vs time for Tactix 123 composite specimens	7
Figure 35: Predicted DOC vs Measured DOC for Tactix 123 specimens	8
Figure 36: Stress free temperature (T _{SF}) vs measured DOC for Tactix 123 and CAT	В
specimens5	9
Figure 37: Comparison of stress free temperature for Tactix 123 and CAT B 6	0
Figure 38: Measured warpage and temperature during EB cure as a function of predicte	d
resin degree of cure for Tactix 123 and CAT B for a 50 (s ⁻¹) irradiation 6	0
Figure 39: Temperature and warpage vs predicted DOC for RS13 specimen 6	2
Figure 40: Temperature and warpage vs predicted DOC for RS23 specimen 6	2
Figure A. 1: Calculated dose rate vs time for RS09	9
Figure A. 2: Calculated dose rate vs time for RS10	9
Figure A. 3: Calculated dose rate vs time for RS12	9
Figure A. 4: Calculated dose rate vs time for RS14	0
Figure A. 5: Calculated dose rate vs time for RS15	0'
Figure A. 6: Calculated dose rate vs time for RS16	'0
Figure A. 7: Calculated dose rate vs time for RS17	'1
Figure A. 8: Calculated dose rate vs time for RS18	'1
Figure A. 9: Calculated dose rate vs time for RS19	1
Figure A. 10: Calculated dose rate vs time for RS20	72
Figure A. 11: Calculated dose rate vs time for RS21	12

Figure A. 12: Calculated dose rate vs time for RS22	72
Figure A. 13: Calculated dose rate vs time for RS23	73
Figure A. 14: Calculated dose rate vs time for RS24	73
Figure A. 15: Calculated dose rate vs time for RS25	73
Figure A. 16: Calculated dose rate vs time for RS26	74
Figure A. 17: Calculated dose rate vs time for RS27	74
Figure A. 18: Calculated dose rate vs time for RS28	74
Figure B. 1: Temperature and warpage vs predicted DOC for RS14 specimen	76
Figure B. 2: Temperature and warpage vs predicted DOC for RS16 specimen	. 76
Figure B. 3: Temperature and warpage vs predicted DOC for RS17 specimen	. 77
Figure B. 4: Temperature and warpage vs predicted DOC for RS21 specimen	. 77
Figure B. 5: Temperature and warpage vs predicted DOC for RS22 specimen	. 78
Figure B. 6: Temperature and warpage vs predicted DOC for RS24 specimen	. 78
Figure B. 7: Temperature and warpage vs predicted DOC for RS25 specimen	. 79
Figure B. 8: Temperature and warpage vs predicted DOC for RS26 specimen	. 79
Figure B. 9: Temperature and warpage vs predicted DOC for RS27 specimen	. 80
Figure B. 10: Temperature and warpage vs predicted DOC for RS28 specimen	. 80
Figure C. 1: Temperature, warpage and dose vs time results for specimen RS13	82
Figure C. 2: Temperature, warpage and dose vs time results for specimen RS14	82
Figure C. 3: Temperature, warpage and dose vs time results for specimen RS15	82
Figure C. 4: Temperature, warpage and dose vs time results for specimen RS16	82

Figure C. 5: Temperature, warpage and dose vs time results for specimen RS17	83
Figure C. 6: Temperature, warpage and dose vs time results for specimen RS18	83
Figure C. 7: Temperature, warpage and dose vs time results for specimen RS19	83
Figure C. 8: Temperature, warpage and dose vs time results for specimen RS20	83
Figure C. 9: Temperature, warpage and dose vs time results for specimen RS21	84
Figure C. 10: Temperature, warpage and dose vs time results for specimen RS22	84
Figure C. 11: Temperature, warpage and dose vs time results for specimen RS23	84
Figure C. 12: Temperature, warpage and dose vs time results for specimen RS24	84
Figure C. 13: Temperature, warpage and dose vs time results for specimen RS25	85
Figure C. 14: Temperature, warpage and dose vs time results for specimen RS26	85
Figure C. 15: Temperature, warpage and dose vs time results for specimen RS27	85
Figure C. 16: Temperature, warpage and dose vs time results for specimen RS28	85

LIST OF TABLES

Table 1: Cure conditions for metallic specimens with Tactix 123 resin
Table 2: Cure conditions for composite specimens with Tactix 123 resin
Table 3: Cure conditions for composite specimens with CAT B resin
Table 4 Comparison between dose rate, total dose measured from dosimeter and
calculated from temperature profiles using Equation 8; degree of cure measured
after EB exposure
Table 5 Measured stress free temperature (T_{SF}) and warpage after EB cure
Table 6: Measured stress free temperature (T _{SF}) and warpage after thermal post-cure 41
Table 7 Comparison between dose rate, total dose measured from dosimeter and
calculated (Equation 8); degree of cure measured by DSC after EB exposure 44
Table 8: Measured stress free temperature ($T_{\rm SF}$) and warpage after EB cure
Table 9: Comparison between warpage vs stress free temperature and warpage vs
gelation degree of cure

1 INTRODUCTION AND LITERATURE REVIEW

The present work is a result of a joint collaboration between the Department of Mechanical Engineering at Mcgill University, the National Research Council of Canada (IAR-NRC) in Ottawa and EMS Technologies in Montreal, relevant to the monitoring of residual stresses during electron beam processing of epoxy resins. The goal of this research is to show that residual stresses developed in an electron beam cured resin are considerably lower that those developed during an equivalent thermally cured resin.

1.1 MOTIVATION FOR RESEARCH WORK

Throughout the years, companies working in the space industry have used advanced materials in their space craft designs in order to improve their technical and financial competitiveness. In the last decade, advanced composite materials have taken an unprecedented role in satellite structure design. At the present time, 10% of a communication satellite is made out off composite materials. The most common composite structures in the space industry are:

- Reflectors (Figure 1);
- Support structures for radiating components (Figure 1);
- Printed circuit boards (Figure 2);
- RF components.

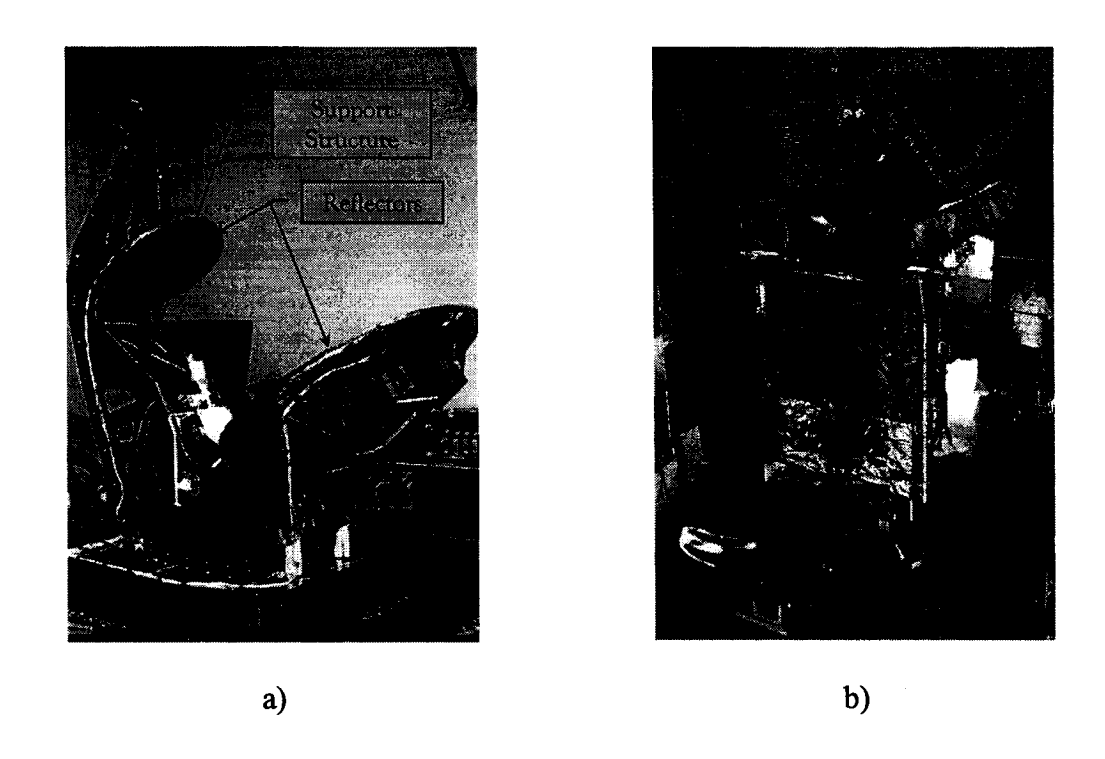


Figure 1: a) RF component support structure; b) Satellite in testing

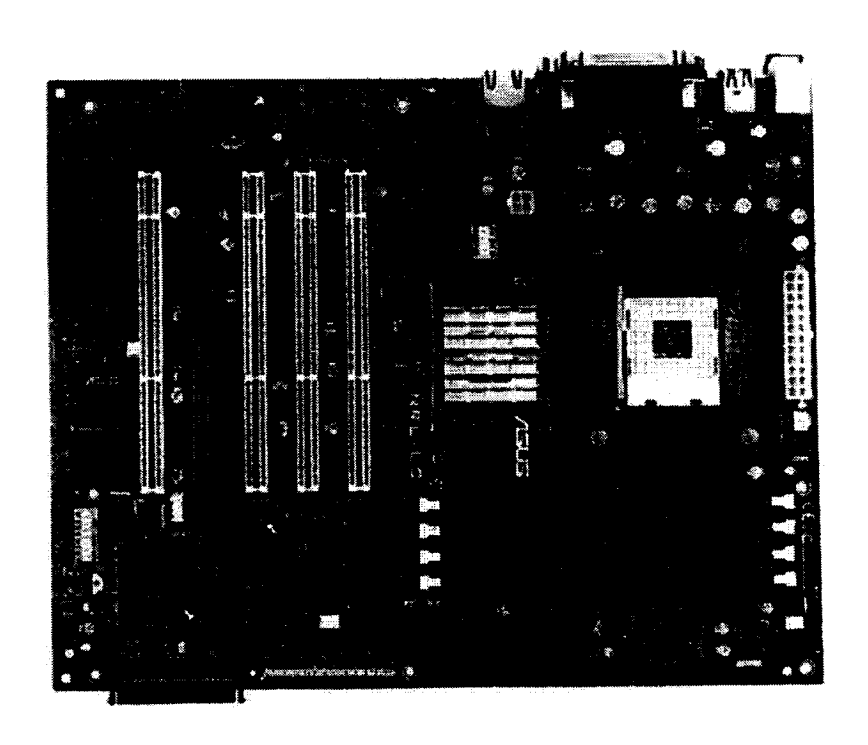


Figure 2: Printed circuit board

1.1.1 Space composites

Reflectors and RF support structures are made, almost, entirely out of a particular type of composite material called sandwich panel. These unique materials are fabricated from two laminates bonded to a honeycomb core using a film adhesive (Figure 3). The laminates used for these assemblies are commonly made out of high modulus carbon fibres embedded in a resin matrix. The fabrication of a laminate is shown in Figure 4. The honeycomb core material is mainly aluminium or Corex.

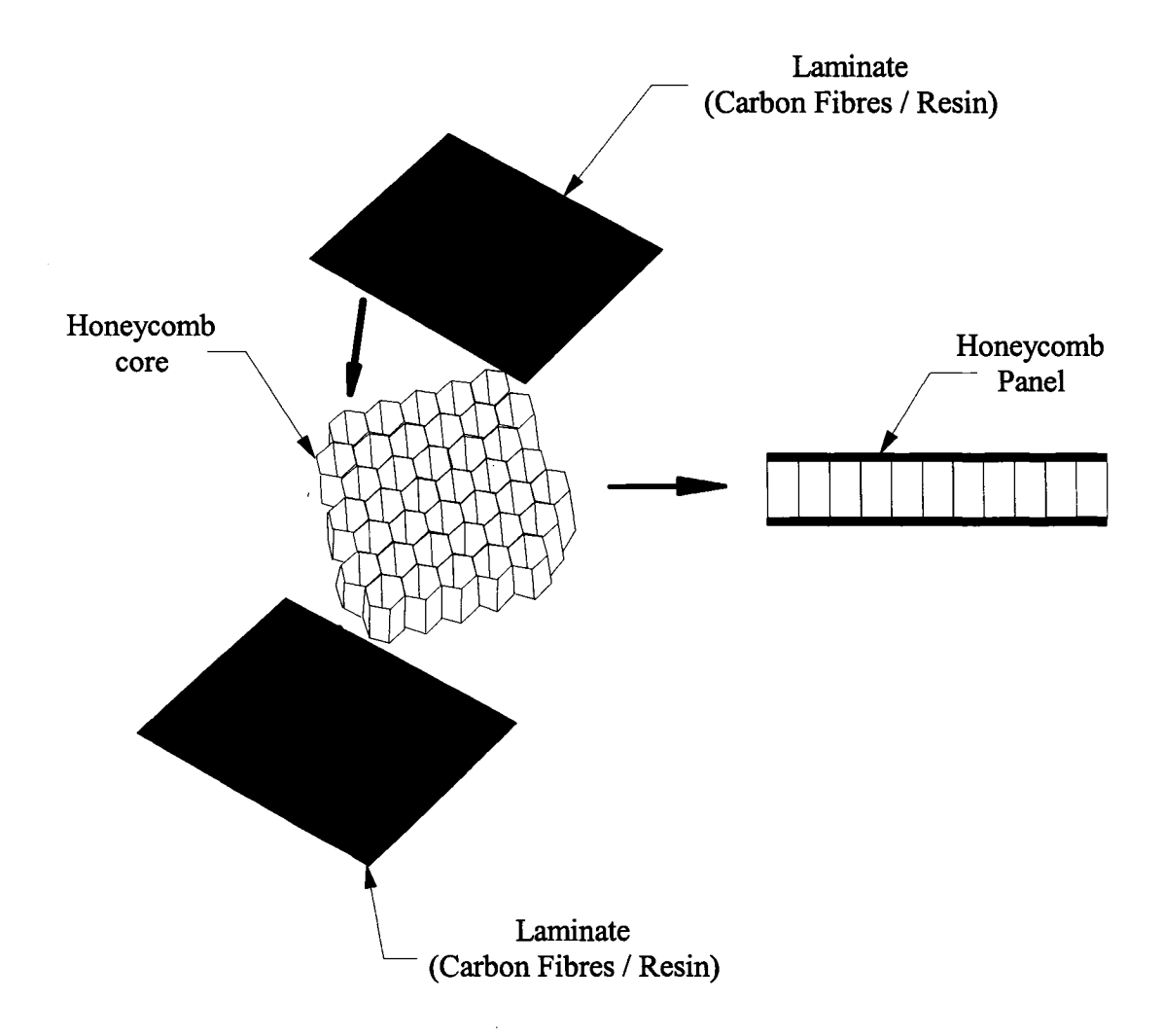


Figure 3: Honeycomb panel assembly

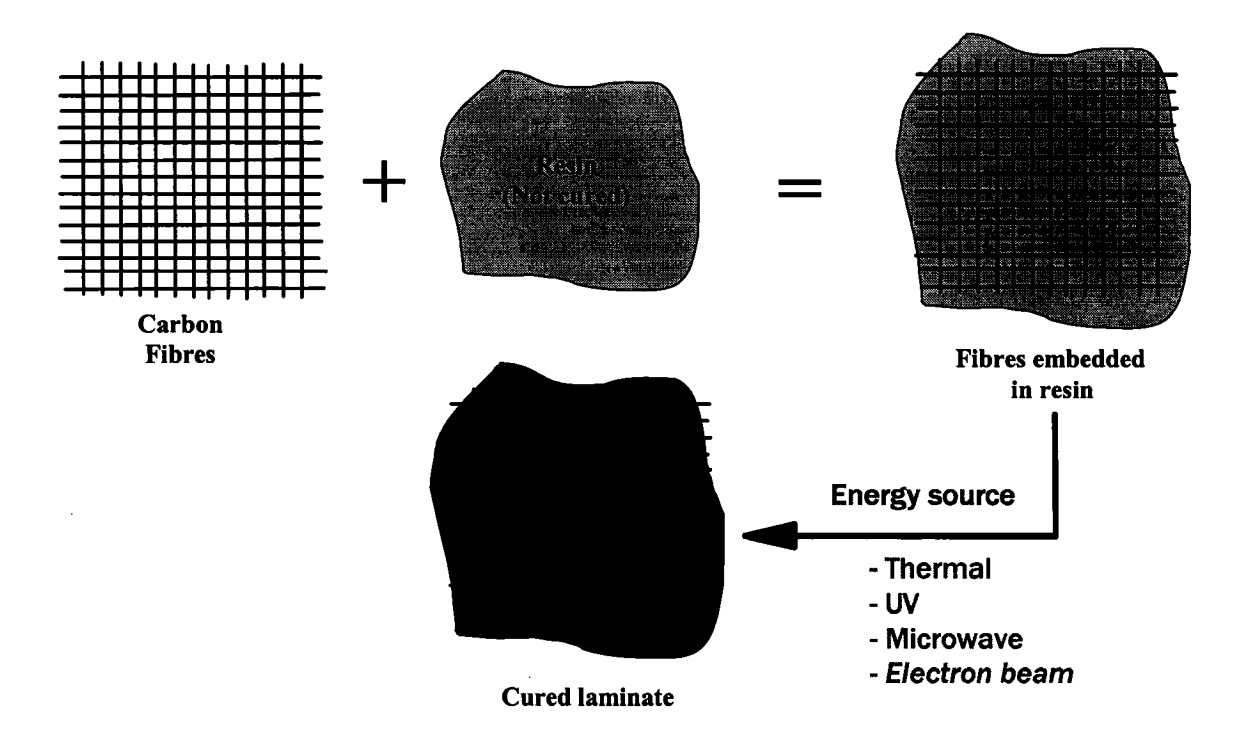


Figure 4: Laminate sheet fabrication

The resin being a polymer can be divided into two major groups based on their thermal processing behaviour. Polymers that can be heat-softened in order to be process into a desired shape are call *thermoplastics*. Thermoplastics can be recycled and re-processed by application of heat and pressure. In comparison, *thermosets* are polymers whose individual chains have been chemically linked by covalent bonds during the polymerization or by subsequent chemical or thermal treatment during fabrication. Once cured, these crosslinked networks resist heat softening, creep, and solvent attack, but cannot be reprocessed. Such properties make thermosets suitable materials for space composites, coating and adhesive applications.

1.1.2 Resin polymerization process

The word polymer is derived from the classical Greek words *poly* meaning «many» and *meres* meaning «parts» [1]. Simply stated a polymer is a long-chain molecule that is composed of a large number of *repeating units* of identical structure. Certain polymers, such as proteins, cellulose, and silk are found in nature, while many others, including polystyrene, polyethylene, epoxies and nylon are produced only by synthetic routes.

Elastomers capable of high extension under ambient conditions find important applications. In addition to natural rubber, there are synthetic elastomers such as nitrile and butyl rubber. Other polymers may have characteristics that permit their formation into long fibres suitable for the space and textile industries.

In contrast to the usage of the word *polymer*, those commercial materials, other than elastomers and fibres that are derived from the synthetic polymers are called *plastics*. A typical commercial plastic resin may contain two or more monomers in addition to various additives and fillers. These are added to improve properties such as processabillity, thermal or environmental stability and mechanical properties of the final product.

The birth of polymer science may be traced back to the mid-nineteenth century [1]. In the 1830s, Charles Goodyear developed the vulcanization process that transformed the sticky latex of natural rubber to a useful elastomer for tire use. In 1847, Christian F. Schönbein reacted cellulose with nitric acid to produce cellulose nitrate. This was used

in the 1860s as the first man made thermoplastic. In 1907, Leo Baekeland produced Bakelite (phenol-formaldehyde resin) and glyptal (unsaturated-polyester resin) was developed as a protective coating resin by General Electric in 1912. In the 1960s and 1970s witnessed the development of a number of high-performance polymers that could compete favourably with more traditional materials, such as metals, for automotive, aerospace and space applications.

The polymerization of a thermoset resin can be described in four distinct steps (Figure 5). Initially, (step 1), the resin is in its liquid state containing a large number of monomers, catalysts and initiators. No energy source is present to break the initiator chemical bonds in order to start the polymerization process.

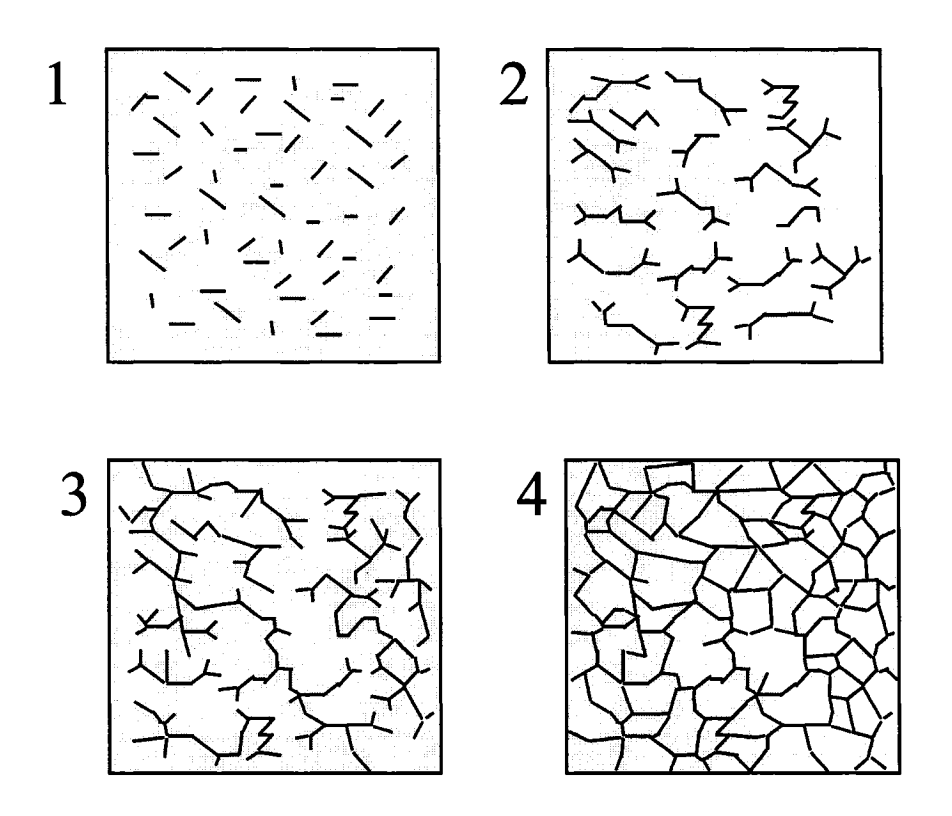


Figure 5: Polymerization steps

Once the energy source is activated, (step 2), the initiators start the chemical reactions and thus long chains of polymers are formed. The density of the resin increases and the temperature rises due to exothermic chemical reaction. As the reaction progresses, (step 3), the polymer chain formation decreases as the monomers are consumed and the density becomes so high that the chemical exchanges become difficult. Lastly, the reaction stops (step 4) and the resin is solidified.

Two important events happen during the curing process: gelation and vitrification of the resin. The gelation is the point in the curing cycle at which a dramatic increase in viscosity occurs due to initial network formation. This transition comes with a significant increase in the resins mechanical properties and thus its load caring capability. The vitrification is the transition from the amorphous solid state to the melt state. The temperature that marks this transition is called the glass-transition temperature T_g .

1.1.3 Polymerization techniques

The most common thermoset resin curing techniques are:

- Room temperature
- Oven curing
- Autoclave
- Electron beam curing
- UV

Out of these, the thermal methods (ie. Oven and autoclave curing) are the most frequently used in the aerospace industry. The availability of toughened resin systems that provide excellent mechanical properties for space and aerospace applications is one of the main advantages of this technique. High processing costs, high tooling cost and considerable residual stresses development in the cured structures are amongst its main drawbacks.

Room temperature curing is mostly used to bonde doublers, joints and fibreglass pads on composite structures (Figure 1a). The main disadvantage of this technique is that it has a 24 hour cure time.

Electron beam (EB) processing is a composite manufacturing technology that consists of curing thermosets resins by irradiation using a source of high-energy electrons [1]. Applications of this technique to the automotive and aerospace industry would enable the fast curing of large components that would be difficult and expensive to produce with conventional thermal processing technologies such as autoclave and oven processing. During EB curing, the polymer cross-linking reaction is triggered by room-temperature electron irradiation. Faster curing, close to room temperature curing, potential for lower residual stress in the part, low tooling and processing cost, long shelf lives of resins, environmental friendly, possibility to cure large composite structures which are impossible to fit in an autoclave, are some of the main advantages of the EB processing. Poor interlaminar shear strength and little qualification data for space and aerospace industries are some of its main drawbacks.

1.1.4 Thermal distortions and residual stresses

Composite structures often have to survive for 15 years under extreme environmental conditions. Since space has no atmosphere, their temperature could rise up to 200°C (473° Kelvin) and drop to -269°C (4° Kelvin) in just a couple of minutes. The highest temperatures are reached when the structure is exposed to the solar flux, and the lowest temperature is obtained when the structure is shadowed from the sun. Under these conditions, thermal stability becomes a very important factor in the spacecraft design. Residual stresses trapped in the structure, during the curing phase of the composite, are significant contributors to the structures deformation during temperature changes. The following list identifies other different contributors to the residual stress development [2]:

- Non-uniform thermal strains in direction of the fibre vs transverse of the fibre;
- Resin cure shrinkage strain;
- Non-uniform resin flow;
- Tooling effects.

Residual stresses cause matrix microcracking, warpage or springback of the final component and can be very costly to control. Designers often account for residual stresses by assuming that the composite is stress-free at the curing temperature and that stresses will develop as the part is cooled down to room temperature and beyond. Therefore, the stress-free temperature (T_{SF}) is a measure of the level of residual stresses present in the part after processing. Figure 6a shows an example of the microcraking effects and Figure 6b shows a possible spring in effect on a cured structure. One way to

reduce the level of residual stresses in a structure is to reduce the curing temperature of the curing process.

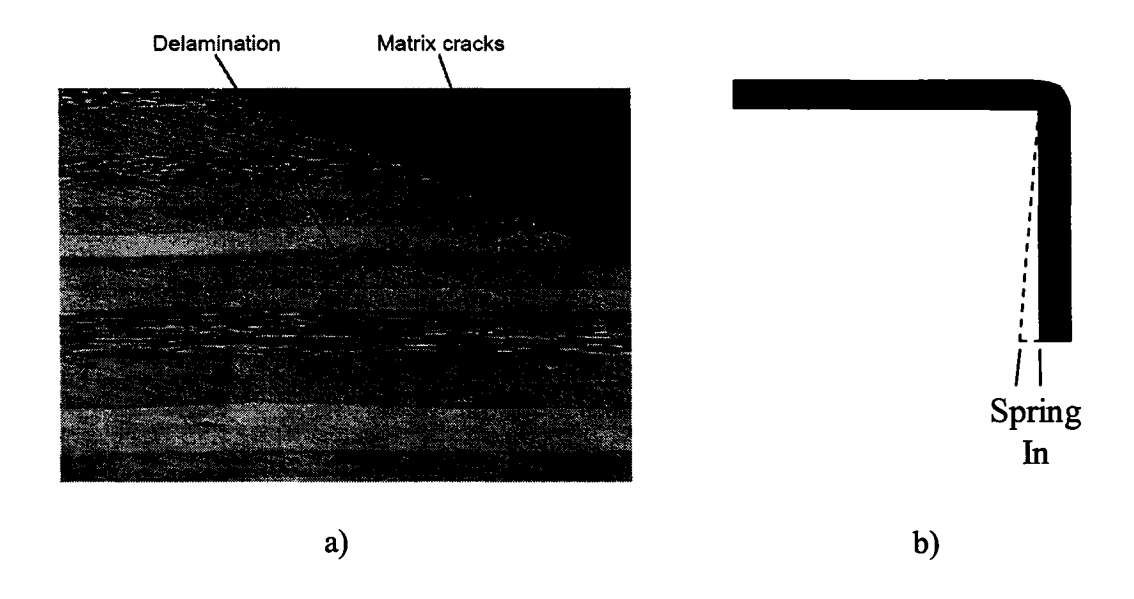


Figure 6: a) Microcraking of composites; b) Spring In of structure

For the EB process, the study of residual stresses development has been very limited [1]. The presence and magnitude of residual stresses are generally assessed by measuring the final component warpage or distortion. The question of how these stresses develop during cure remains unanswered. It has been found that the level of residual stresses arising from EB curing can be low, compared to thermal curing. Knowledge of why and how stress develops is critical to understanding how it can be controlled. Furthermore, the understanding of residual stresses development will help defining the practical limits of controlling residual stresses during EB curing. Also, while it may be theorized that "locking-in" residual stress at a low temperature may be possible, the effects of post-cure required to complete the cure process are still unclear.

1.2 LITERATURE REVIEW

1.2.1 Electron beam overview

Chens et al [3] wrote a complete literature review of electron beam curing of composites.

Electron beam curing of fibre-reinforced composites is an attractive technique that offers the potential to produce cost effective composite structures [3]. EB curing of composites possesses many advantages in comparison with conventional thermal curing process: Faster curing, close to room temperature curing, potential for lower residual stresses in the part, low tooling and processing cost, long shelf lives of resins, environmental friendly, possible to cure large composite structures which are impossible to fit in an autoclave etc.

It has been found [3] that resin systems (mainly epoxies + photoinitiators), which cure via cationic mechanism under EB irradiation, are chosen to manufacture high performance composite structures because of their low shrinkage and high thermal and mechanical properties. All reinforcement materials, which are conventionally used for advanced composite materials, such as carbon fibre, aramid fibre and glass fibre, can be used for EB cured composites.

Research shows that some of the composites cannot reach full cure, even after a very high dosage of the electron beam irradiation [3]. The reason might be the low temperature during the EB curing. When the degree of cure reaches a certain stage, the reactive

species don't have enough energy to move and are «trapped» in the resin. To solve this problem, a thermal post-cure at elevated temperature is usually used to improve the degree of cure and mechanical properties. The dose rate is another influence factor of EB curing. The direct influence of dose rate is the processing time and the rate of temperature rise in the part. Appropriate dose rate should be selected to avoid overheating in the part. Dose rate can also influence the total dose requirement for fully cure and properties of composite. Furthermore, temperature plays an important role in the EB curing. EB curing processed under different temperatures might result in different properties of the composites. An increase of the process temperature, results in a higher degree of cure for the same dose level.

With respect to residual stress, no precise data or information was yet available [3]. All that is known is that composite materials cured in an autoclave contain residual stresses induced by the different sources mentioned in section 1.1.4. It is expected that EB cured composites will have lower residual stresses due to their lower processing temperatures. Efforts have been made to develop projects to monitor the residual stress in process of EB curing composite patch repair in the Institute for Aerospace Research (IAR) of the National Research Council of Canada.

1.2.2 Thermal cure residual stress overview

Like other load-bearing structures, aging aircraft may contain damaged or cracked structural components resulting from fatigue and corrosion during service and the degraded structural components must be replaced or repaired to extend their service lives.

Because of the superior properties of advanced fibre composites, composite patch repair

is recognized as an efficient and economical repair technology, yet thermal residual stresses induced by the bonding process of composite patch repairs cause adverse effects on the fatigue performance.

Cho and Sun [4] and D. Djokic [5], both focused their work on lowering the thermal residual stresses induced during processing in composite patch repair in metallic aircraft structures. Based on Albat [6] ground work, they have found that by optimizing the curing cycle induced residual stresses in a composite patch could be reduced. Moreover, it has been shown that the reduction of thermal stresses from the modified bonding cycle can substantially improve the fatigue performance of the repair. Furthermore, the two-step curing strategy was successful in maximizing final cure properties and reducing residual stresses. However, the adhesive required extended processing in its initial curing step, before it could be post-cured without viscoelastic relaxation. Slow cooling and lowered post-cure temperature strategies were successful, but at the cost of prolonged times and lowered adhesive properties. Finally, with the use of multi-step cure cycles a good compromise was achieved between lowered residual stresses and maximized adhesive properties. In these cycles, the initial segment at an intermediate temperature shortened processing times significantly.

No residual stress literature was found relative to electron beam (EB) processing. This finding was the initial incentive to proceed with the investigation of the development of residual stresses in EB cured composites. Considering that EB cured parts are well-

known to cure at low temperatures, the potential of lowering considerably the residual stresses is appealing.

1.3 RESEARCH OBJECTIVES

The objective of this work is to asses the development of residual stresses during onset electron beam curing. In order to achieve that goal the following tasks are conducted:

- Design and manufacturing of a test fixture that is insensitive to EB field;
- Test twenty specimens containing two types of EB resins (CAT B and Tactix 123);
- Compare stress-free temperature of EB and thermally cured specimens;
- Apply various dose rates, irradiation cycles and heat transfer coefficients in order to better understand their impact on residual stress development.
- Thermal post cure certain specimens to asses the impact on residual stresses;
- Measure gelation DOC and temperature using parallel plate rheology test;
- Establish a relationship between the warp temperature, stress free temperature and the gelation temperature;
- Predict the resin degree of cure at which residual stresses develop using a simple cure kinetics model.

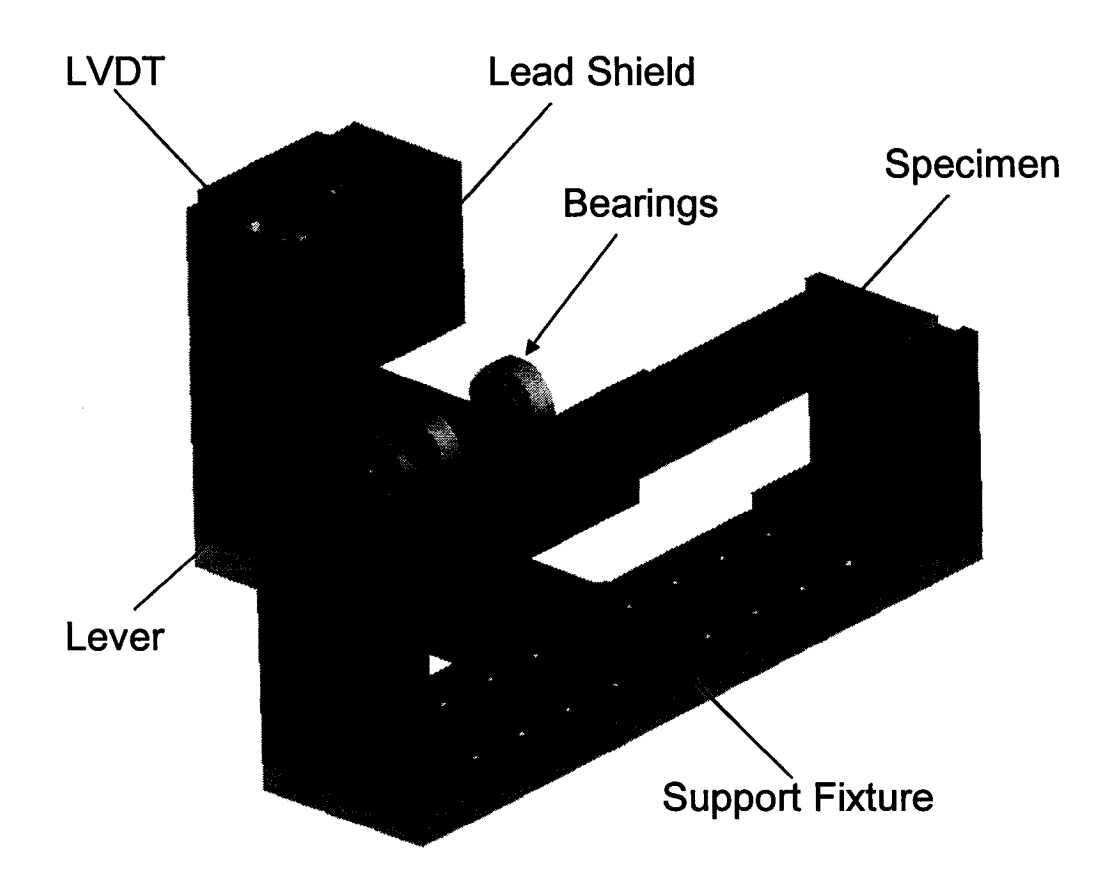
2 EXPERIMENTAL PLAN

2.1 TEST APPARATUS

The experimental technique used here was developed from the work of Djokic *et al.* [7], which used a fixture to measure warpage of thermally cured bonded patch specimens. The fixture enabled the understanding of residual stresses development and optimization of the cure cycle in order to reduce the level of residual stresses for repair of components using composite patches. The main objective in the present work was to adapt this technique for the measurement of specimen warpage during EB irradiation. Therefore, the instrumentation shielding was the main focus of the fixture design. It is important to mention that the objective of the proposed technique was to measure the residual stresses development by monitoring warpage evolution but not the actual magnitude of the warpage. The stress-free temperature (T_{SF}) was used to assess the level of residual stresses corresponding to a particular curing condition.

The key design considerations in the development of the test fixture were as follows: simplicity of design, adequate measurement sensitivity and insensitivity to EB radiation. In order to meet all the main design considerations, the fixture developed in [7] was modified by replacing the strain gauge displacement measuring system with an LVDT mounted outside the beam area. The specimen warpage was transmitted to the LVDT by a lever mounted on bearings. The LVDT was isolated from the beam using a lead shield as shown in Figure 7. It is known that with electron radiation, lead produces more secondary radiation than using a low atomic number material (ex: plastic) yet the choice

of lead was made due to the lack of volume space available for the shielding and that the secondary radiations generated by the lead were contained by the thick concrete walls surrounding the curing setup. Specimen alignment features have been added to ensure proper specimen positioning. The LVDT LD400-2.5 Series model manufactured by Omega Inc. was chosen because it offered a span of displacement of \pm 2.5 mm and high resolution (0.01 mm). The displacement measured by the LVDT was calibrated with a micrometer over the full range.



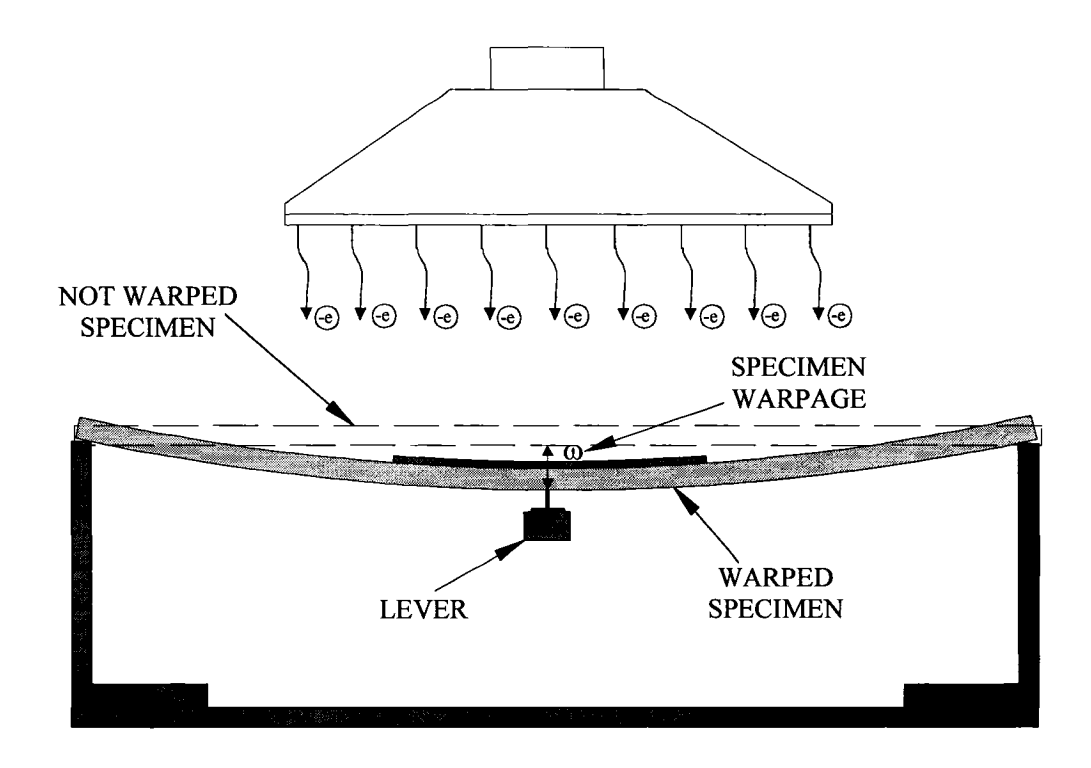


Figure 7: Schematic of the test fixture

2.2 SPECIMEN PREPARATION

2.2.1 Metallic specimen

The metallic specimens were manufactured using a procedure developed for composite patch repair presented in [7]. The metallic specimens consisted essentially of a steel-aluminium strip in which two metal plates are joined by a curing resin. The difference in the coefficients of thermal expansion of the materials, combined with a temperature change induced by the EB exposure will induce the warpage of the specimen. Warpage will occur only if the two metals are bonded by the resin layer. Hence, the occurrence of the warpage indicates that the resin can support stresses. The adherent metals and their thicknesses were selected to maximize the warpage within the LVDT range. For this set of experiments, a 3 mm thick aluminum substrate, and a steel patch with a thickness of 1.5 mm were used (Figure 8). Dow Chemical's Tactix 123 resin with 3 wt% CD 1012

photoinitiator (Sartomer Co.) was used the bonding agent. Standardized techniques for bonding surface preparation of aluminum substrates were implemented; using mechanical abrasion (grit-blasting), 1 % silane solution coupling agent and BR 127 primer applications. Steel patch bonding surfaces were chemically cleaned and grit-blasted. In order to maintain bondline thickness during vacuum compaction, a 0.2 mm thick glass scrim cloth was inserted between the two metals. The stacked layers were secured with flashbreaker tape along the bondline edge. This was also done to minimize resin migration and excessive bleed-out. The assembled specimen was covered with nylon breather cloth and vacuum bagged (Figure 9). Prior to EB exposure, vacuum was applied to ensure adequate bonding pressure.

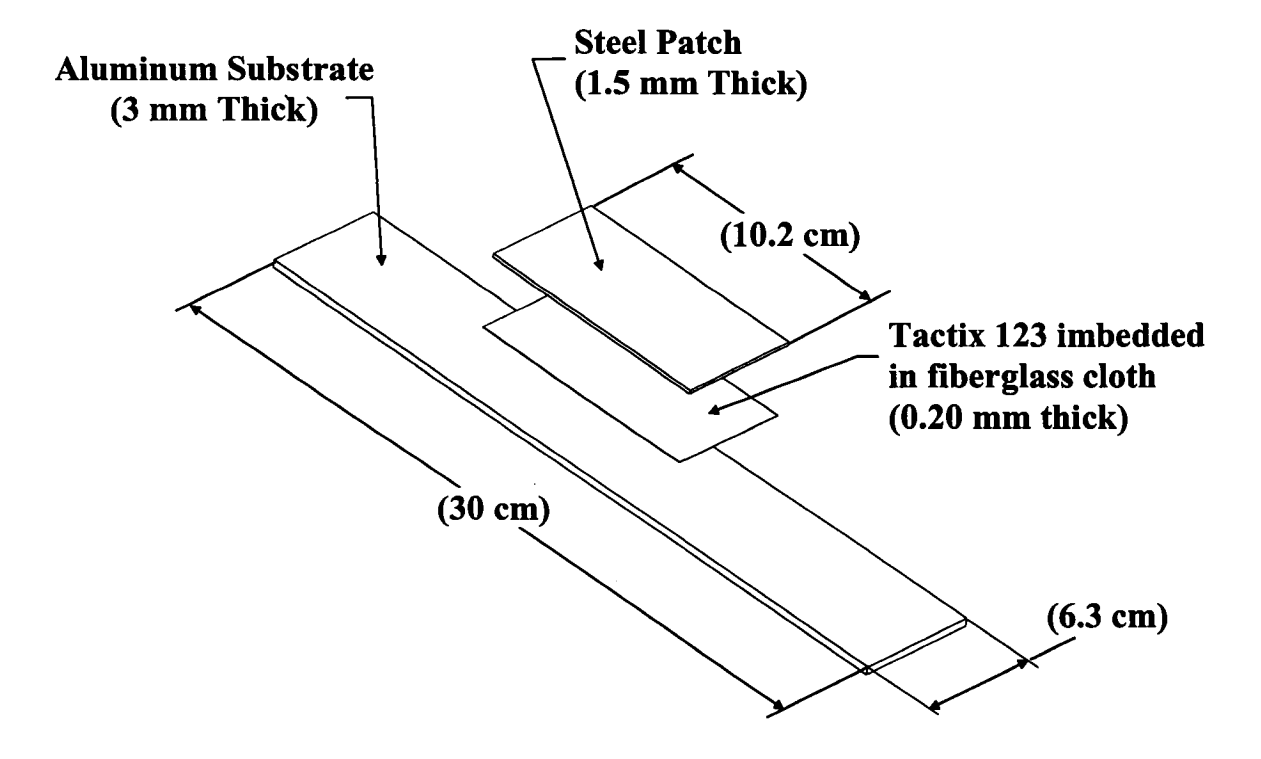


Figure 8: Metallic specimen components



Figure 9: Metallic specimen vacuum bag assembly

2.2.2 Composite specimen

The composite specimens consisted of an unbalanced (asymmetric) composite laminate, designed to warp with temperature change. The principle of the unbalanced composite specimen is similar to the metallic specimen (aluminum-steel) used in Section 2.2.1. Similarly to the metallic specimen, the adherent laminates and their thicknesses were selected to maximize the warpage within the LVDT range. For this set of specimens, substrate and patch were each made from 12 plies of AS4/3501-6 unidirectional carbon fibre and assembled as shown in Figure 10. Dow Chemical's Tactix 123 resin with 3 wt% CD 1012 photoinitiator (Sartomer Co.) and CAT B resin system from Applied Poleramic Inc. were used as adhesives. In order to maintain bondline thickness during vacuum compaction and irradiation, a (0.2 mm) glass scrim cloth was inserted between the two laminates. The stacked layers were secured with flashbreaker tape along the

bondline edge. This was also done to minimize resin migration and excessive bleed-out. The assembled specimen was covered with release film, nylon breather cloth and vacuum bagged (Figure 11). Just prior to EB exposure, vacuum was applied to ensure adequate bonding pressure.

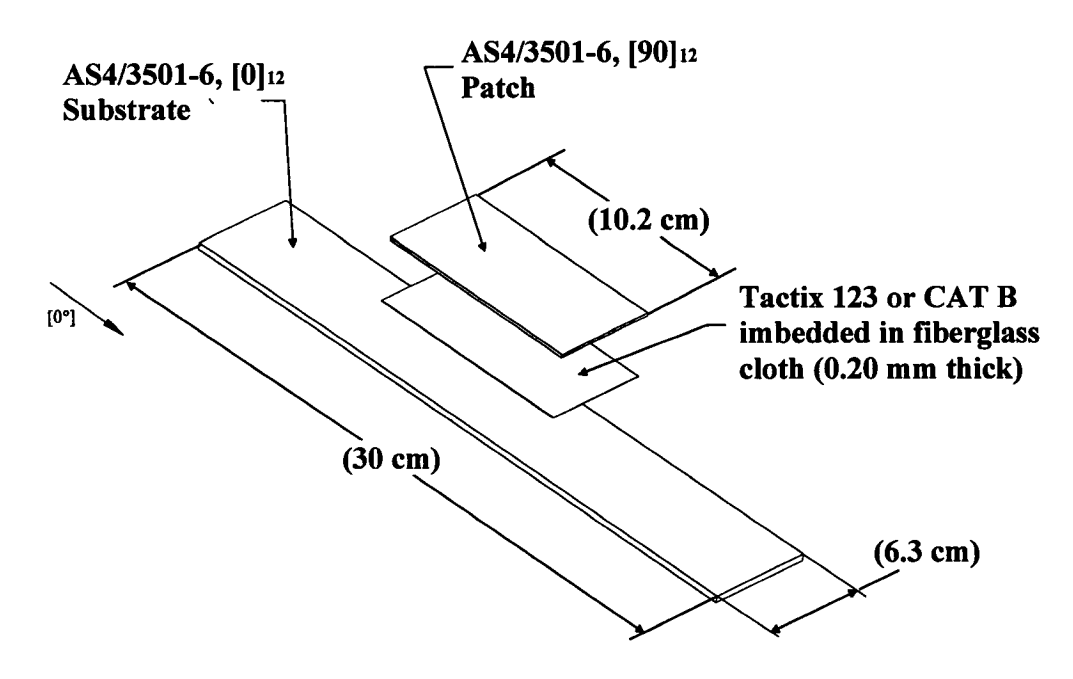


Figure 10: Composite specimen components

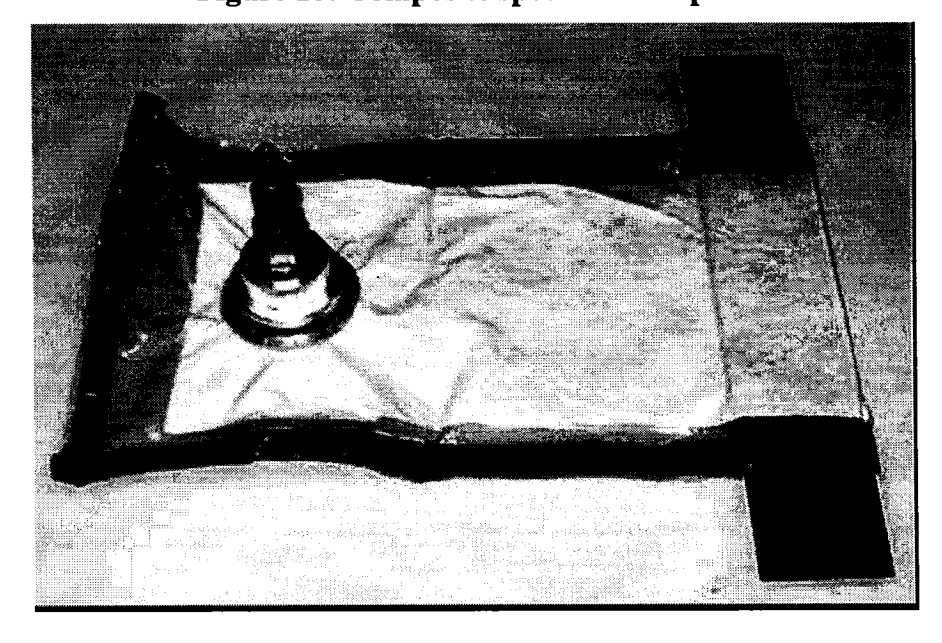


Figure 11: Composite specimen vacuum bag assembly

2.2.3 Resin coupons

Resin coupons were installed on to each specimen in order to investigate the resin degree of cure after EB irradiation. In Figure 12, a typical resin coupon assembly is shown. Initially, the aluminium foil was cleaned using solvent (MEK or Acetone) wipes. The clean surface was then sprayed with release agent and then left to dry. Once the first coat of release agent had dried, a second coat was applied and left to dry. The aluminium foil was then crimped to create the fold lines shown in Figure 12. Using a syringe, 0.5 ml of resin was transferred to the aluminium foil and the foil was folded to create a pouch. The pouch was then sealed with flashbreaker tape. Once all these steps were completed the resin coupon was mounted on the specimen and strapped with flashbraker tape.

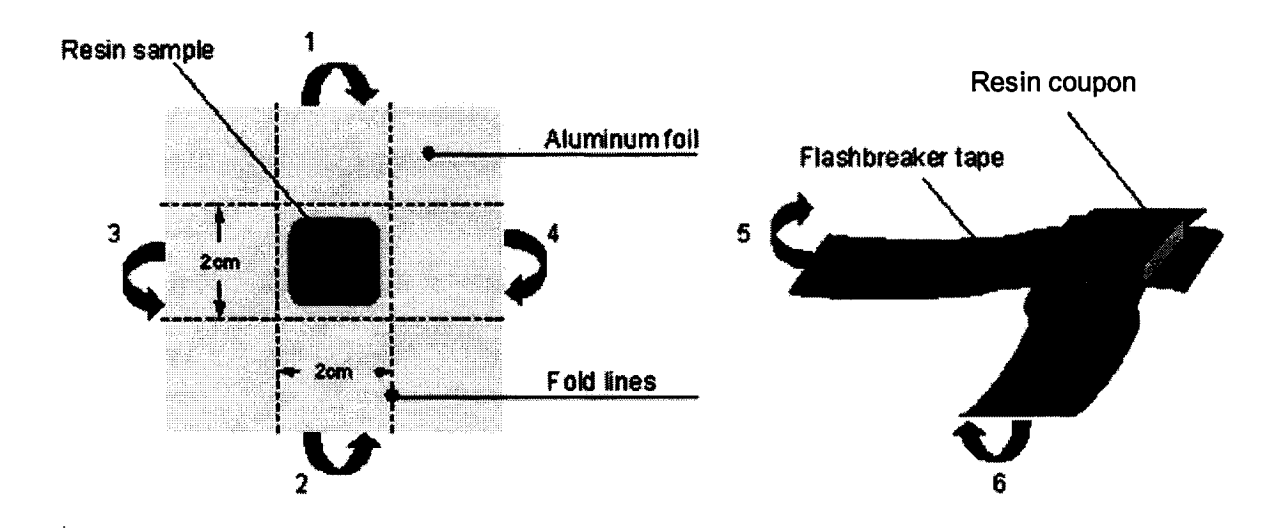


Figure 12: Resin coupon fabrication

2.3 TEST CONDITIONS

2.3.1 E-Beam cure

2.3.1.1 Test setup

The residual stress testing was performed at the Laboratory for Research on Electron Beam Curing of Composites of the University of Dayton Research Institute. The EB accelerator was a 3 MeV S-Band RF Linac gun with a power of 500 W. The following procedure was used for all tests.

The apparatus was first positioned so that the specimen was directly under the EB gun horn at a distance of approximately 30 cm (Figure 13a). Direct current excitation voltage (16 V) from an external source was applied to the LVDT. The specimen was placed on the support brackets and the vacuum bag was connected to a vacuum pump (Figure 13b). The specimen temperature monitored with thermocouples mounted on the top (TC1) and bottom (TC3 and TC4) surfaces of the specimen. In order to monitor the environment temperature during processing a thermocouple (TC2) was places on the support fixture (Figure 14). All thermocouples were connected to the data acquisition system. Temperature and displacement data were acquired using an InstruNet iNet-100 DAQ board at 5 Hz rate.

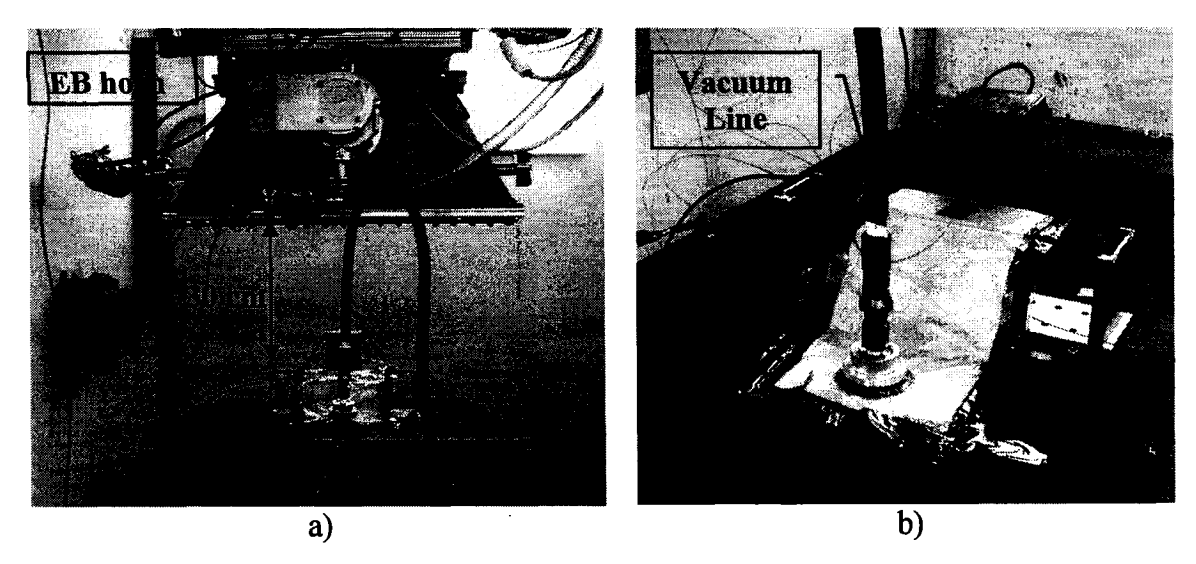


Figure 13: a) Photograph of the test setup, b) Close up showing the specimen and vacuum bag.

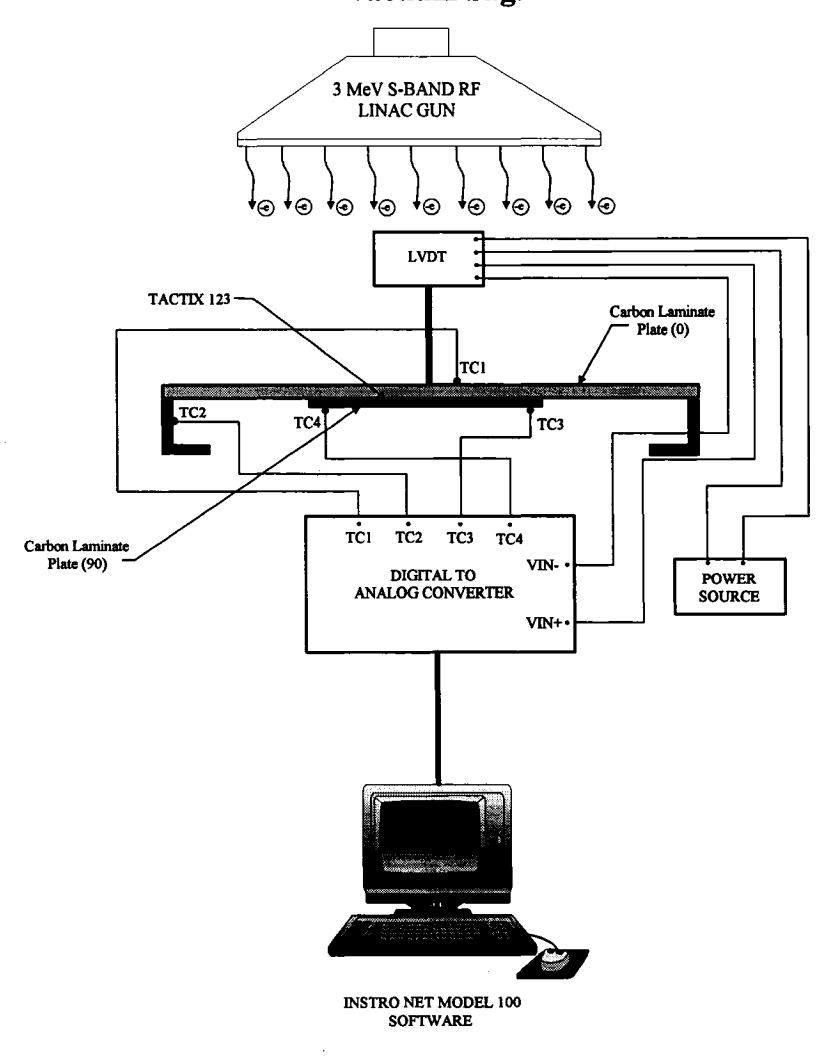


Figure 14: Test setup schematic.

2.3.1.2 Cure conditions

Twenty test specimens were prepared and exposed to different EB irradiation times and pulse rates summarized in Table 1, 2 and 3.

Metallic specimens with Tactix 123 resin

Four metallic specimens were prepared and exposed to different EB irradiation times and pulse rates. From Table 1, RS09 and RS10 was exposed to the same pulse rate (50 s⁻¹), but RS10 was exposed to a higher total dose (600 seconds for RS09 vs 960 seconds for RS10). RS11 was exposed at a higher pulse rate (75 s⁻¹), while RS12 was exposed at a lower pulse rate (25 s⁻¹). Prior to testing, the average dose rate (kGy/min) was calculated from the total dose measured by ten radiachromic films mounted on an aluminum plate. The plate was placed on the specimen support in order to measure the actual dose that will be seen by the specimen as shown in Figure 15.

Table 1: Cure conditions for metallic specimens with Tactix 123 resin

Test	Specimen	RESIN	Pulse rate (s ⁻¹)	Time (sec)
			50	300
1	RS09		Cool down	300
		Tactix 123	50	300
			50	480
2	RS10		Cool down	240
			50	480
	RS11		75	320
3			Cool down	240
			75	320
	RS12		25	600
			Cool down	240
4			25	600
Ì			Cool down	500
			75	240

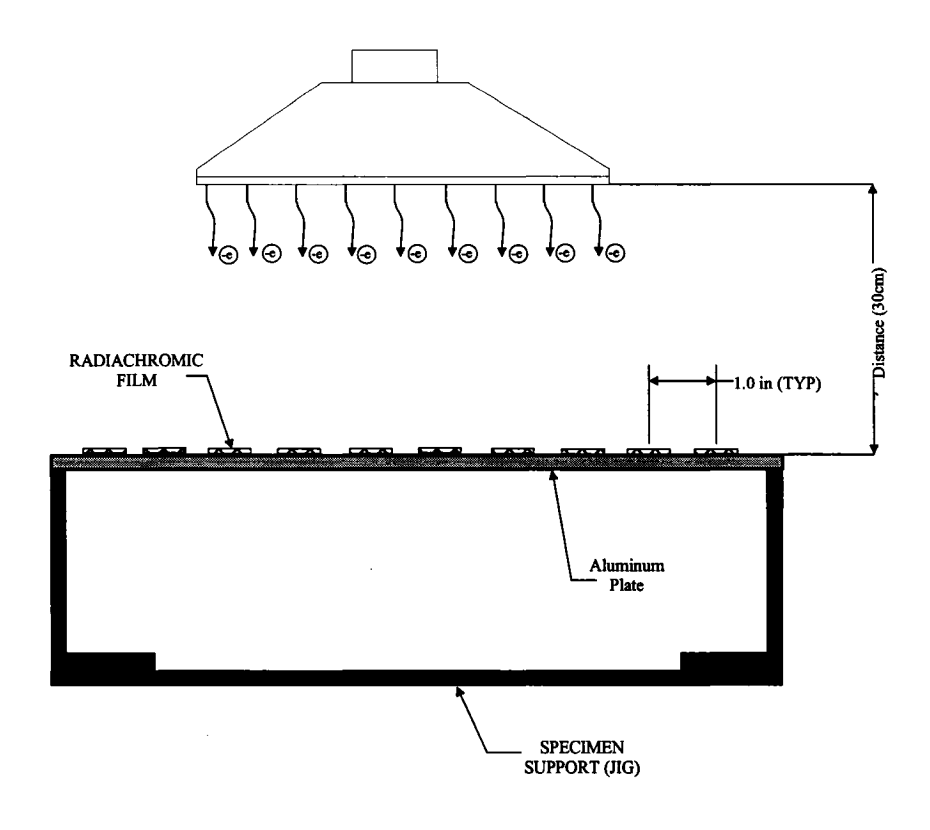


Figure 15: Dose rate measurement.

Composite specimens with Tactix 123 resin

For specimens RS13, RS14, RS16, RS17, RS18, RS21 to RS24 (Table 2), the irradiation time was selected such that the total dose seen by the specimens remained relatively the same. From Table 2, RS13, RS14, RS27 and RS28 are at the same pulse rate (25 s⁻¹) but RS13 and RS14 were exposed to three radiation cycles and a higher radiation time exposure compared to RS27 and RS28. RS16, RS17, RS23 and RS24 are also at the same dose rate (50 s⁻¹) and total dose (KGy), but RS16 and RS17 were exposed to two radiation cycles compared to one for specimens RS23 and RS24. For specimens RS25 to RS28, the total dose and the dose rates were varied in order to observe their effect on

residual stresses. In several tests, two specimens were tested using the same conditions in order to measure test repeatability.

Table 2: Cure conditions for composite specimens with Tactix 123 resin

Test	Specimen	RESIN	Pulse rate (s ⁻¹)	Time (sec)
	RS13 RS14		25	275
			Cool down	240
5			25	275
	K514		Cool down	240
			25	275
	RS16		50	194
6	RS17***	Tactix 123	Cool down	240
			50	194
	RS21 RS22***		75	132
7			Cool down	240
			75	132
8	RS23 RS24***		50	388
9 .	RS25		25*	10 cycles of 30 sec+1 cycle of 100 sec
10	RS26**]	25*	8 cycles of 30 sec
11	RS27		25	
12	RS28		25	147

^{80%} Beam width.

Composite specimens with CAT B resin

For specimens RS15 and RS18 (Table 3), the irradiation time was selected such that the total dose seen by the specimens remained relatively the same. The choice of pulse rates for specimens RS15 and RS18 was copied from RS13/RS14 and RS16/RS17 respectively (see Table 2), in order to be able to compare the test results. For specimens RS19 and

Low starting temperature Fan used during testing

RS20, the total dose and the dose rates were varied by exposing the specimens to sixteen, 30 second, irradiation cycles and one 100 second cycle, in order to see the effects of short irradiation time exposures on temperature rise of the specimen and residual stress development.

Table 3: Cure conditions for composite specimens with CAT B resin

Test	Specimen	RESIN	Pulse rate (s ⁻¹)	Time (sec)
	RS15	CAT B	25	275
			Cool down	240
13			25	275
			Cool down	240
			25	275
:	RS18		50	194
14			Cool down	240
			50	194
15	RS19***		25*	16 cycles of 30 sec+1 cycle of 100 sec
16	RS20**		25*	16 cycles of 30 sec+1 cycle of 100 sec

^{*: 80%} Beam width.

Improvements to the metallic dose measurement setup were necessary in order to represent more accurately the testing environment. Figure 16 shows radiochromic film dosimeters mounted between the substrate and patch parts of a "dummy" specimen (no EB resin adhesive present), mounted in the test fixture and placed in the same location as in the actual irradiation tests. With this configuration, the radiochronic films were in the same environment as the resin, thus giving a more accurate approximation of the average dose rate seen by the resin. The beam width was adjusted to control the dose rate (kGy/min) seen by the specimen for a particular pulse rate (s⁻¹). All dose rates for

^{**:} Low starting temperature

^{***:} Fan used during testing

specimens RS13 to RS18, RS21 to RS24, RS27 and RS28 were measured and calculated with a 40% beam width. Specimens RS19, RS20, RS25 and RS26 were measured and calculated with an 80% beam width. As an example, for a particular pulse rate, a 40 % beam width will give a higher dose rate than an 80% beam width, due to the focusing of the beam on a smaller surface area with the same amount of electrons being projected.

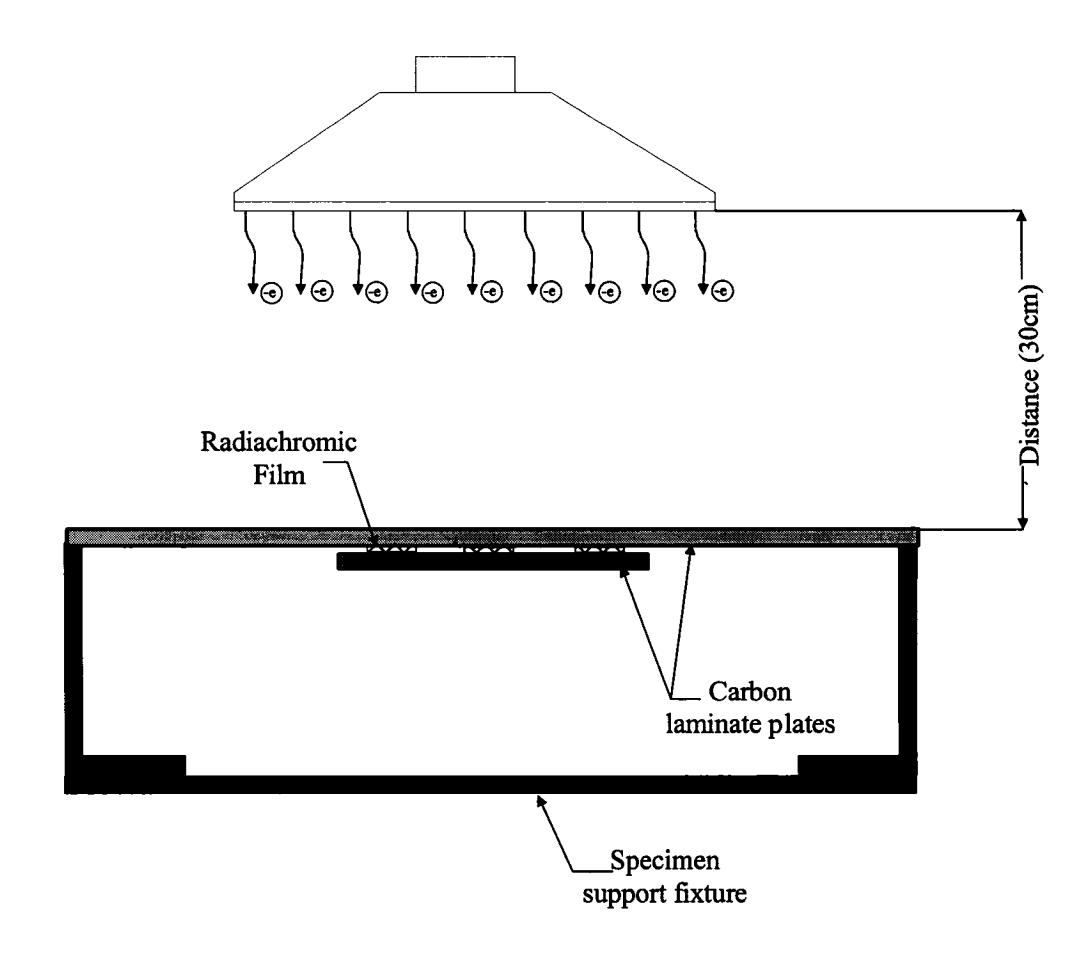


Figure 16: Composite dose rate measurement.

2.3.2 Thermal cure

Following irradiation, EB cured (RS09, RS10, RS11, RS12) specimens were thermally post-cured in a convection oven at 160 °C for 1 hour. The specimen warpage was measured during post-cure using the instrumented cantilever beam, as in [7]. In addition, two uncured specimens (with unexposed Tactix 123) were thermally cured at 160 °C and 205 °C for 1 hour in order to compare the stress free temperature obtained for a thermal cure versus an EB cure. Temperature and warpage data were recorded at 0.1 Hz sampling rate. The linear portion of specimen warpage vs. temperature curve during final cool-down was used to estimate the T_{SF} .

2.4 DATA REDUCTION

The average dose rate $\dot{\overline{D}}$ $\binom{kGy}{\sec}$ exposed to the specimen during the irradiation phase is one of the most important parameter that needs to be quantified. The following thermal energy balance equation for the specimen is assumed:

$$Q_{in} - Q_{out} = \rho V c_p \Delta \dot{\overline{T}} \tag{1}$$

where Q_{in} $\binom{kJ}{\mathrm{sec}}$ is the heat generated by the EB irradiation field, Q_{out} $\binom{kJ}{\mathrm{sec}}$ is heat lost to the environment, ρ is the volume mass of the material $\binom{kg}{m^3}$, V is the total volume of the substrate $\binom{m^3}{}$, c_p is the material specific heat $\binom{kJ}{kg} \cdot {}^{\circ}K$ and $\Delta \dot{T}$ is the

average rise in the specimens temperature (${}^{\circ}K/\text{sec}$). Figure 17 shows schematically the energy balance for each specimen during the curing phase.

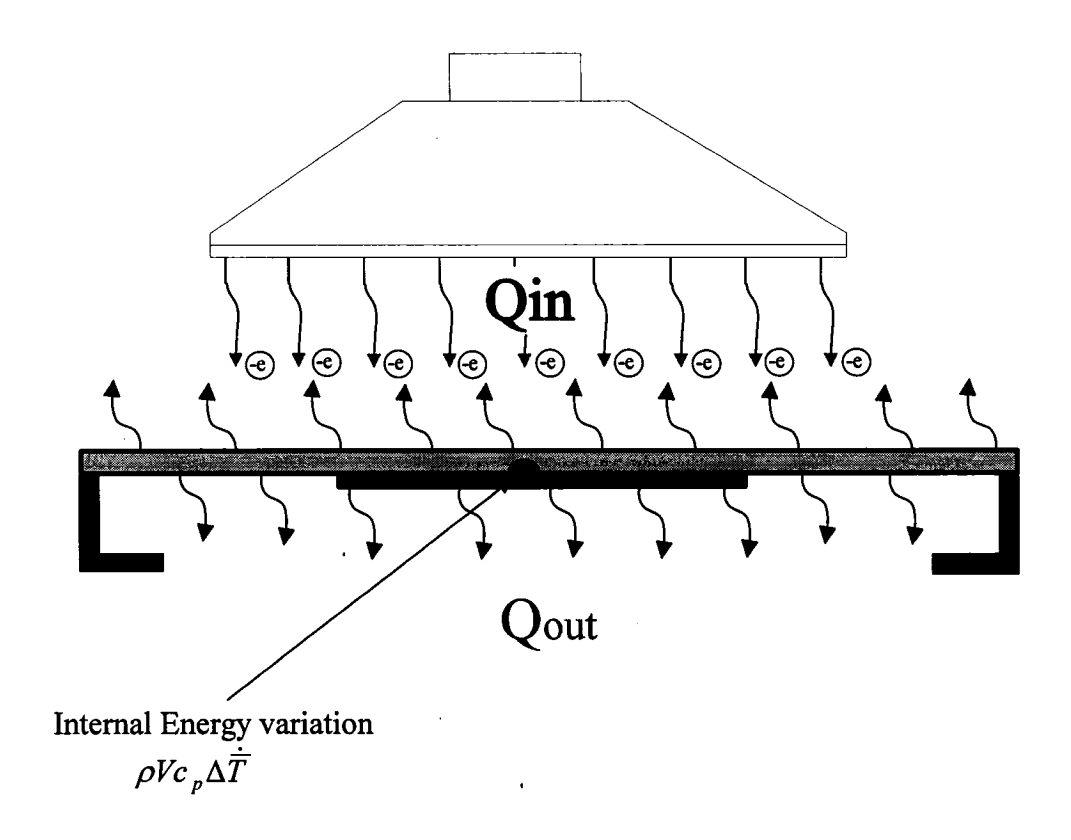


Figure 17: Specimen energy balance

Assuming that the energy generated by the EB irradiation is directly proportional to the dose rate $(\dot{\overline{D}})$ and that the heat exchange lost to the environment is mainly convective, Q_{in} and Q_{out} can be defined as follows:

$$Q_{in} = \rho V \dot{\overline{D}} \tag{2}$$

$$Q_{out} = hA\Delta \overline{T} \tag{3}$$

Where h $(kJ_{m^2} \cdot {}^{\circ}K \cdot \sec)$ is the heat transfer coefficient, A (m^2) is convection surface area, $\Delta \overline{T}$ $({}^{\circ}K)$ is the average gradient temperature between the specimen and the environment.

The convection coefficient (h) was calculated from the measured temperature evolution during the test. During the specimen EB irradiation period both Q_{in} and Q_{out} , in (1), are non zero. However, during the cool down period Q_{in} is zero as the beam is turned off. Thus equation (1) is reduced to

$$Q_{out} = -\rho V c_p \Delta \dot{\bar{T}} \tag{4}$$

By substituting (4) into (3) the following relation is obtained:

$$hA = -\frac{\rho V c_p \Delta \overline{T}}{\Lambda \overline{T}} \tag{5}$$

In equation (5) the average temperature change and the average temperature gradient are extracted from acquired thermocouple data as follows:

$$\Delta \dot{\overline{T}}(t) = \frac{\begin{bmatrix} Tc3(t+5) + Tc4(t+5) \\ 2 \end{bmatrix} - \begin{bmatrix} Tc3(t-5) + Tc4(t-5) \\ 2 \end{bmatrix}}{\underbrace{(t+5) - (t-5)}_{10 \text{ sec time span}}}$$
(6)

$$\Delta \overline{T}(t) = \frac{1}{10} \sum_{t=5}^{t+5} \left[\underbrace{\frac{Tc3(t) + Tc4(t)}{2}}_{Avg\ at\ t=t} - \underbrace{\frac{1}{10} \sum_{t=5}^{t+5} Tc2(t)}_{Avg\ air\ Temp\ during\ 10\,\text{sec}} \right]$$
(7)

where, Tc2(t) is the thermocouple TC2 temperature reading, Tc3(t) is the thermocouple TC3 temperature reading and Tc4(t) is the thermocouple TC4 temperature reading (see Figure 14).

By substituting equation (2), (3) and (5) into (1) we can isolate the $\dot{\overline{D}}$ as follows:

$$\dot{\overline{D}} = \frac{1}{\rho V} \left(\rho V c_p \Delta \dot{\overline{T}} + h A \Delta \overline{T} \right) \tag{8}$$

Equation (8) enables to monitor the evolution of dose rate with time (\bar{D}) in order to detect any irregularities in the irradiation process.

3 EXPERIMENTAL RESULTS

Preliminary tests in which the fixture alone was exposed to the EB irradiation, confirmed that the electron beam did not affect the LVDT signal. Next, a specimen without bonding resin was irradiated and again, the beam was found not to affect the LVDT signal and no warpage was measured as the temperature of the specimen changed. These preliminary tests demonstrated that the fixture thermal expansion did not affect the warpage measurement during or after irradiation.

3.1 E-BEAM CURED SPECIMENS

3.1.1 Metallic specimens

Table 4 presents a comparison of the average EB dose rate and total dose obtained from dosimeter measurements and calculations based on the measured temperature profile. Good agreement for tests RS09, RS10 and RS12 was found. In these cases, the beam dose rate was constant during the irradiation. However, for RS11 the calculated dose rate was significantly lower than the measured dose rate. In this case, the beam was applied at a high pulse rate (75 s⁻¹) and it was evident, from temperature measurements, that the accelerator could not maintain this high pulse rate throughout the duration of the irradiation (Figure 18). The same behaviour was observed for the third exposure for specimen RS12 (see Figure A. 3). Appendix A presents pulse rates results for RS09, RS10 and RS12. Table 4 also shows the resin degree of cured (DOC) measured from resin samples collected from the specimen after EB cure. The DOC (α) was measured

with a differential scanning calorimeter (DSC), using a dynamic scan rate of 5 °C/min. This technique measures the heat of reaction of a resin and allows the derivation of the DOC (α) with the following equation:

$$\alpha = 1 - \frac{\text{Heat of reaction of a partialy cured re sin}}{\text{Heat of reaction of an uncured re sin}}$$
(9)

Therefore, a resin that is fully cure will have an $\alpha=1$, and a resin that is uncured will have an $\alpha=0$.

A slight increase of the degree of cure between specimens RS09 and RS10, this was explained by the fact that RS10 was exposed to a higher total dose. RS11 degree of cured (DOC) was expected to be the highest due to the fact that it was exposed to a higher pulse rate (75 s⁻¹), yet the dose rate results (Figure 18) show that the EB gun was unable to maintain the dose rate at a constant level for 75 s⁻¹ thus directly impacting the final degree of cure. Finally, RS12 obtained an equivalent DOC as RS10 due to its higher pulse rate (75 s⁻¹) final radiation curing phase which restarted the polymerization of the resin by activating some of the initiators that haven't been activated by the two subsequent (25 s⁻¹) radiation phases.

Table 4 Comparison between dose rate, total dose measured from dosimeter and calculated from temperature profiles using Equation 8; degree of cure measured after EB exposure.

G.	Dose Rate (kGy/min)		Total Dose (kGy)		Degree of
Specimen	Measured	Calculated	Measured	Calculated	cure
RS09	6.7	6.4	67	64	0.76
RS10	6.8	6.4	109	102	0.80
RS11	6.9	11.5	74	123	0.74
RS12	3.4* 7.0**	3.5* 11.5**	96	116	0.80

^{*} Dose rate corresponding to the first and second EB irradiation at pulse rate of 25 s⁻¹ (see Table 1)

^{**} Dose rate corresponding to the third EB irradiation at pulse rate of 75 s⁻¹ (see Table 1)

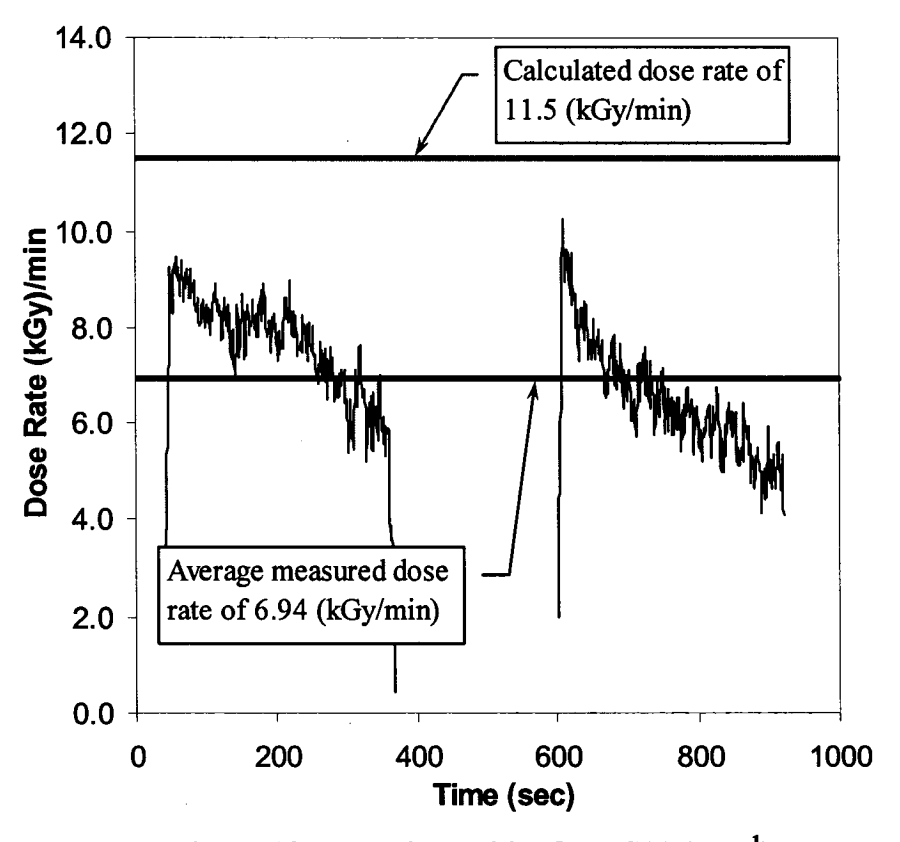


Figure 18: Beam instability for RS11 (75 s⁻¹)

Figure 19 shows the specimen temperature during and between radiation doses. The specimen heated up rapidly during irradiation and cooled down when the beam was switched off. Figure 19 also illustrates the noticeable difference between the dose rate and resulting temperature profile between RS09 and RS12. For the first EB exposure, specimen RS09 received 32 kGy at 6.7 kGy/min compared to 34 kGy at 3.4 kGy/min for sample RS12. This dose rate difference resulted in a maximum temperature for the first cycle of 54 °C at 300 seconds for RS09 compared to 43 °C at 600 seconds for RS12. Measured temperatures for RS10 and RS11 were similar to RS09.

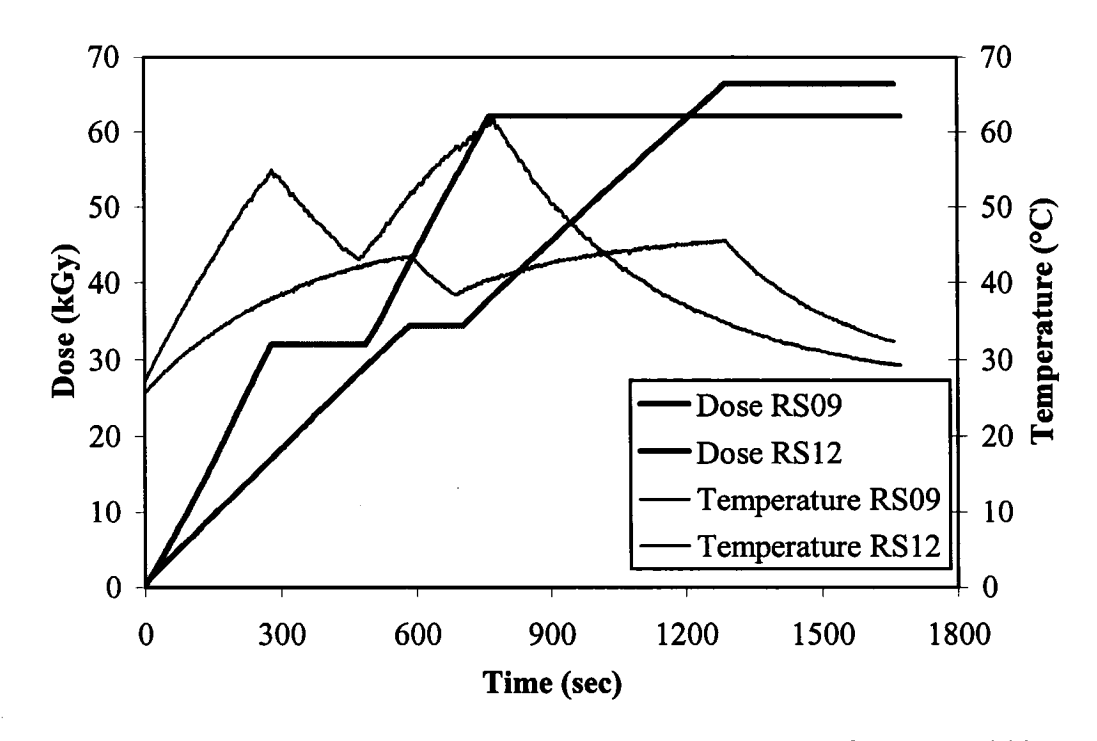


Figure 19 Calculated EB dose and measured temperature for tests RS09 and RS12. Note that RS12 was exposed for a total dose of 96 kGy; the third EB irradiation is not shown.

Figure 20 shows a typical response for the warpage and temperature measured during a test. The result shown is for specimen RS12, which received three successive EB doses

(Table 1). When the beam was activated for the first time, the temperature increased rapidly and a "negative" warpage was observed. The warpage reached a minimum (-0.07 mm) at 152 seconds before returning to zero after 300 seconds. This behaviour was attributed to the load transfer capability of the crystallized resin at the beginning of the test. This resin system is known to crystallize when stored for a prolonged period at room temperature. It is believed that the resin at the interface between the aluminium substrate and the steel patch was initially crystallized. Consequently, it was rigid enough to transfer load and allow the specimen to warp as the temperature changed. As the resin temperature increased, the resin de-crystallized and became fluid. Then, the aluminium substrate and steel patch could slide between each other and the warpage diminished.

After about 320 seconds, the specimen started to warp in the negative direction. At this point, the resin has gelled and its elastic modulus was high enough to transfer load between the substrate and the patch. The warpage reached a minimum (-0.027 mm) when the specimen temperature reached a maximum (43 °C) at 600 seconds. At this point, the beam was deactivated and the temperature decreases rapidly, causing the warpage to change in the positive direction. This is an indication that the substrate and the patch acted as a bimetallic strip bonded by the cured resin. Subsequent EB exposures produced the same warpage behaviour associated with the temperature changes in the specimen. Finally, at the end of the test, the specimen was found to be warped indicating the presence of residual stresses induced during cure.

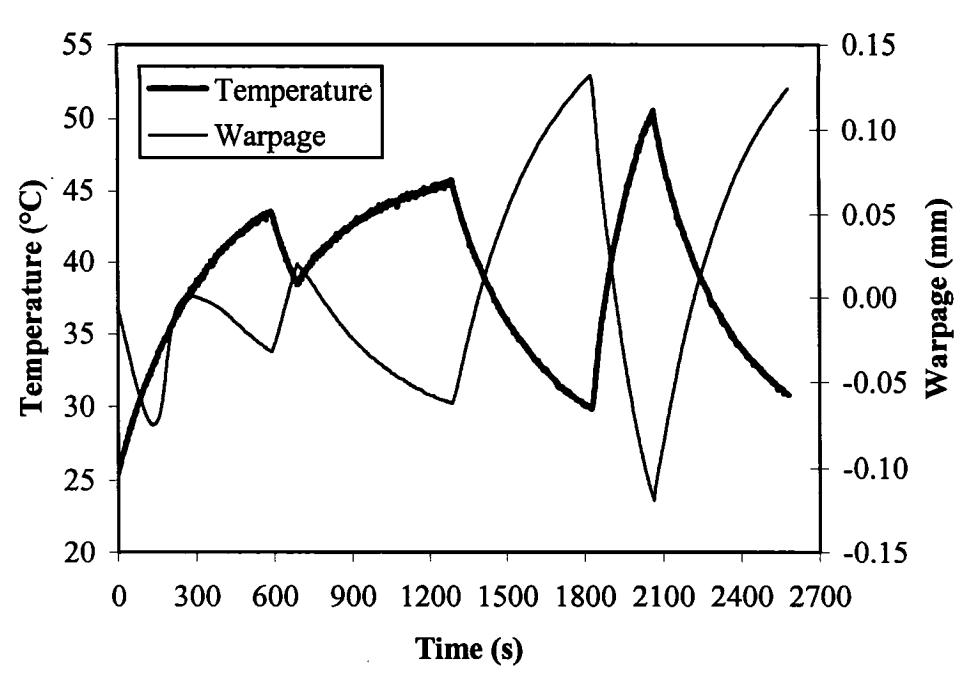


Figure 20: Measured warpage and temperature during EB curing for test RS12.

Figure 21 shows the variation of warpage with specimen temperature. The results for all specimen tested are superposed on the graph. The initial warpage observed before the resin de-crystallized was observed for all specimens. The intersection of the measured warpage-temperature curve with the horizontal axis corresponds to the stress-free temperature, T_{SF} , for a given curing condition. Subsequent reheating and cooling of the sample followed a straight line, as expected from the behaviour of a bimetallic strip. From this graph, the stress-free temperatures for each test were determined and are summarized in Table 5. From Table 5, RS09 and RS10 had similar results at respectively 44 °C and 43 °C. Specimen RS12 had the lowered T_{SF} at 37 °C while RS11 had the highest at 54 °C.

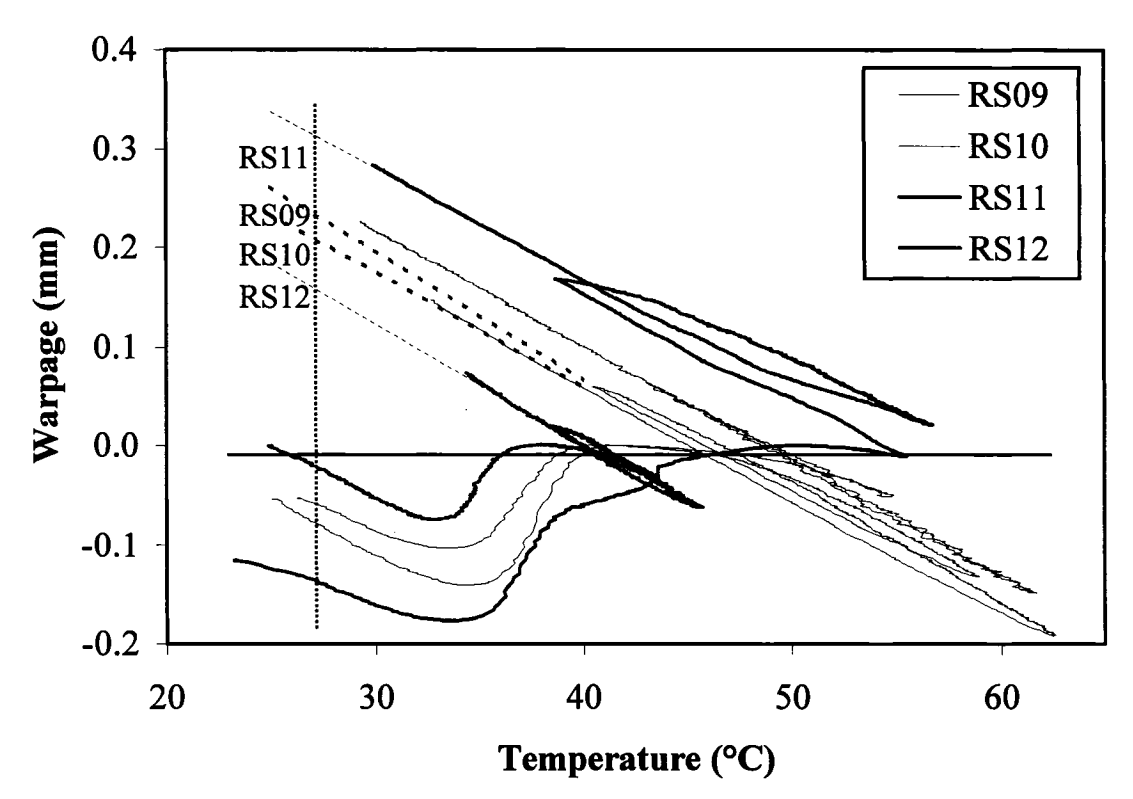


Figure 21 Measured warpage during EB curing as function of specimen temperature for all tests.

Table 5 Measured stress free temperature (T_{SF}) and warpage after EB cure

Specimen	T _{SF} (°C)	Warpage (mm)
RS09	44	0.26
RS10	43	0.23
RS11	54	0.34
RS12	37	0.18

Table 5 also shows the final warpage measured after the EB cure for all the specimens. The warpage was measured from the extrapolation of the warpage temperature response shown in Figure 21. The dotted line on the graph represents the extrapolated linear curve fit used to determine the final specimen warpage at room temperature. The specimen warpage was consistent with the T_{SF} measured. Again, RS09 and RS10 had similar warpage while RS12 had the lowest warpage and RS11 the highest warpage. It is interesting to notice, from Table 5, that RS12 specimen, despite having one the highest DOC (0.8) (Table 4) also has the lowest stress free temperature (T_{SF} = 34°C). This result tends to suggest that the stress free temperature (T_{SF}) is mainly influenced by the initial radiation phase as for the DOC is mainly influenced by the maximum dose rate seen by the resin. From these results, we can conclude that RS12 has the lowest level of residual stresses.

3.1.2 Thermal post-cure effects

The results from the 160 °C thermal post-cure are presented in Figure 22 and summarized During the post-cure cycle, all specimens showed a linear Table 6. warpage/temperature relationship. However, as seen in Table 6, the final warpage measured after the post-cure decreased slightly. More importantly, compared to the results presented in (Table 5) the measured change in T_{SF} during post-cure was very small (less than 7 °C). This result confirms that the thermal post-cure cycle did not induced additional residual stresses in the specimens. This is an important finding since a postcure cycle is often required to fully cure the resin after EB irradiation in order to increase mechanical properties. Here, the resin degree of cure after post-cure, measured from DSC, showed that the samples were fully cured ($\alpha = 1.0$). Therefore, it was demonstrated that it is possible to achieve a fully cured resin with a thermal post-cure without affecting the low residual stresses level locked-in at a low cure temperature during the EB irradiation. Again, in-situ measurements of the specimen warpage and temperature both during EB irradiation and thermal post-cure allowed to precisely determine the onset of residual stresses development and stress-free temperature.

Table 6: Measured stress free temperature (T_{SF}) and warpage after thermal post-cure

Specimen	T _{SF} (°C)	Warpage (mm)	
RS09	48	0.13	
RS10	50	0.18	
RS11	48	0.13	
RS12	38	0.15	

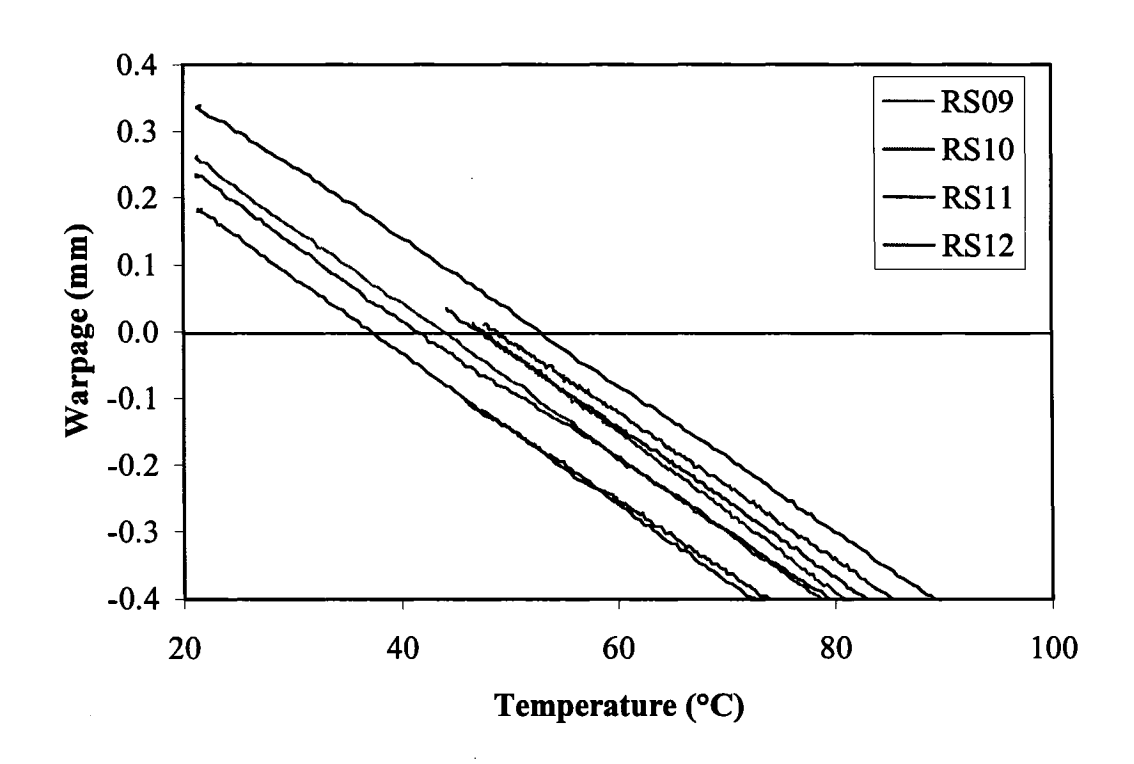


Figure 22: Measured warpage during post-cure. Note that data above 90°C is not shown on figure.

3.1.3 Composite specimens

Table 7 shows that the average measured dose rate (dosimetry) was on average 25% lower than the calculated dose rate. The same trend was observed for the total dose. This phenomenon might be caused by a spike in the beam during the first stages of the irradiation process. As shown in Figure 23, the calculated dose rate was higher in the first 180 seconds of the irradiation and then stabilized. This initial spike in the calculated dose rate might be an artefact coming from the temperature measurements or a real behaviour of the EB gun used (Section 3.1.1). This discrepancy between the measured and calculated dose rate will be addressed in further improvements to the experimental technique, but does not alter the trends observed in this study as this problem occurred in all tests (see Appendix A for results). Table 7 also shows the resin degree of cure (DOC) measured from resin coupons collected from the specimen after EB cure.

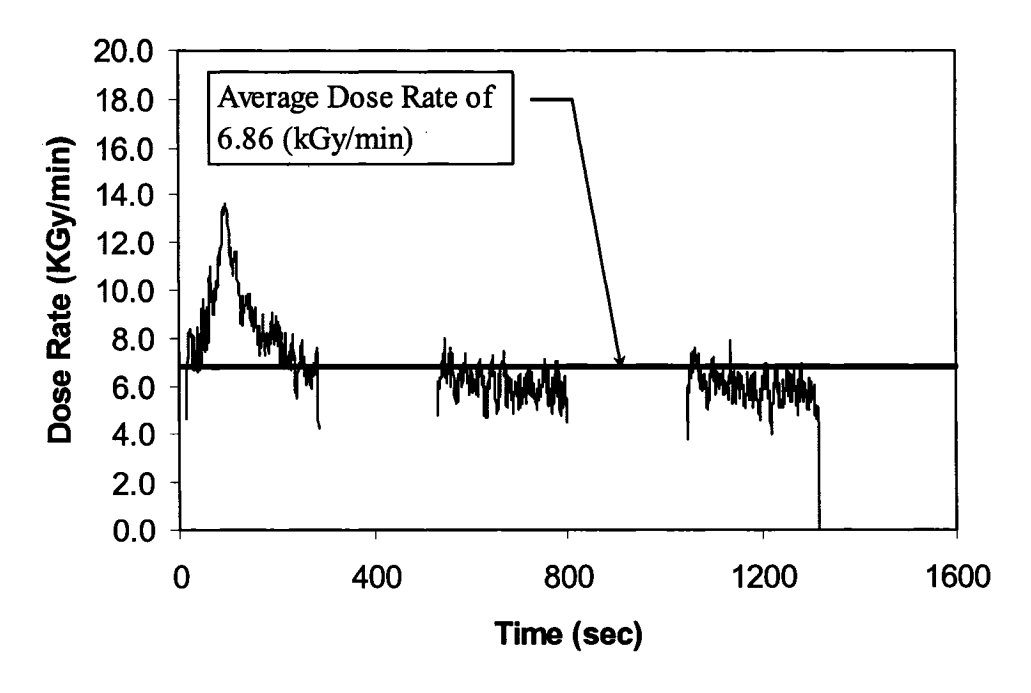


Figure 23: Calculated dose rate vs time for RS13. The measured average dose rate was 6.86 kGy/min.

The degree of cure was calculated from the residual heat measured from thermal curing in a differential scanning calorimeter (DSC), using a dynamic scan rate of 5 °C/min. The area of the exothermic heat flow measured was divided with the total heat of reaction obtained from uncured resin: 578 J/g and 429 J/g for Tactix 123 and CAT-B respectively.

Table 7 Comparison between dose rate, total dose measured from dosimeter and calculated (Equation 8); degree of cure measured by DSC after EB exposure.

Specimen	Dose Rate (kGy/min)		Total Dose (kGy)		Degree of
_	Measured	Calculated	Measured	Calculated	cure
RS13	6.9	8.0	93	110	0.72
RS14	6.5	8.0	89	110	0.75
RS15	6.9	8.3	93	110	0.73
RS16	13.6	17.0	89	110	0.82
RS17	13.0	17.0	83	110	0.87
RS18	13.0	17.0	84	110	0.82
RS19	2.8	3.8	27	37	0.53
RS20	2.8	3.8	27	37	0.47
RS21	19.1	25.0	86	110	0.87
RS22	18.4	25.0	80	110	0.90
RS23	13.6	17.0	88	110	0.87
RS24	13.6	17.0	88	110	0.90
RS25	2.9	3.8	19	25	0.65
RS26	2.9	3.8	12	15	0.59
RS27	7.6	8.0	34	37	0.83
RS28	7.6	8.0	19	20	0.79

The DSC results for all of the specimens show that the degree of cure of the resin increased with the dose rate (Figure 24). This result was also true for the metallic specimens. This result confirms that the dose rate has an important effect on the final DOC.

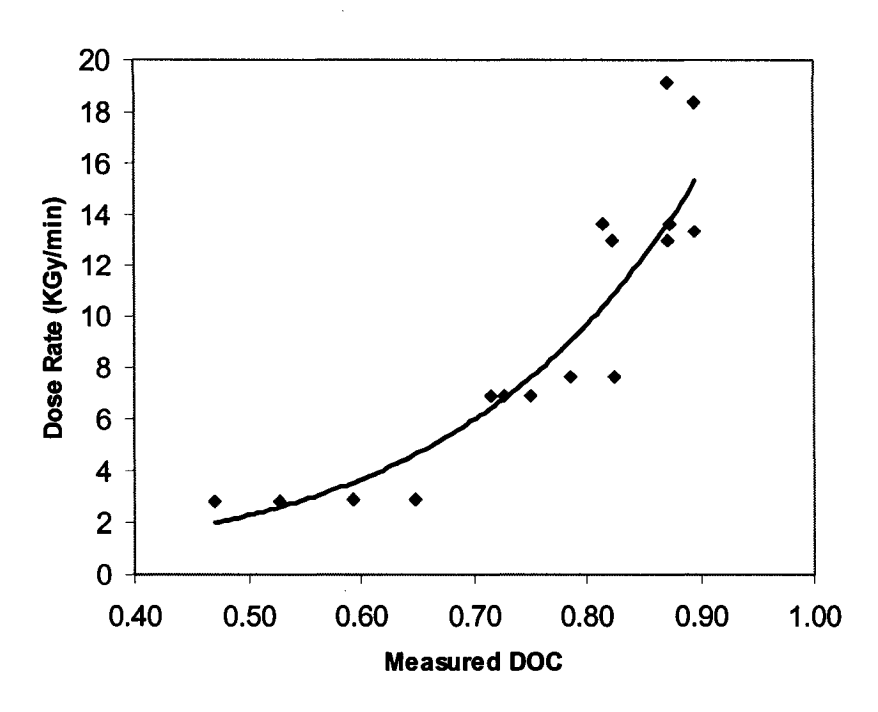


Figure 24: Dose rate vs measured DOC for Tactix 123 and CAT B specimens

Figure 25 shows the variation of specimen temperature and dose during and between doses for three different specimens (RS13, RS21 and RS25). The specimen temperature increased during irradiation and decreased when the beam was turned off. Figure 25 illustrates the significant effect of dose rate on the specimen temperature profile. During their first EB exposures, specimen RS13 received 39 kGy at 6.9 kGy/min compared to 49 kGy at 21.4 kGy/min for specimen RS21. This dose rate difference resulted in a maximum temperature of 54 °C at 287 seconds for RS13 compared to 76 °C at 530 seconds for RS21. Furthermore, from Figure 25, RS25 had received 1.14 kGy at 4.3 kGy/min and reached a maximum temperature of 33 °C. These results confirm that an increase in the dose rate increases the maximum temperature of the specimen.

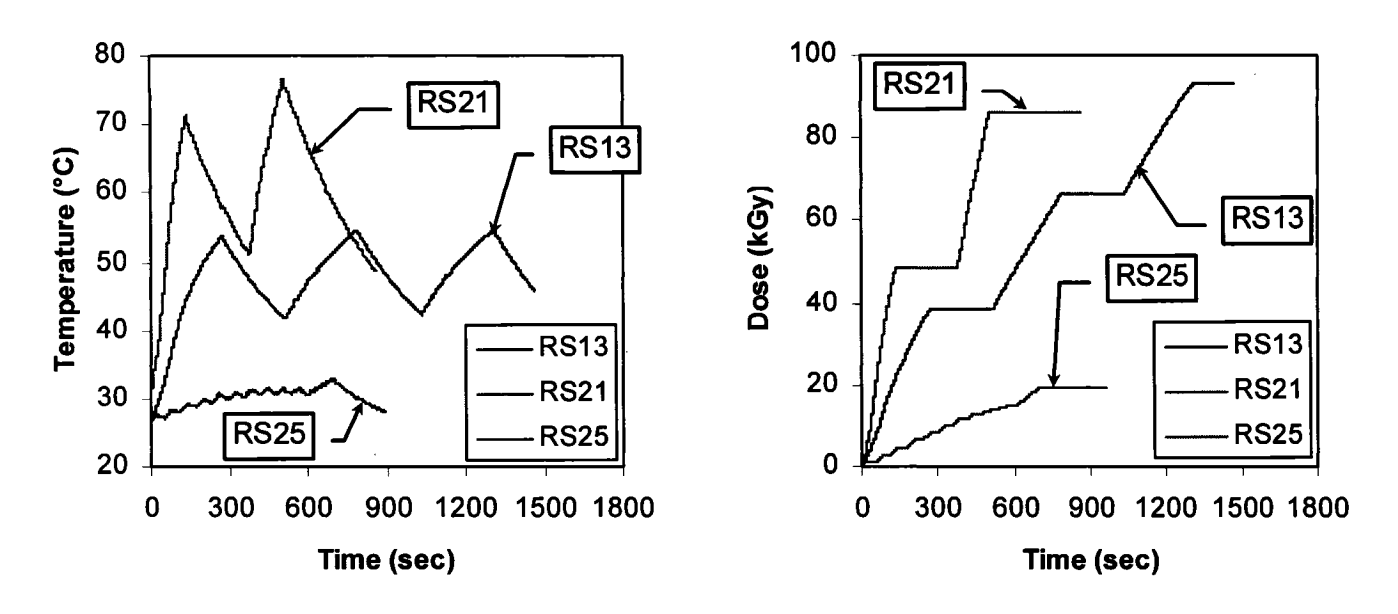


Figure 25: a) Calculated EB dose and b) Measured temperature for specimens RS13, RS21 and RS25.

Measured temperatures for RS14, RS15, RS27 and RS28 were similar to RS13. Measured temperatures for RS16, RS18, and RS23 were similar to RS21. Finally, measured temperatures for RS19, RS20 and RS26 were similar to RS25.

Figure 26 shows the effect of the heat transfer coefficient on the maximum temperature and the stress free temperature (T_{SF}). A fan was used to increase the heat transfer coefficient for specimens RS17, RS22 and RS24. The results presented in Figure 26 and 27 show that both the maximum and the stress free temperatures decreased with the increase of the heat transfer coefficient. The maximum temperature was decreased by 20% and the stress free temperature by 2-11%. It is clear that the convection coefficient has a definite influence on the temperature profile evolution during cure and thus on the stress free temperature.

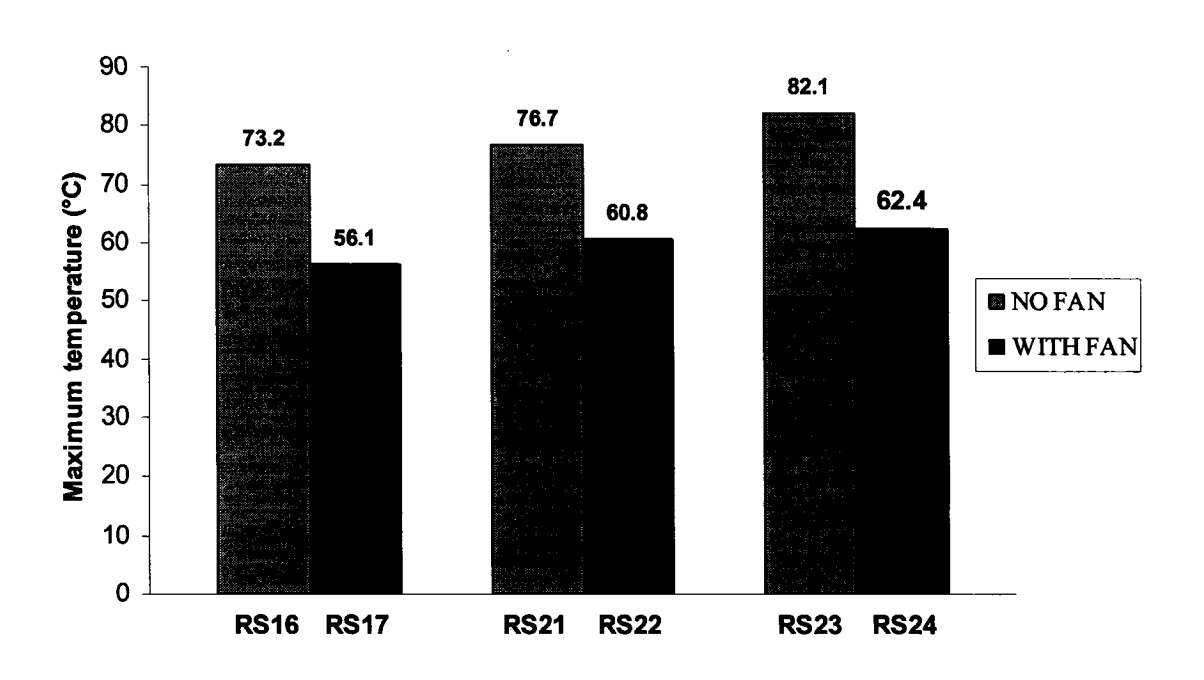


Figure 26: Maximum temperature comparison between fan and no fan test setup

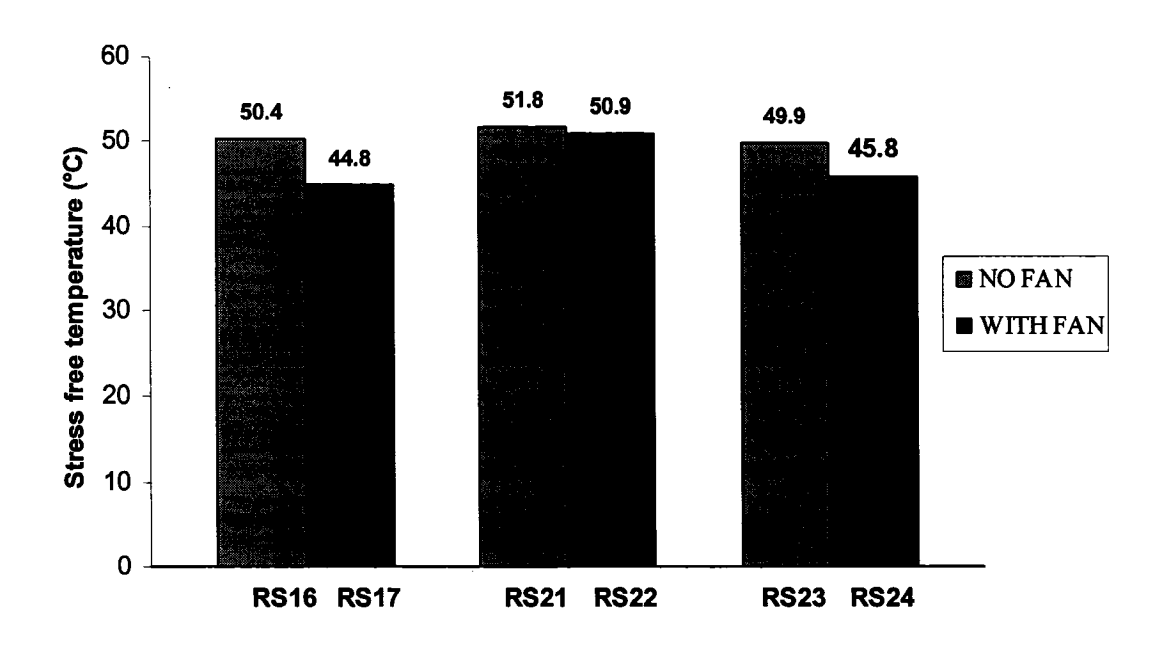


Figure 27: Stress free temperature comparison between with fan and no fan test setup

Figure 28 shows a typical response for the warpage and temperature measured during the first irradiation cycle. Figure 28a) shows the result obtained with the metallic specimens. When the beam was turned on, the temperature increased rapidly and a negative warpage was observed (1a). The warpage reached a minimum (-0.07 mm) at 152 seconds before returning to zero after 300 seconds. This behaviour was attributed to the finite load transfer capability of the initially crystallized resin (Tactix 123). This resin system was known to crystallize when stored at room temperature, which made it rigid enough to transfer load and allowed the specimen to warp as the temperature changed. As the resin temperature increased, the resin de-crystallized and became fluid, allowing the aluminium substrate and steel patch to move relative to each other and causing the warpage to go back to zero (2a). After about 300 seconds, the specimen started to warp again in the negative direction (3a). At this point, the resin has gelled and its modulus was high enough to transfer load between the substrate and the patch (4a). The warpage reached a minimum (-0.045 mm) when the specimen temperature reached a maximum (43°C) at 600 seconds. At this point, the beam was deactivated and the temperature decreased, causing the warpage to change in the positive direction (5a).

To address the crystallization problem, the composite specimens were heated in an oven at 40°C just before the test in order to de-crystallize the resin. Then the specimens were cooled to room temperature before test. As shown in Figure 28b), the initial warpage minimum observed for the metallic specimen (Figure 28a) was not present 1b.

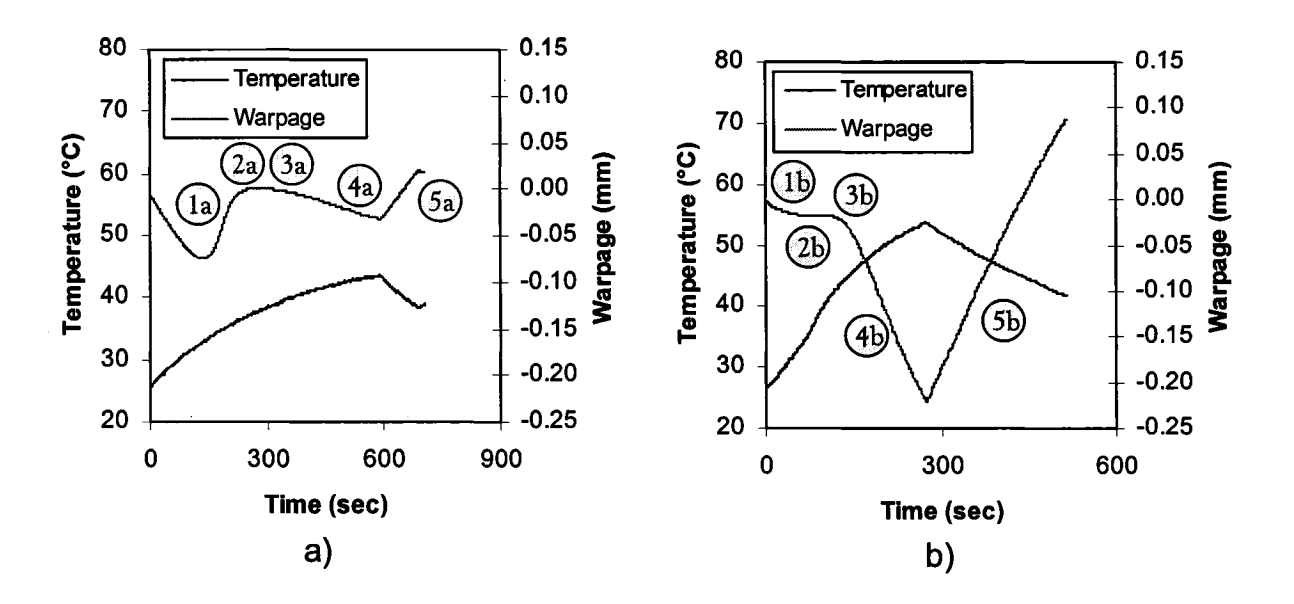


Figure 28: Measured warpage and temperature for a 25 s⁻¹ irradiation for a) metallic specimen (RS12), b) composite specimen (RS13).

Only a very slight negative warpage, attributed to the friction between the fibreglass scrim cloth and the top and bottom laminates was observed. This initial warpage eventually stabilized after 45 seconds (2b). After about 125 seconds, the specimen started to warp again in the negative direction (3b). At this point, the resin has gelled and its modulus was high enough to transfer load between the substrate and the patch (4b). The warpage reached a minimum (-0.221 mm) when the specimen temperature reached a maximum (53.7°C) at 288 seconds. At this point, the beam was deactivated and the temperature decreased rapidly, causing the warpage to change in the positive direction (5b). This is an indication that the substrate and the patch were effectively bonded by the cured resin. Subsequent EB exposures produced the same warpage behaviour associated with the temperature changes in the specimen. At the end

of the test, the specimen was found to be warped, indicating the presence of residual stresses induced during cure. This result confirmed that the composite specimen worked adequately and that the initial warpage caused by the crystallized Tactix 123 resin was eliminated by preheating the specimen before the test. Figure 28 also shows that the composite specimen solved the resolution of the testing method as the magnitude of the warpage for similar irradiation conditions was increased by of factor of five compared to the metallic specimen.

Figure 29 and Figure 30 show the variation of warpage with specimen temperature. The results for Tactix 123 and CAT B specimens are presented in Figure 29 and 30 respectively. The initial small warpage attributed to friction was observed in all cases. Figure 30 illustrates how the stress free temperature was derived from a warpage vs temperature diagram. The intersection of the measured warpage-temperature curve with the horizontal axis corresponds to the stress-free temperature, $T_{\rm SF}$, for a given curing condition. Subsequent reheating and cooling of the sample followed a straight line, as expected for a bonded unsymmetric laminate. The stress-free temperatures for each test were determined from the warpage-temperature graph and are summarized in Table 8. In general, $T_{\rm SF}$ increased with the dose rate. The lowest stress free temperatures were obtained for specimens RS19, RS20, RS25 and RS26 with an irradiation cycle consisting of successive short irradiation periods of 30 seconds each.

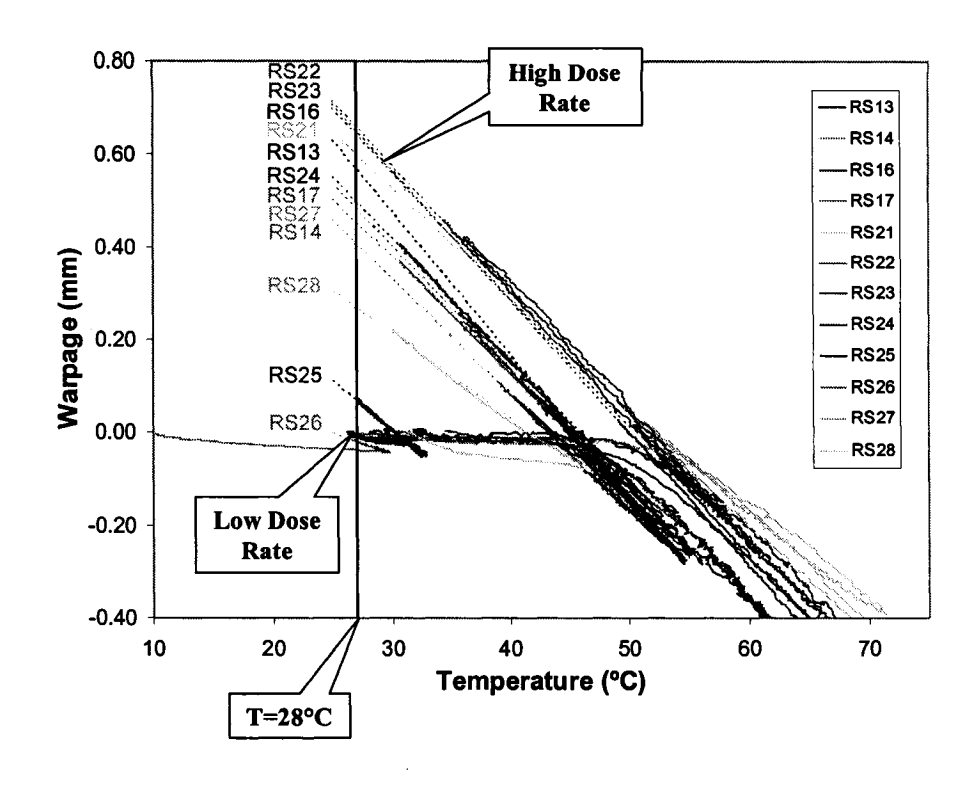


Figure 29: Measured warpage during EB curing as function of specimen temperature for Tactix 123 specimens.

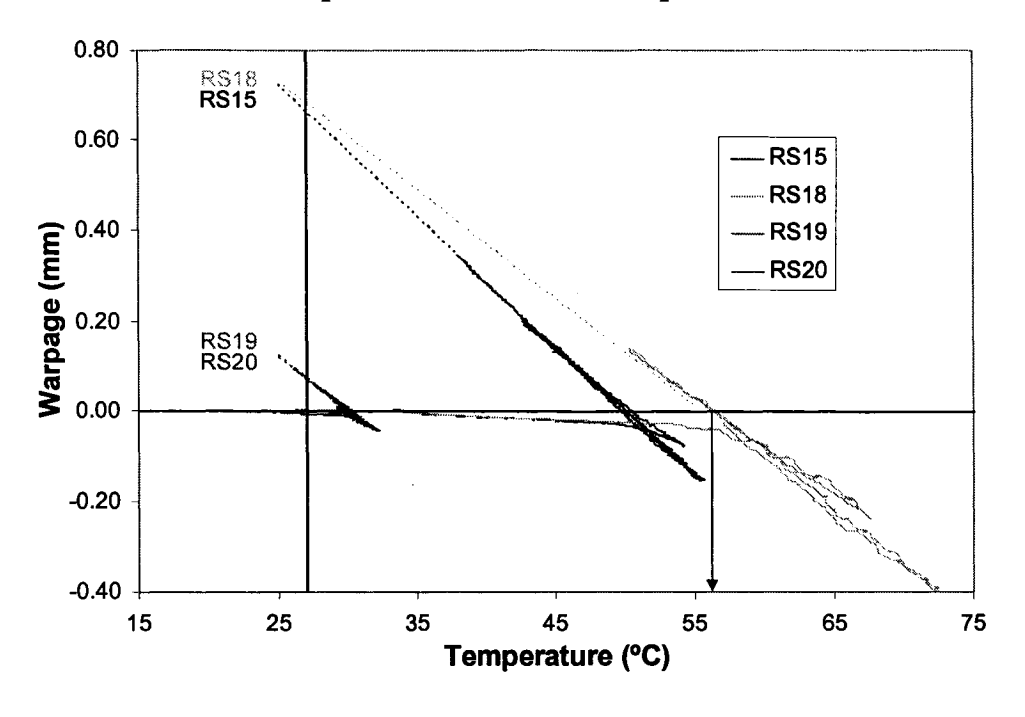


Figure 30: Measured warpage during EB curing as function of specimen temperature for CAT B specimens.

Table 8 also shows the final warpage after the EB cure for each specimen. The shown values were determined from extrapolation of the warpage-temperature response shown in Figure 29 and 30. The dotted line on the graph represents the extrapolated linear curve fit used to determine the final specimen warpage at room temperature. The specimen warpage was consistent with the $T_{\rm SF}$ measured and was generally proportional to the dose rate, with the lowest warpage observed for specimens RS19, RS20, RS25 and RS26. A linear relationship between the stress free temperature and the warpage was observed, as shown in Figure 31.

Table 8: Measured stress free temperature (T_{SF}) and warpage after EB cure.

	Tactix 123			CAT-B	
Specimen	T _{SF} (°C)	Warpage (mm)	Specimen	T _{SF} (°C)	Warpage (mm)
RS13	45	0.63	DC15	50	0.72
RS14	43	0.46	RS15	50	0.72
RS16	50	0.70	RS18	55	0.73
RS17	45	0.54	K516	33	0.73
RS21	52	0.65		-	
RS22	51	0.71			
RS23	50	0.71			
RS24	50	0.71			
RS25	30	0.11	RS19	30	0.12
RS26	25	0.00	RS20	30	0.12
RS27	45	0.50			
RS28	42	0.30			Ì

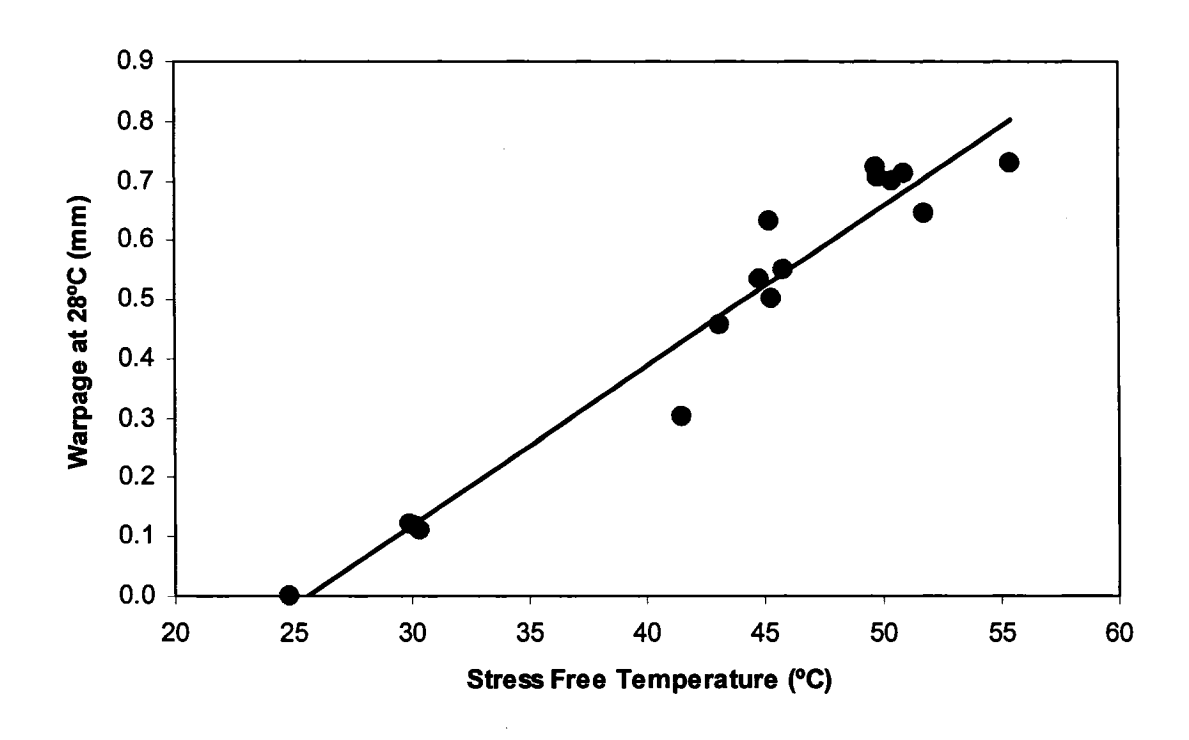


Figure 31: Specimen warpage at 28°C vs stress free temperature (T_{SF})

3.2 THERMAL CURED SPECIMENS

Stress-free temperatures of 161 °C and 177 °C were obtained for the specimens cured thermally at 160 °C and 205 °C respectively. The RS12 EB cured and thermally post-cured stress free temperature was 38°C. The stress-free temperature obtained from the EB cure process was only minimally increased by the thermal post-cure cycle. Figure 32 clearly illustrates the difference in stress free temperature (123°C) between the EB cured/thermal post-cured and thermal cured processes. In comparison, the 160 °C curing of the specimen with the same resin, only thermally cured, induced much higher level of residual stresses as observed by a higher T_{SF} and final warpage. These results confirm that EB cured and thermally post-cured specimens have considerably less residual stresses than the thermally cured specimen.

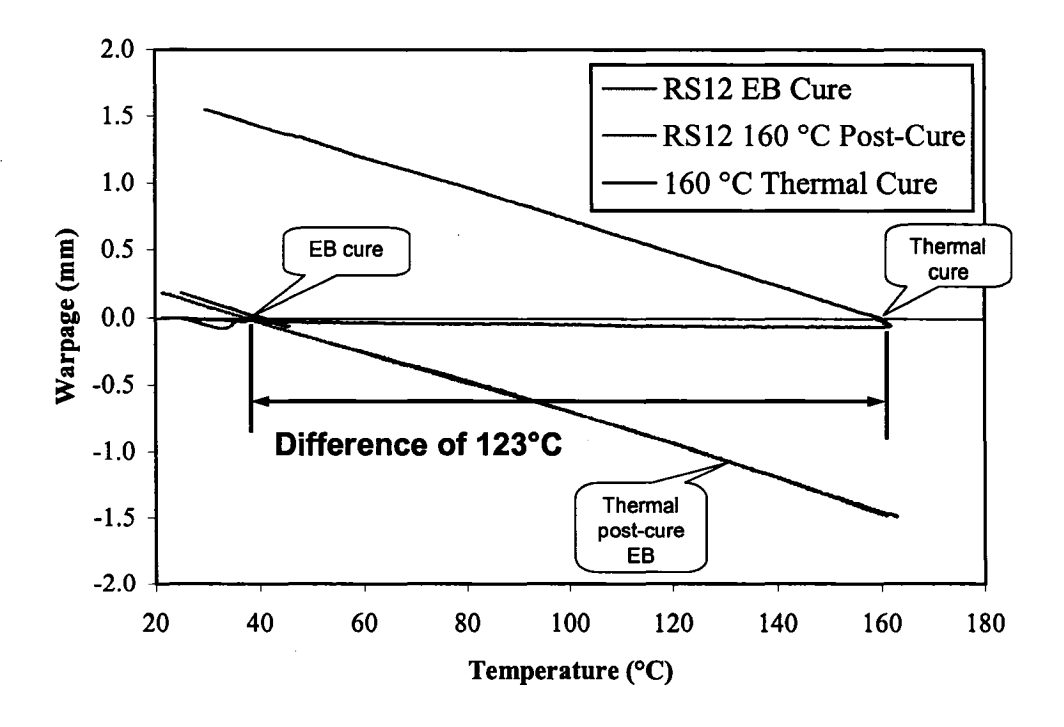


Figure 32: Comparison of RS12 EB cure and post-cure response with a specimen cured thermally at 160°C

4 MODELING AND DISCUSSION

In order to understand the relationship between the development of residual stresses and the stress free temperature obtained for a particular EB cycle, a cure kinetics model was used to predict the resin degree of cure. This was done for Tactix 123 experiments only since no cure kinetics model has been developed. The degree of cure (α) is a measure of the degree of completion of the cure reaction and is generally defined as the ratio of the cumulative heat evolved during a reaction to the total heat of reaction, i.e.:

$$\alpha = \frac{1}{\Delta H_R} \int_0^t \left(\frac{dq}{dt} \right) dt \tag{9}$$

where dq/dt is the specific heat generation rate and ΔH_R is the total heat of reaction of the resin. In the present work the rate of cure, $d\alpha/dt$, is determined based on a radiation cure model described in Mascioni et al. [8] for a DGEBA (diglycidyl ether of bisphenol A) epoxy system, cured using CD1012. The model presented in [8] was modified by Johnston et al. [9] where the term for epoxide monomer concentration, M, was replaced with degree of cure, using the relation:

$$\alpha = 1 - \frac{M}{M_{\odot}} \tag{10}$$

where M_0 is the "initial" epoxide monomer concentration (mol/L). This leads to the following relation for $d\alpha/dt$:

$$\frac{d\alpha}{dt} = k_p \cdot (1 - \alpha) \cdot I \tag{11}$$

where I is the concentration of active centers and k_p is the reaction rate constant. Details in the model description are presented in [9]. Constants for the Tactix 123 and the CD1012 photoinitiator determined in [9] were used to compute the resin cure rate corresponding to the dose rate and temperature measured during irradiation.

Equation 11 was integrated with time to obtain the trends of degree of cure development for all specimens, as presented in Figure 34. In general, the final degree of cure was proportional to the dose rate. The model shows that the specimens cured very fast during the first EB irradiation step.

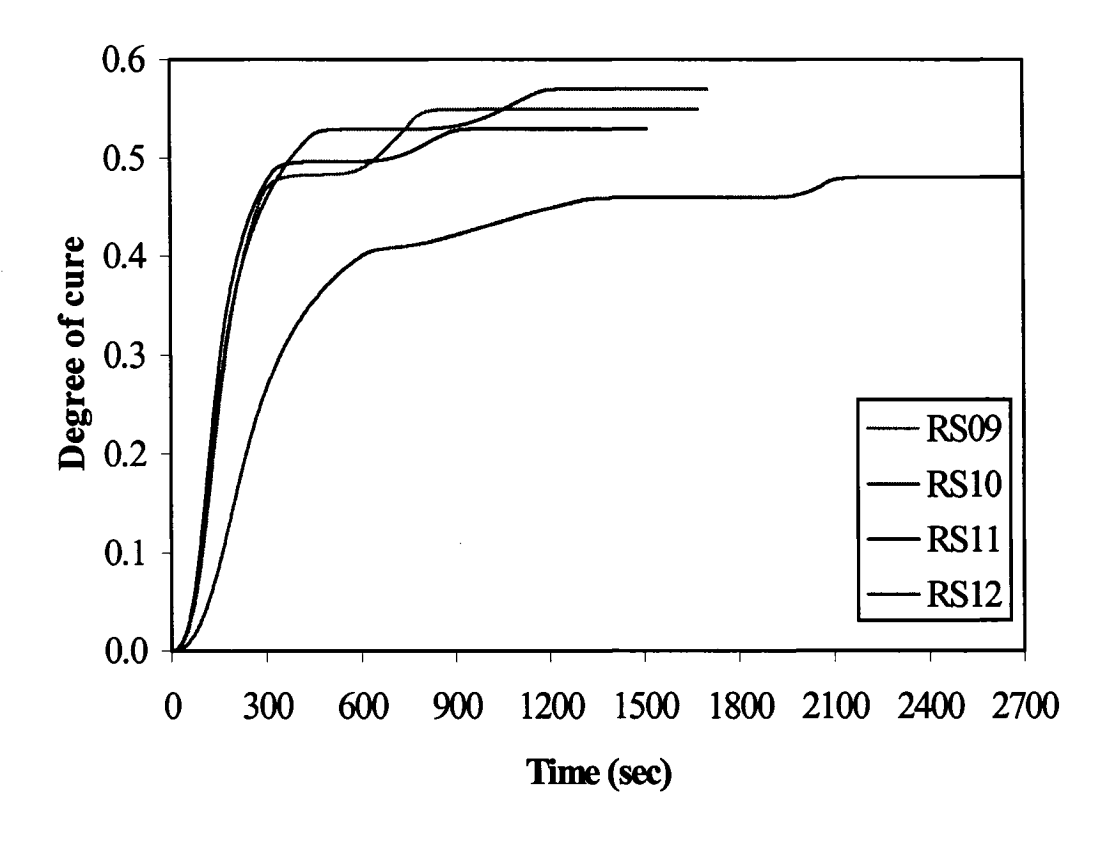


Figure 33: Predicted DOC for Tactix 123 metallic specimens

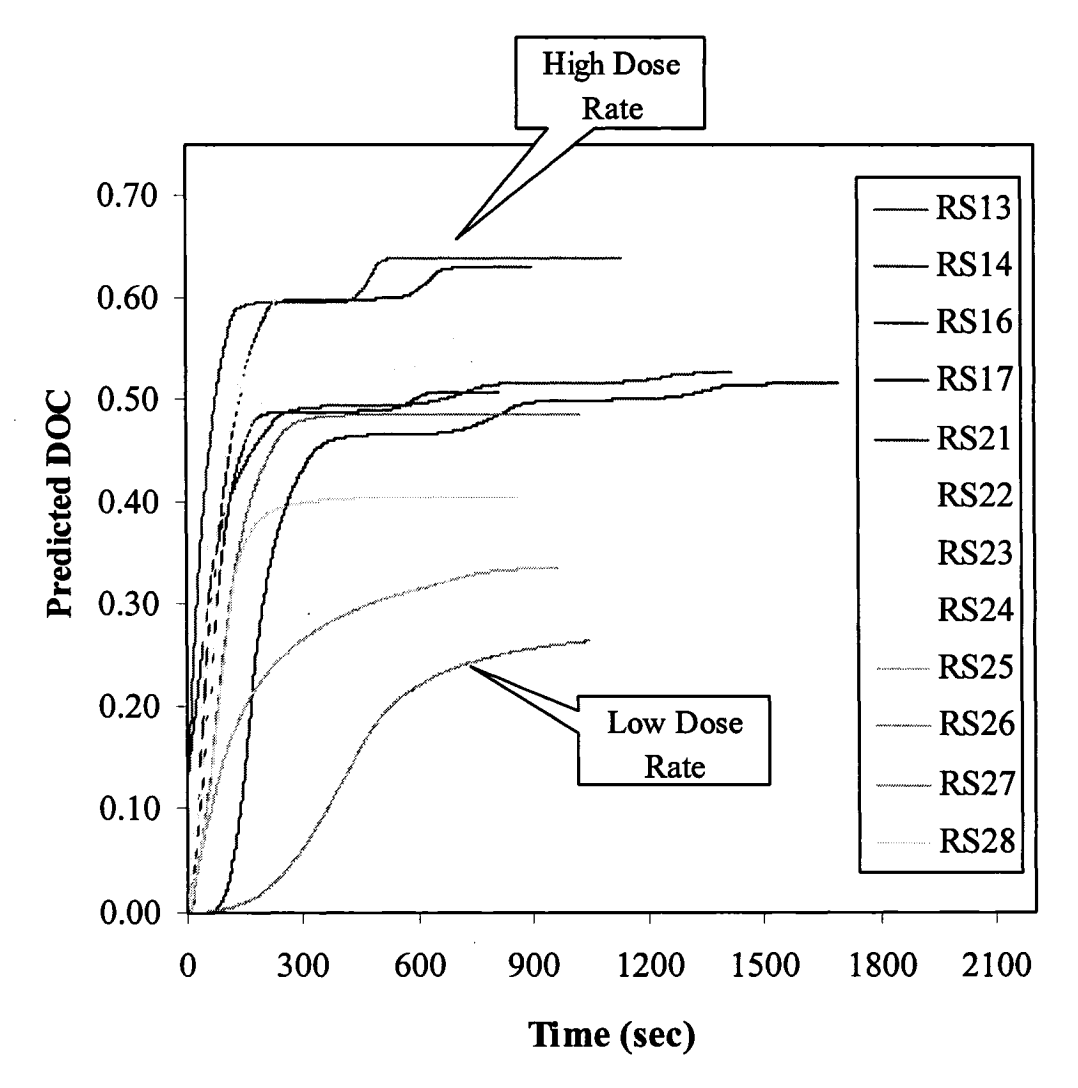


Figure 34: Predicted DOC vs time for Tactix 123 composite specimens

Figure 35 compares the final degree of cure predicted by the model to the degree of cure measured by DSC (Table 7). The measured degree of cure was always higher than the predicted degree of cure. But the trends observed from the cure kinetics model results were consistent with the measured final degree of cure. More work is necessary to improve the accuracy of the model.

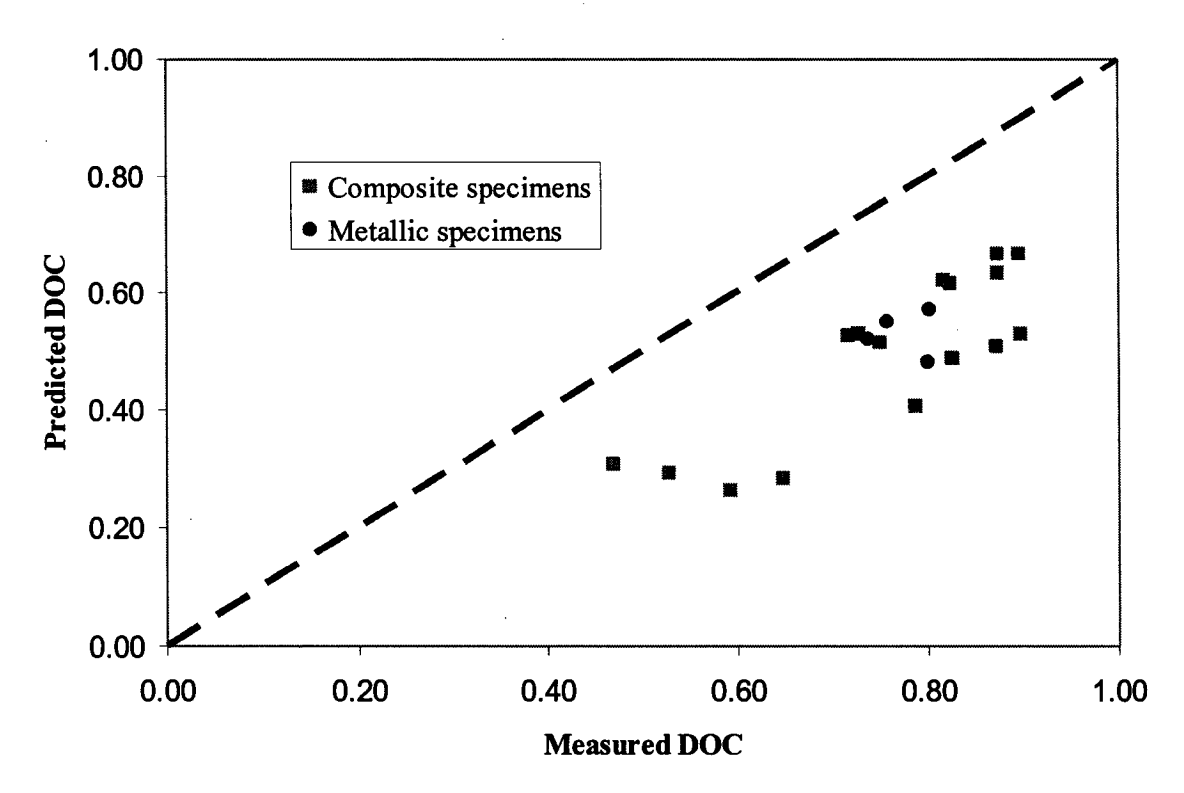


Figure 35: Predicted DOC vs Measured DOC for Tactix 123 specimens

From Figure 36, the stress free temperature (T_{SF}) is proportional to the measured degree of cure (DOC). This shows once again that as energy level (dose rate) increases the degree of cure (DOC) of the resin increases and thus the stress free temperature (T_{SF}) .

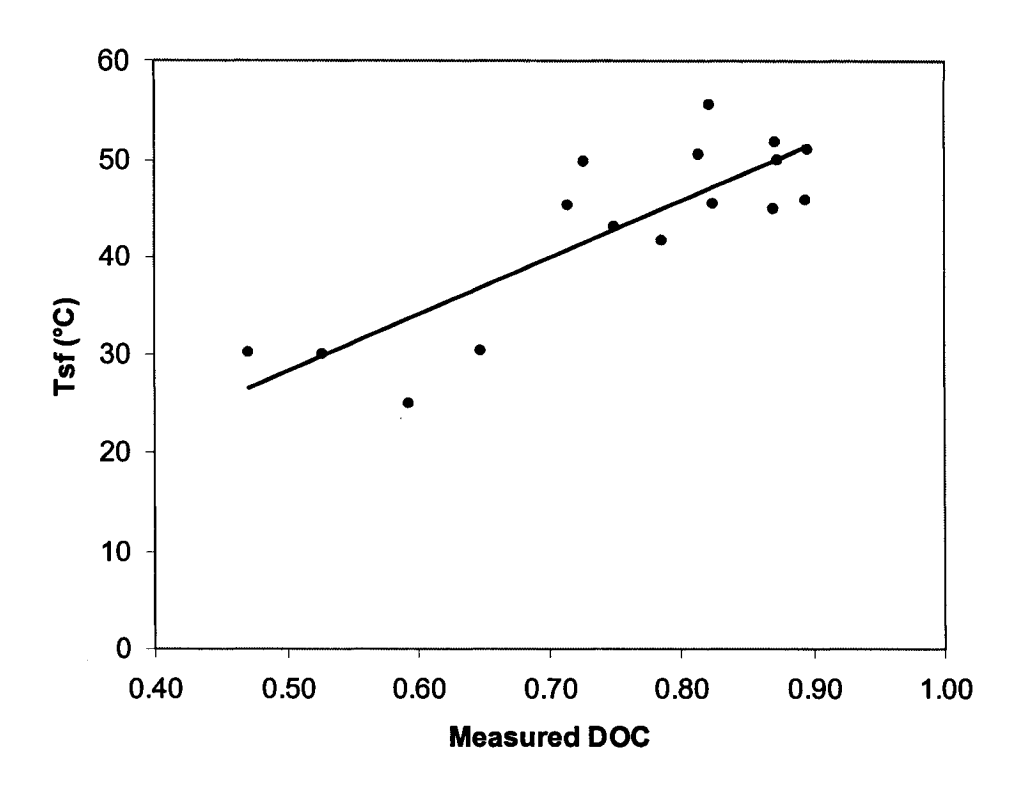


Figure 36: Stress free temperature (T_{SF}) vs measured DOC for Tactix 123 and CAT B specimens

Figure 37 and 38 compare the results obtained between the Tactix 123 and the CAT B resin. From Figure 37, it can be seen that the stress free temperature is 5°C higher for CAT B except for the 25 sec⁻¹ (30 sec cycles) irradiation cycle where the difference is smaller (2°C). From Figure 38, the onset of warpage occurred at a dose of 20 kGy for Tactix 123 compared to 30 kGy for the CAT B resin. As both resins followed a similar temperature profile, the CAT B specimen warped at a later stage which resulted in a higher warpage temperature. Furthermore, when comparing the stress free temperatures of the two specimens, the CAT B specimen proved to develop more residual stresses during the curing phase.

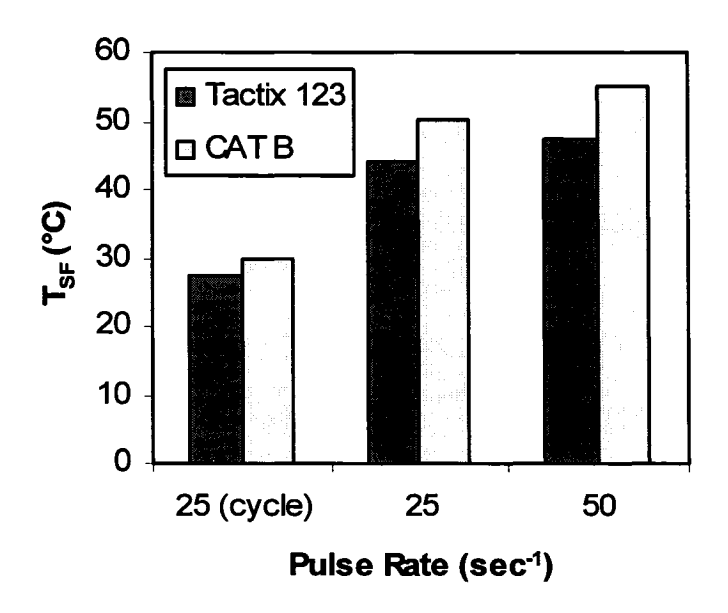


Figure 37: Comparison of stress free temperature for Tactix 123 and CAT B.

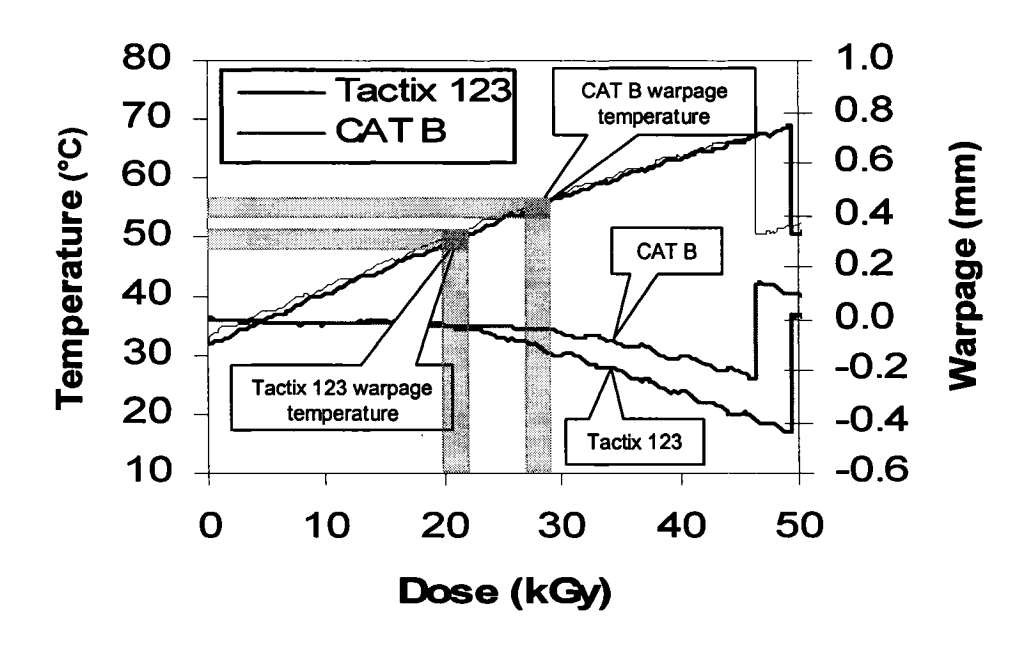


Figure 38: Measured warpage and temperature during EB cure as a function of predicted resin degree of cure for Tactix 123 and CAT B for a 50 (s⁻¹) irradiation.

Figure 39 and 40, show the relationship between the specimen temperature and warpage with the predicted resin degree of cure during the first radiation dose for specimens RS13 and RS23. It is shown that the specimens do not warp during the first stages of the curing process (0 < α < 0.25). Figure 39 and 40, show that RS13 specimen warps at α =0.36 and RS23 specimen warps at α =0.30. The warpage temperatures are T_{warp} = 45 °C and T_{warp} = 49 °C for RS13 and RS23 respectively. Table 9 shows the comparison between the specimen's warpage and stress free temperatures and a comparison between the DOC at warpage and at gelation point.

Table 9: Comparison between warpage vs stress free temperature and warpage vs gelation degree of cure.

Specimen	Temperature (°C)		Degree of cure (DOC)	
	Warpage	Stress Free (T _{SF})	Warpage	Gelation *
RS13	45	45	0.36	0.32.
RS23	49	50	0.31	0.32

^{*:} Gelation DOC measured using parallel plate rheology.

As seen from the table above, the warpage temperature for RS13 ($T_{warp} = 45^{\circ}C$) and RS23 ($T_{warp} = 49^{\circ}C$) were similar to their stress free temperatures ($T_{SFRS13} = 45^{\circ}C$ and $T_{SFRS23} = 50^{\circ}C$) respectively. The same phenomenon was observed for all the other specimens (see Appendix B for results). These results tend to suggest that the specimen's temperature at warpage is directly related to its final stress-free temperature and therefore to the level of residual stresses developed during the curing process. Furthermore, when compared to the gelation DOC measured with the parallel plate rheology, the warpage DOC was found to be a very good approximation

of the gelation point. This result confirms the load caring capacity of the resin when gelation occurs.

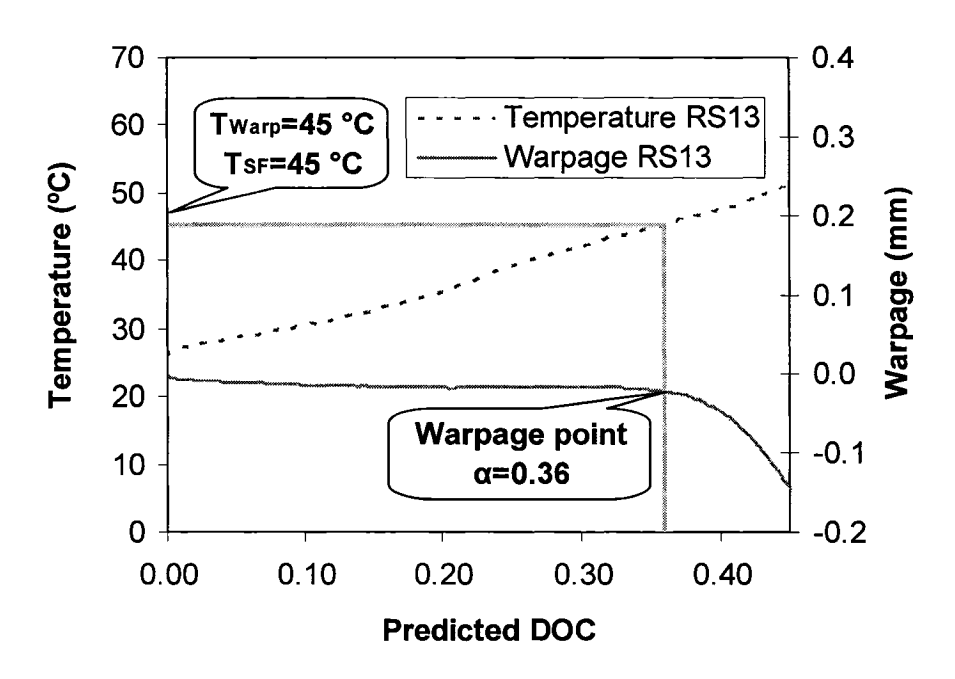


Figure 39: Temperature and warpage vs predicted DOC for RS13 specimen.

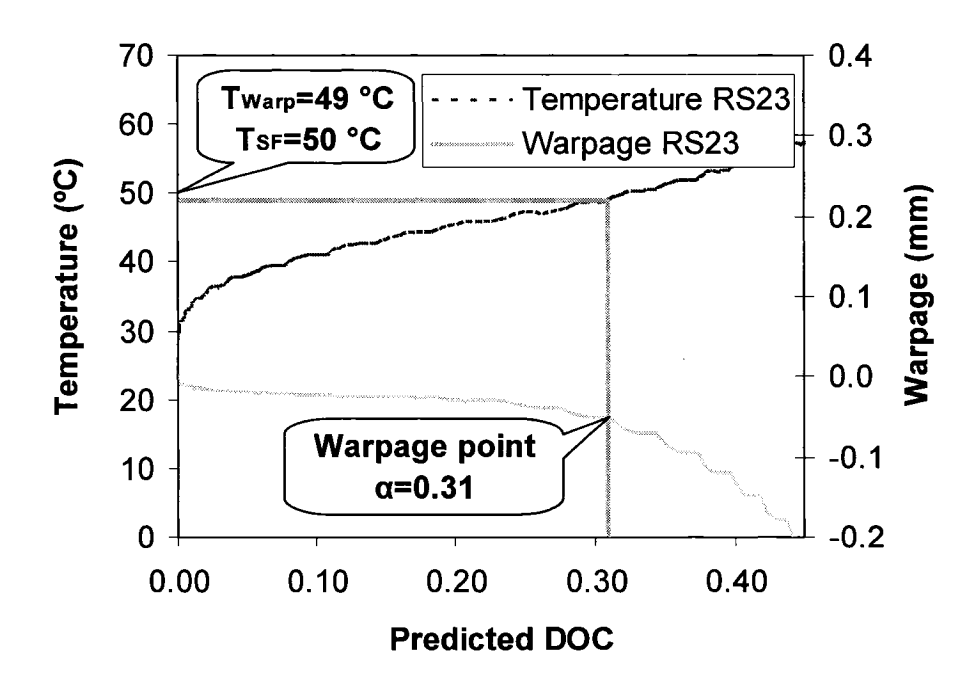


Figure 40: Temperature and warpage vs predicted DOC for RS23 specimen.

5 CONCLUSIONS

A special fixture was designed to measure the warpage of an asymmetrical specimen during the EB process. This fixture was used to monitor the warpage of specimens during and after irradiation at different constant dose rates. A wide variety of experiments using metallic and unbalanced composite specimens were conducted. The study shows that metallic and composite specimen results were relatively the same, thus confirming that the test setup was robust. The results confirmed that the instrumentation was not affected by the EB exposure and that it was possible to monitor the specimen warpage during the EB process. The following conclusions can be drawn from this study:

- The dose rate imposed on a specimen is the main contributor to the development of residual stress in an EB curing process.
- An increase of the heat transfer coefficient has a definite impact on the maximum
 and stress free temperatures of a specimen. The maximum temperature of the
 specimen was decreased by 20% and its stress free temperature was decreased by
 2-11% with the increase of the heat transfer coefficient.
- The specimen temperature at warpage is directly related to the final stress-free temperature and therefore to the level of residual stresses.
- The warpage DOC was found to be a very good approximation of the gelation DOC. This result confirms the load caring capacity of the resin when gelation occurs.

- The stress free temperature for CAT B was about 5°C higher compared to Tactix
 123.
- EB curing followed by a thermal post-cure induces considerably less residual stresses than a standard thermal cure. The stress free temperature of an EB cured and thermally post-cured specimen was 120°C lower than the stress free temperature of thermally cured specimen.

6 RECOMMENDATION FOR FUTURE WORK

The following recommendations can be made for future work on residual stresses development in electron beam cured composites:

- Post curing of all composite specimens in order to confirm the results found with metallic specimens.
- Refinement of the cure kinetic model in order to obtain a better correlation between degree of cure (DOC) predictions and DSC measurements.
- Study on residual stress development in E-Beam cured laminate composites. This
 study is the next step in order to better our understanding of residual stress
 development in EB cured structures.
- Development of the manufacturing process for E-beam cured structures.
- Mechanical qualification program to aerospace and space specifications.

REFERENCES

- [1] J. R. Freid, "Polymer science and technology", University of Cincinnati,
 Prentice Hall PTR, (1995).
- [2] A. Johnston, R. Vaziri, A. Poursartip, "A plane strain model for process induced deformation of laminated composite structures", Journal of Composite Materials, 35 (16), 1435 (2001).
- [3] J. Chen, A. Johnston, L. Petrescue, P. Richer, "Review of Electron Beam Curing of Composites", NRC-IAR Technical Report, (2003).
- [4] J. Choand, C.T. Sun, "Lowering thermal residual stresses in composite patch repairs in metallic aircraft structures", AIAA Journal, 39, 10, 2013-2018, (2001).
- [5] D. Djokic, "Reduction of residual stresses during bonded composite patch repair",

 Master Thesis, The University of New Brunswick Department of Mechanical

 Engineering, New Brunswick, Canada, (2002).
- [6] A.M. Albat, "Thermal residual stresses in bonded composite repair on cracked metal structures", Ph.D. Thesis, The University of British Columbia, Department of Mechanical Engineering, Vancouver, British Columbia, Canada, (1998).

- [7] D. Djokic, A. Johnston, A. Rogers, P. Lee-Sullivan, N. Mrad, "Residual stress development during the composite patch bonding process: Measurement and Modeling", Composites: Part A, 33, 277-288, (2002).
- [8] M. Mascioni, J. Sands, G.R. Palmese, "Real time in-situ spectroscopic characterization of radiation induced cationic polymerization of glycidyl esters".

 SAMPE International Symposium, 47, (2002).
- [9] A. Johnston, K.C. Cole, M. Hojjati, M. Mascioni, G.R. Palmese and V.J. Lopata, "A basic process model for EB curing of composite materials", SAMPE International Symposium, 47, (2002).
- [10] P. Pazdzior, P. Hubert, A. Johnston, D. Djokic, "In-Situ Monitoring of residual Stresses Development During E-Beam Processing", SAMPE International Symposium, 49, (2004).
- [11] P. Hubert, P. Pazdzior, A. Johnston, D. Djokic, "Development of Residual Stresses During E-Beam Processing", SAMPE International Symposium, 50, (2005).

APPENDIX A- DOSE RATE VS TIME RESULTS

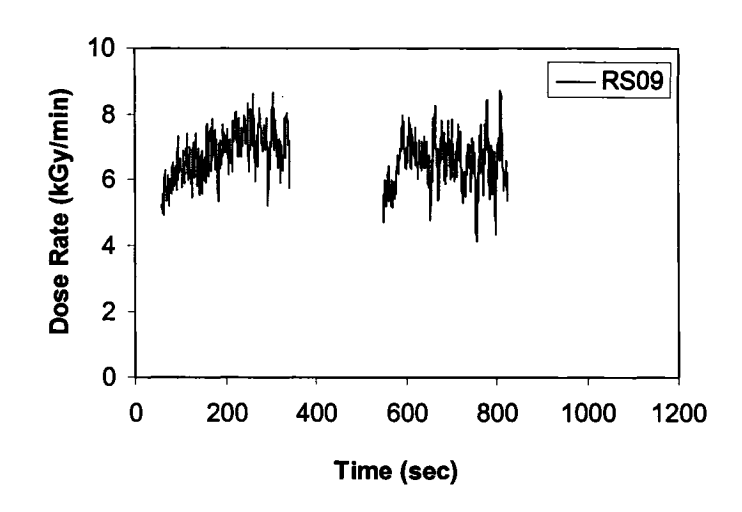


Figure A. 1: Calculated dose rate vs time for RS09

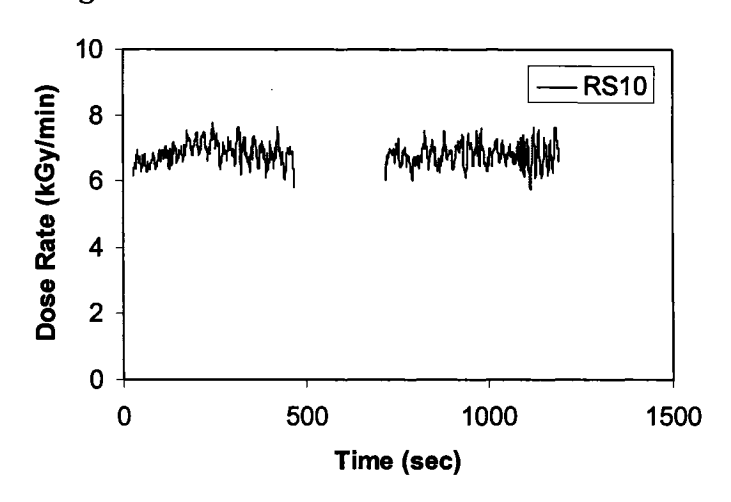


Figure A. 2: Calculated dose rate vs time for RS10

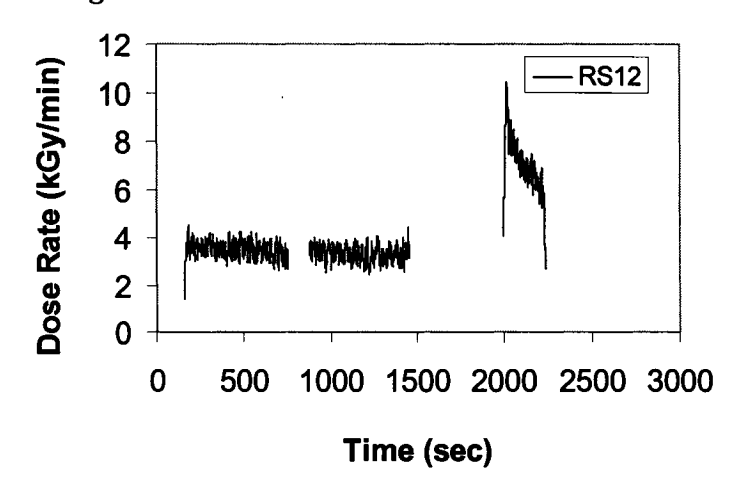


Figure A. 3: Calculated dose rate vs time for RS12

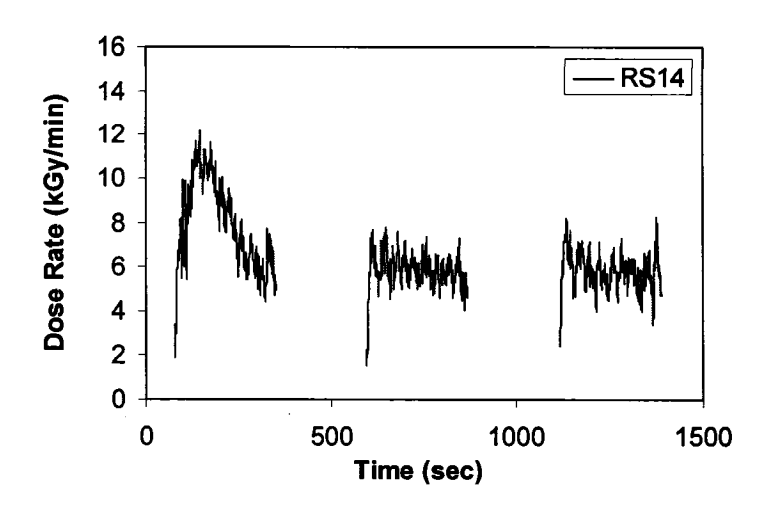


Figure A. 4: Calculated dose rate vs time for RS14

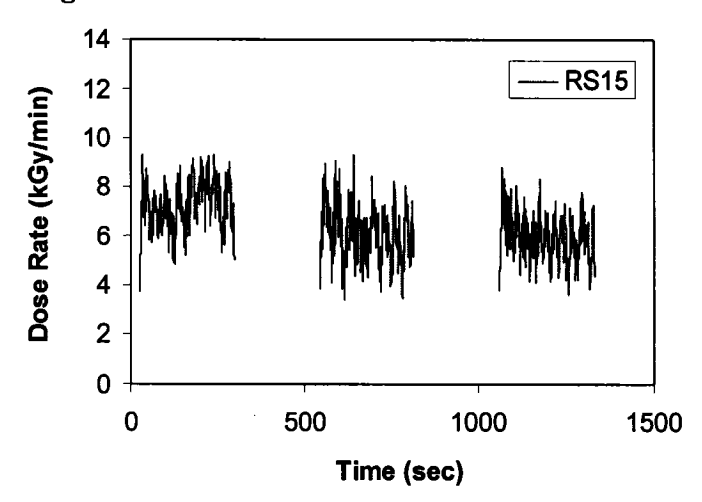


Figure A. 5: Calculated dose rate vs time for RS15

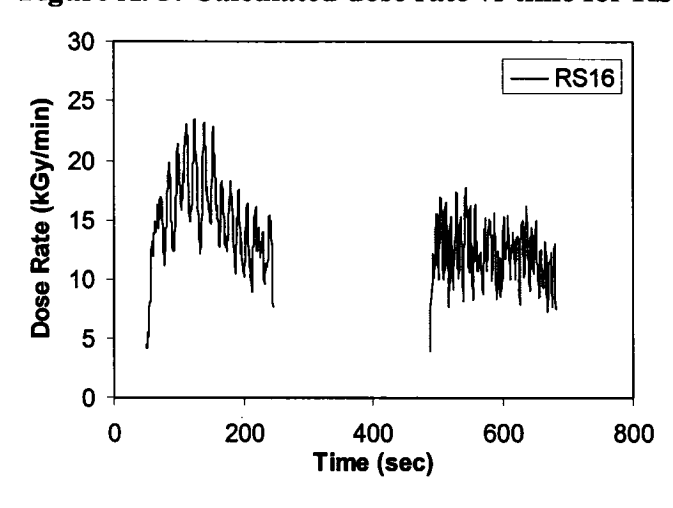


Figure A. 6: Calculated dose rate vs time for RS16

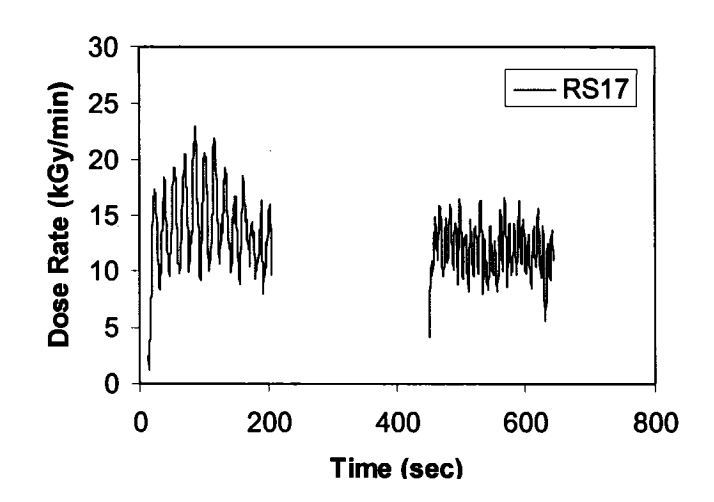


Figure A. 7: Calculated dose rate vs time for RS17

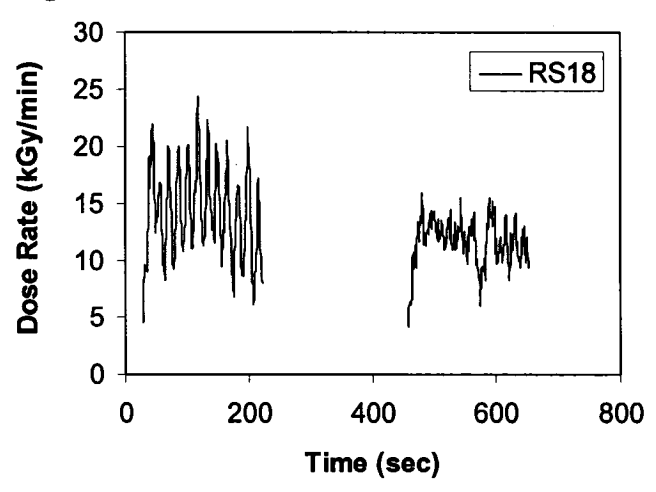


Figure A. 8: Calculated dose rate vs time for RS18

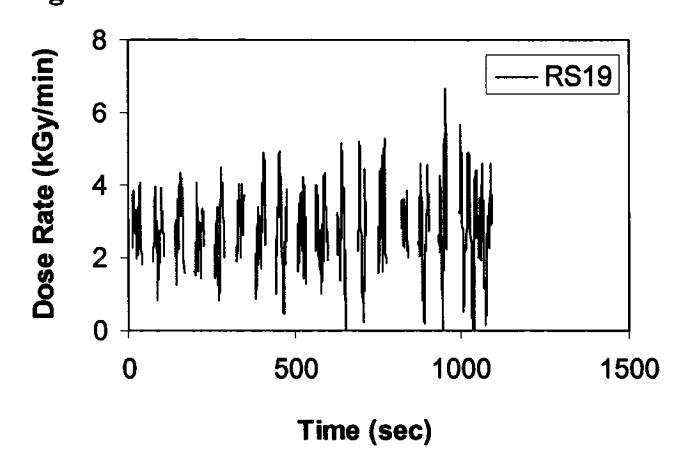


Figure A. 9: Calculated dose rate vs time for RS19

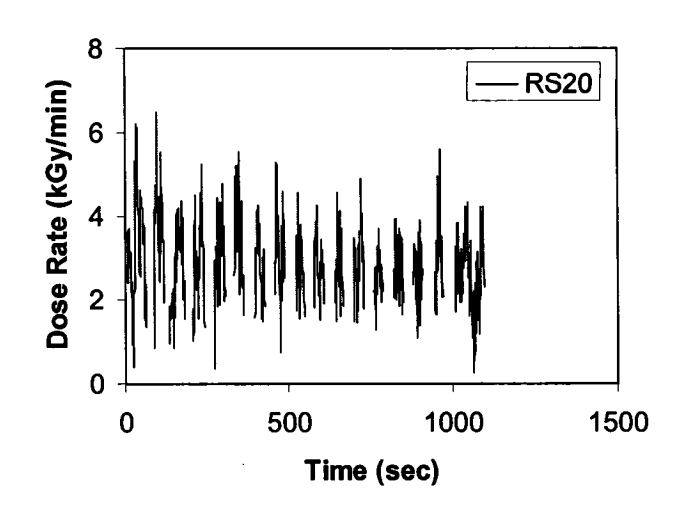


Figure A. 10: Calculated dose rate vs time for RS20

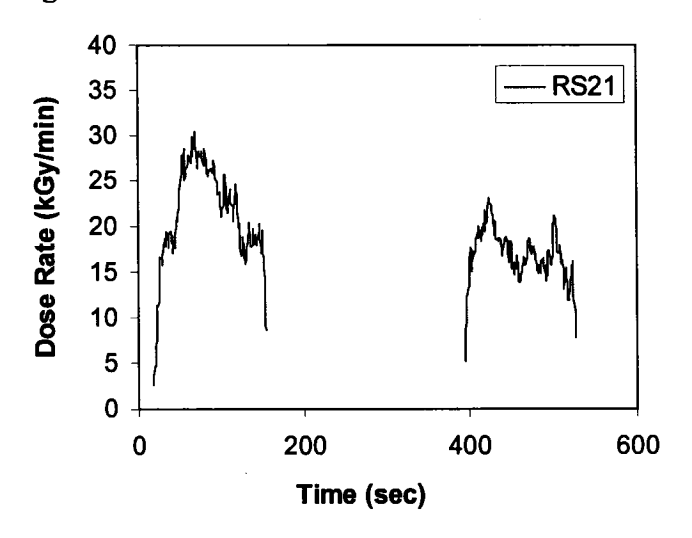


Figure A. 11: Calculated dose rate vs time for RS21

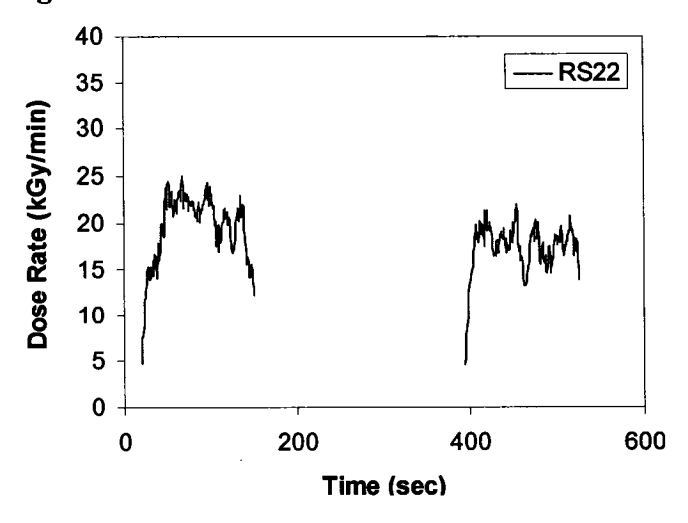


Figure A. 12: Calculated dose rate vs time for RS22

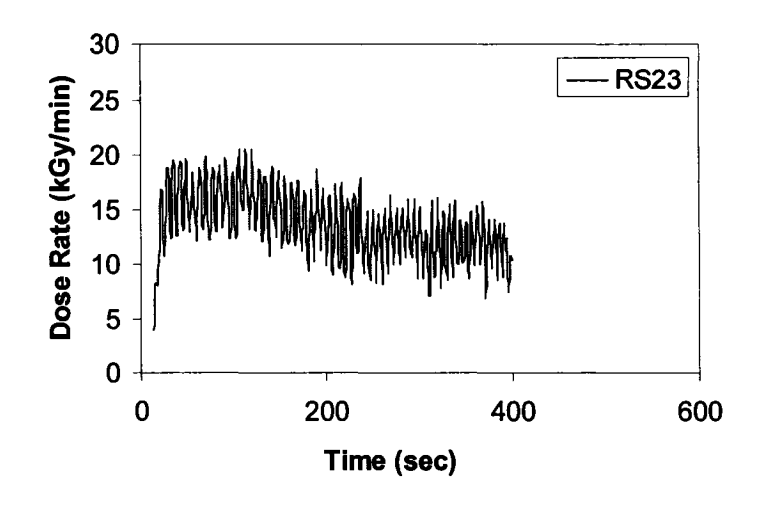


Figure A. 13: Calculated dose rate vs time for RS23

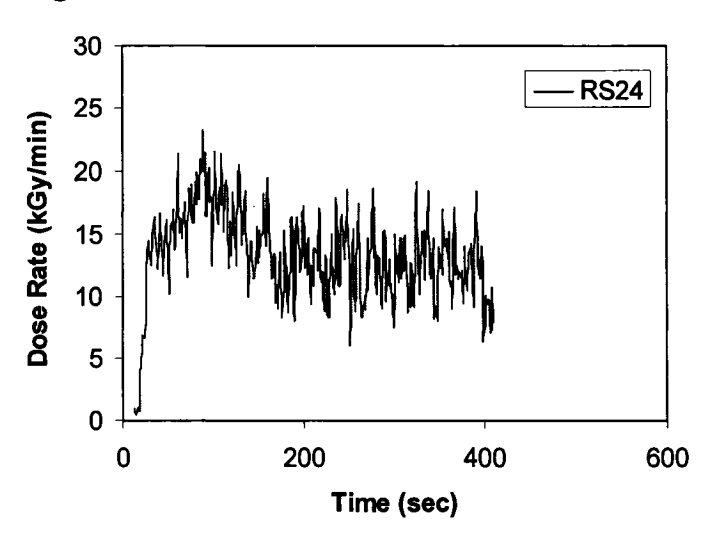


Figure A. 14: Calculated dose rate vs time for RS24

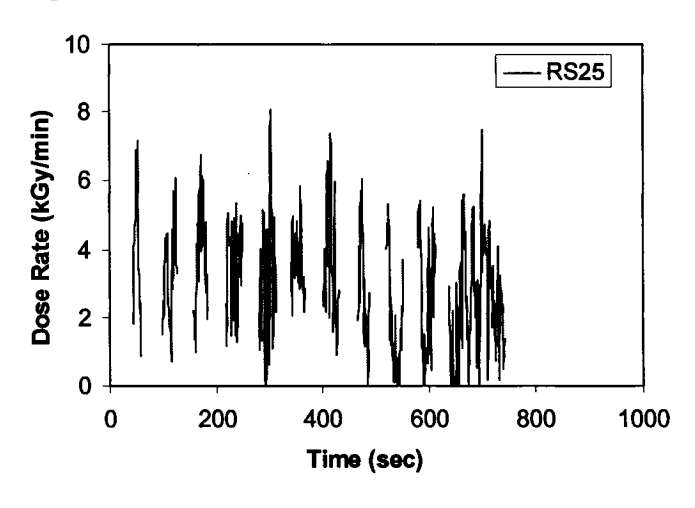


Figure A. 15: Calculated dose rate vs time for RS25

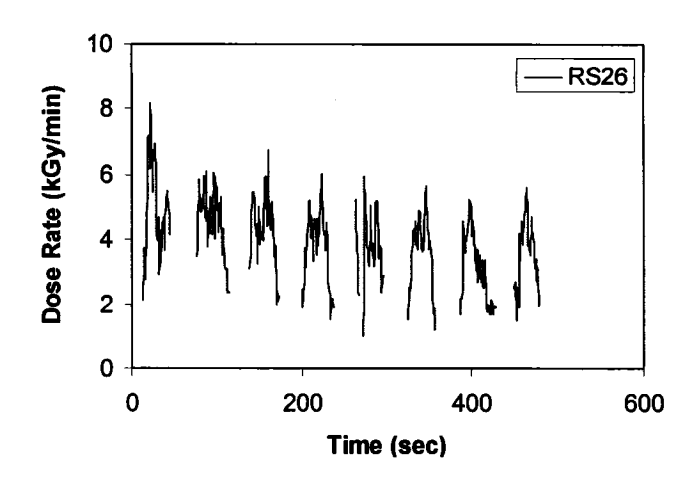


Figure A. 16: Calculated dose rate vs time for RS26

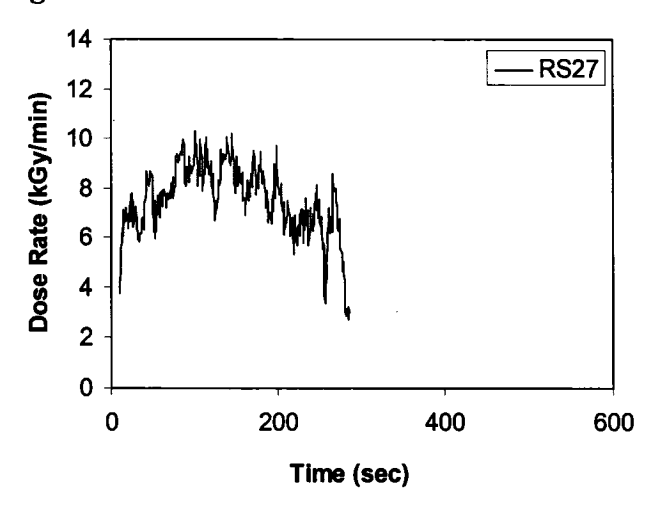


Figure A. 17: Calculated dose rate vs time for RS27

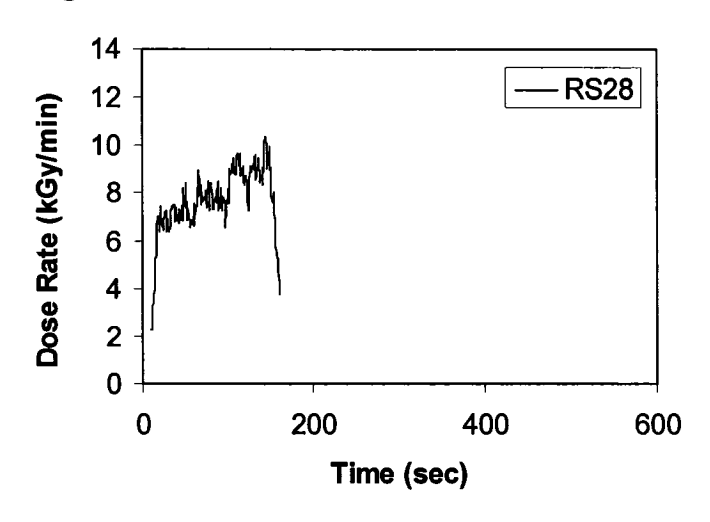


Figure A. 18: Calculated dose rate vs time for RS28

APPENDIX B - TEMPERATURE AND WARPAGE VS PREDICTED DEGREE OF CURE RESULTS

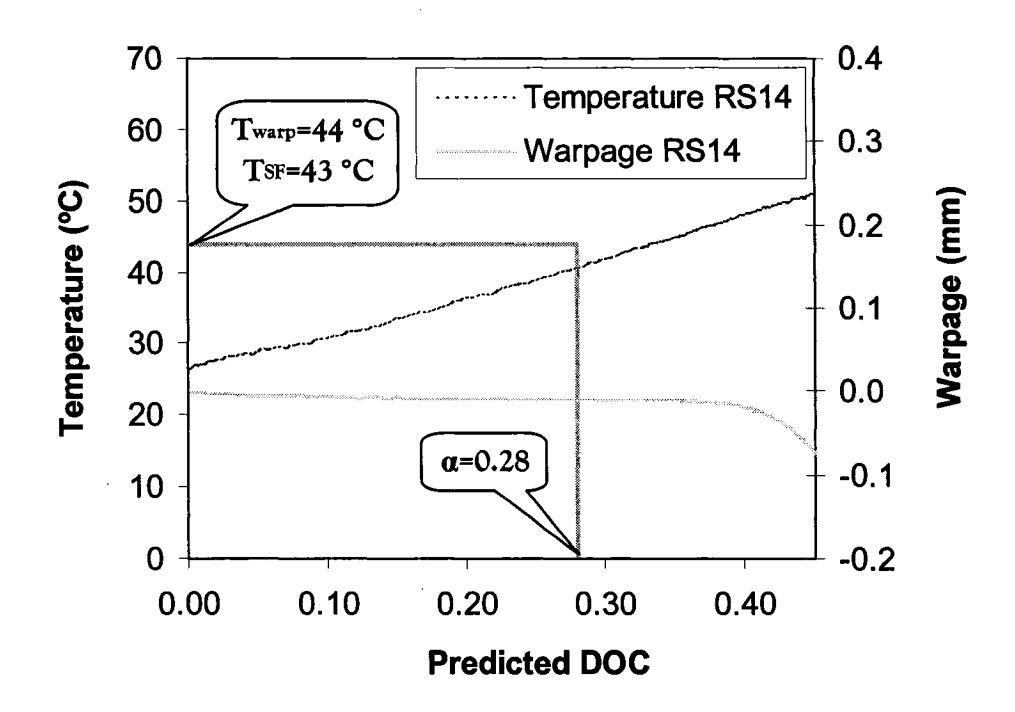


Figure B. 1: Temperature and warpage vs predicted DOC for RS14 specimen.

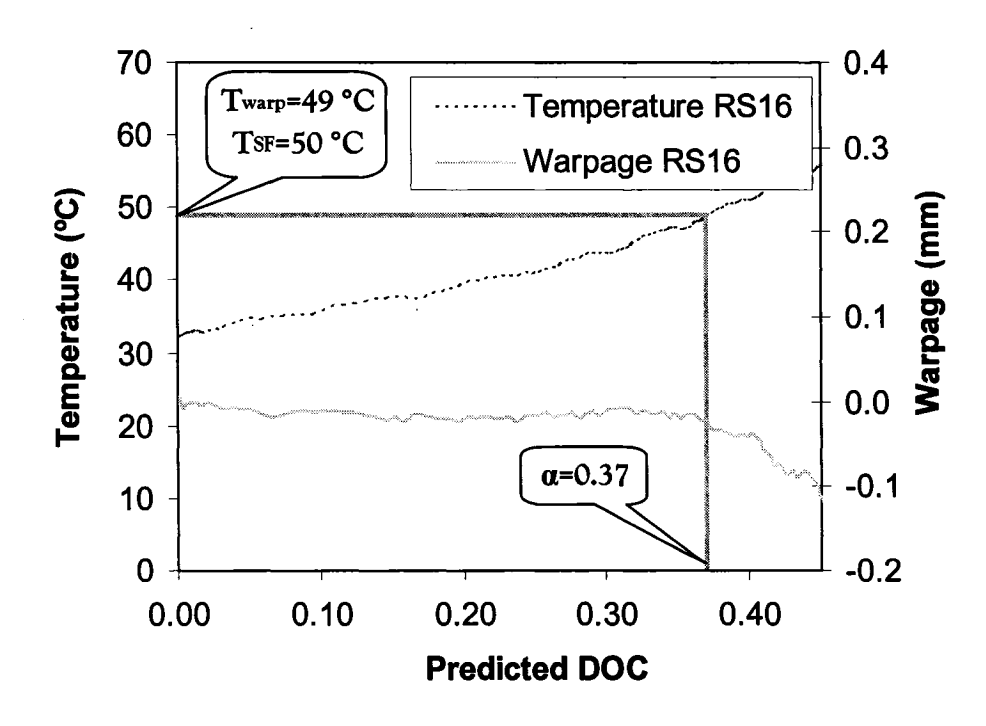


Figure B. 2: Temperature and warpage vs predicted DOC for RS16 specimen.

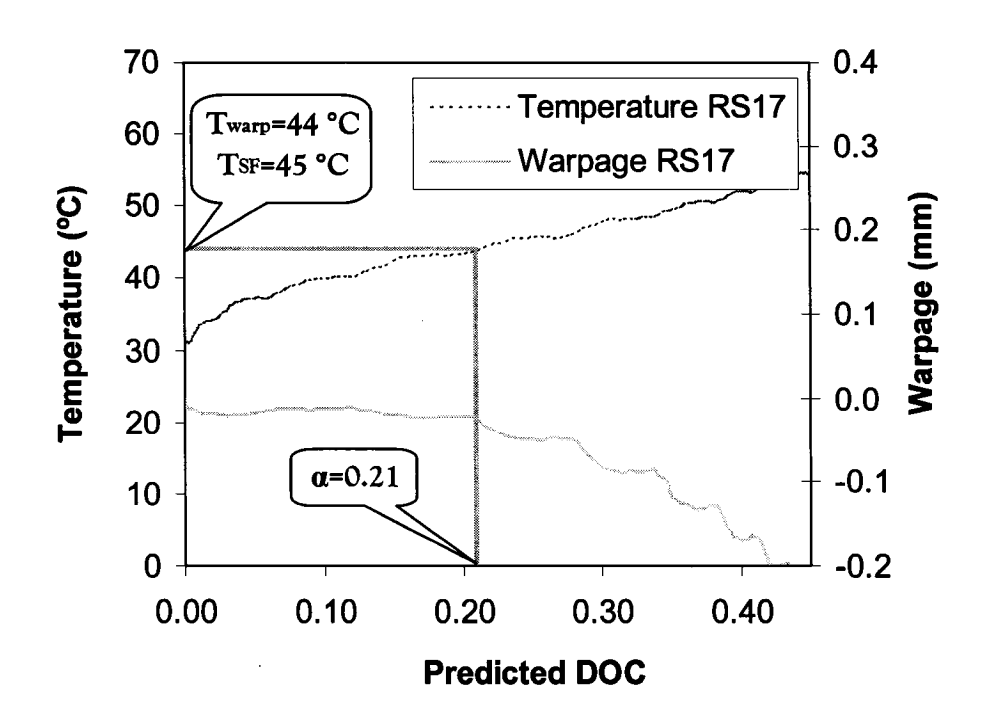


Figure B. 3: Temperature and warpage vs predicted DOC for RS17 specimen.

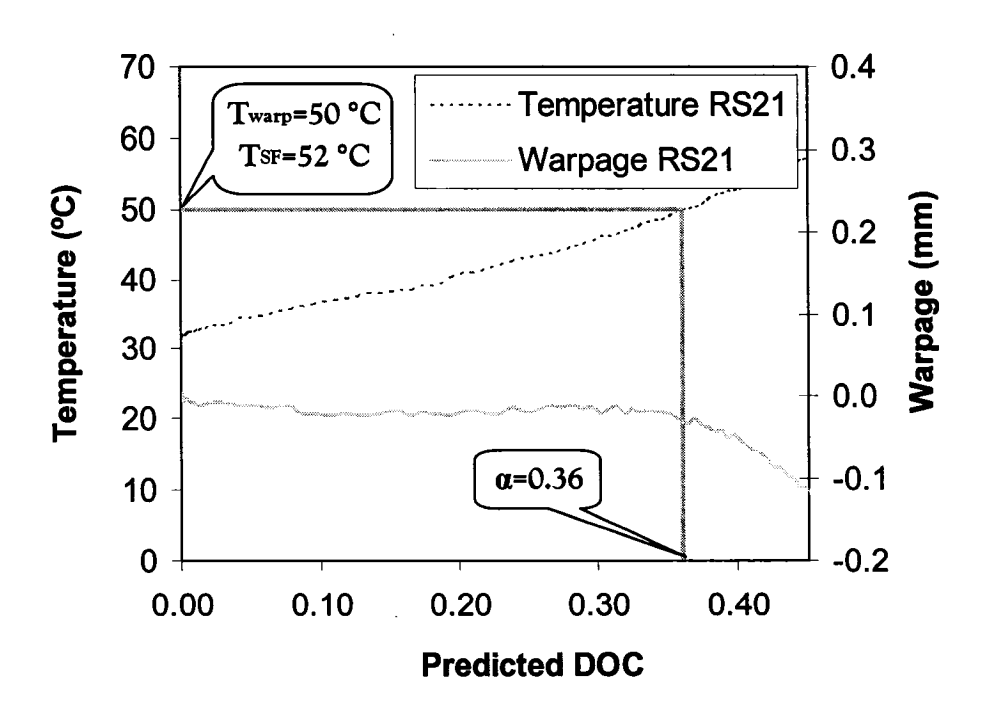


Figure B. 4: Temperature and warpage vs predicted DOC for RS21 specimen.

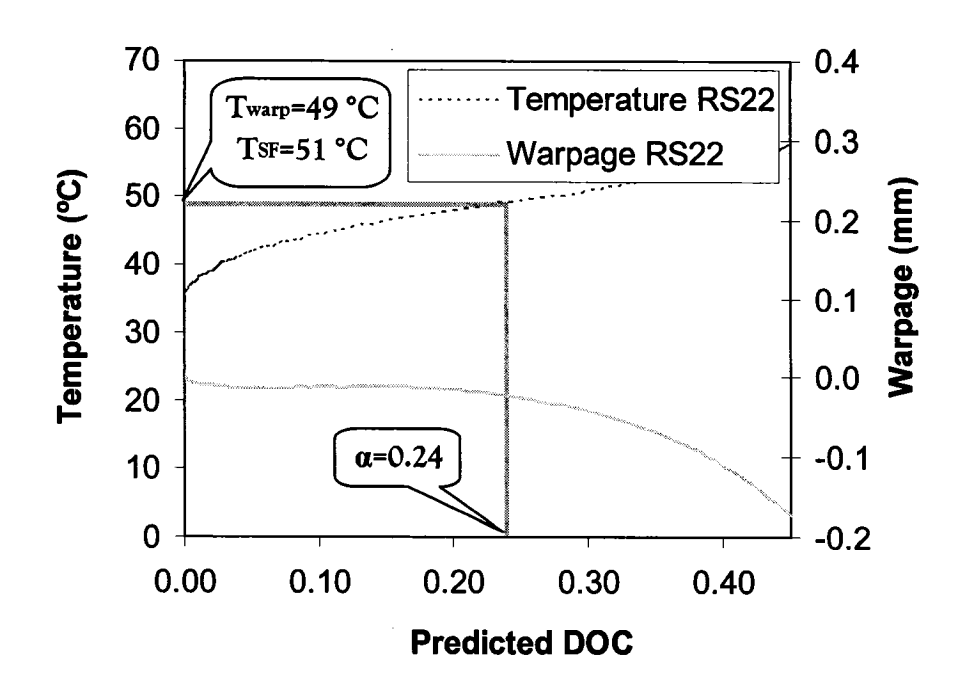


Figure B. 5: Temperature and warpage vs predicted DOC for RS22 specimen.

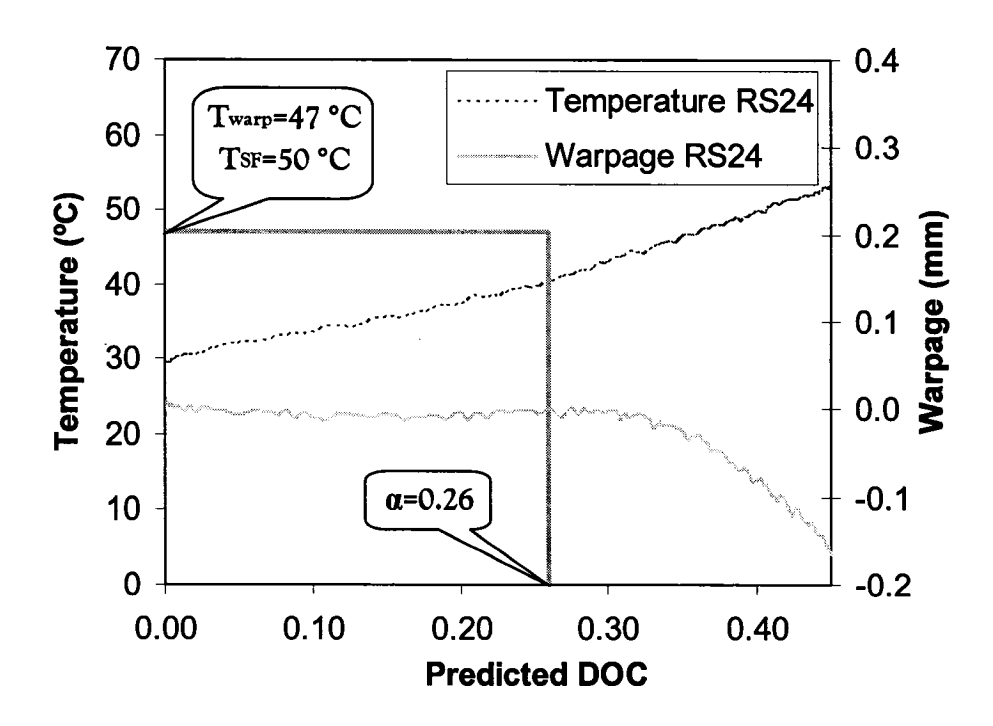


Figure B. 6: Temperature and warpage vs predicted DOC for RS24 specimen.

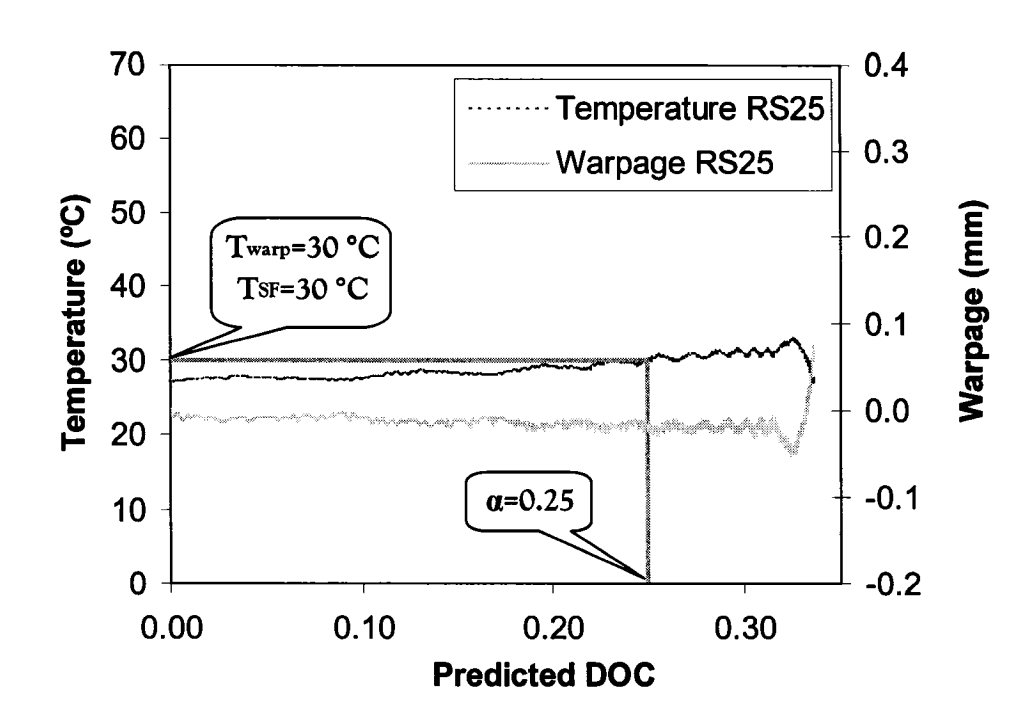


Figure B. 7: Temperature and warpage vs predicted DOC for RS25 specimen.

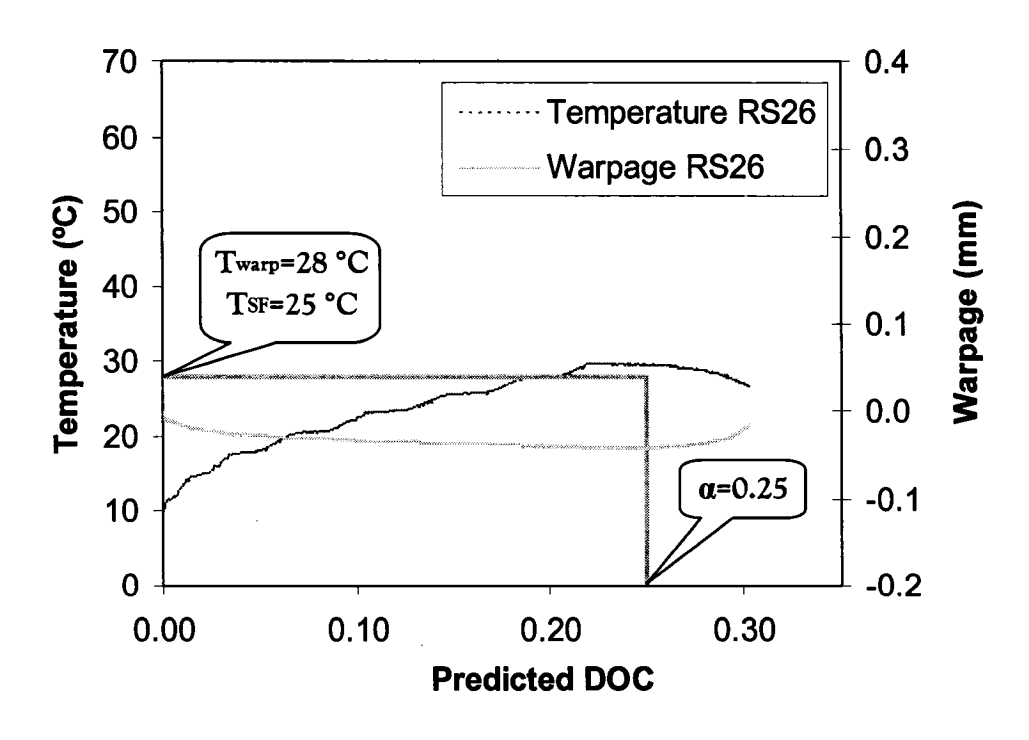


Figure B. 8: Temperature and warpage vs predicted DOC for RS26 specimen.

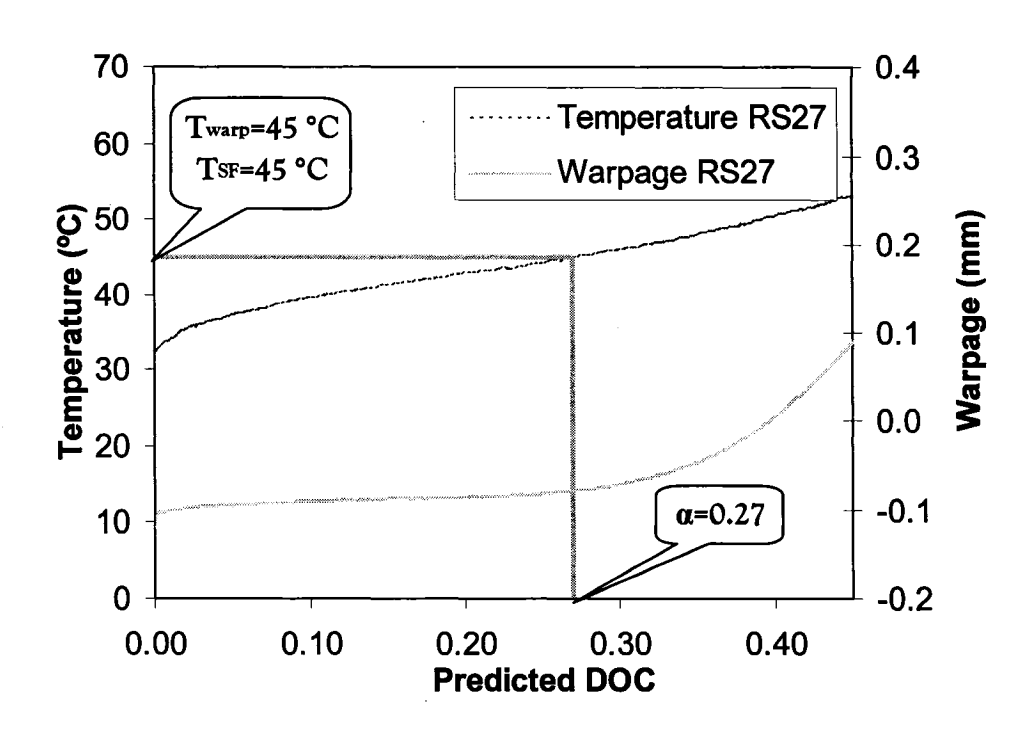


Figure B. 9: Temperature and warpage vs predicted DOC for RS27 specimen.

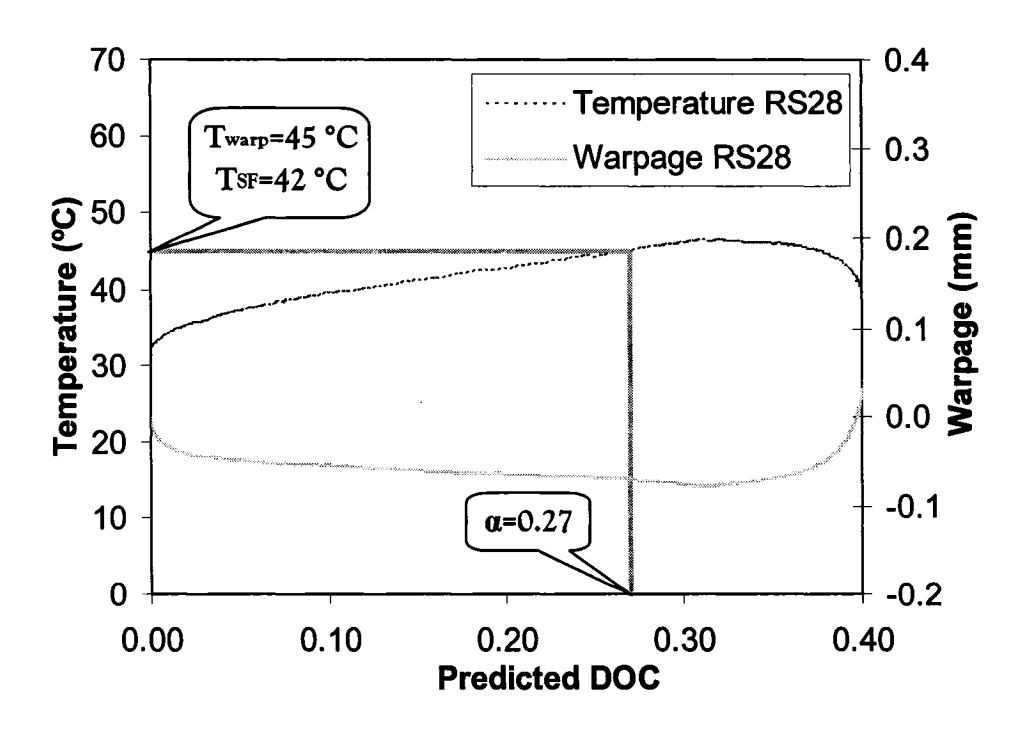


Figure B. 10: Temperature and warpage vs predicted DOC for RS28 specimen.

APPENDIX C – TEMPERATURE, WARPAGE AND DOSE VS TIME OF CURE RESULTS

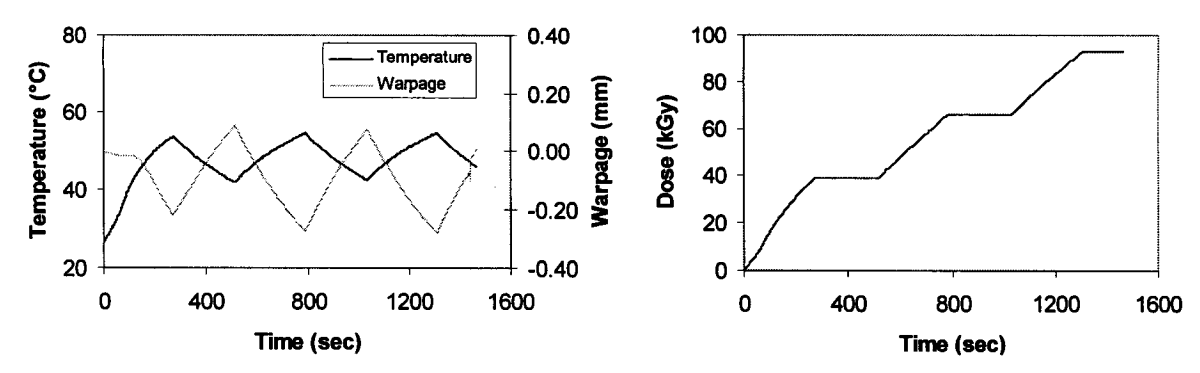


Figure C. 1: Temperature, warpage and dose vs time results for specimen RS13

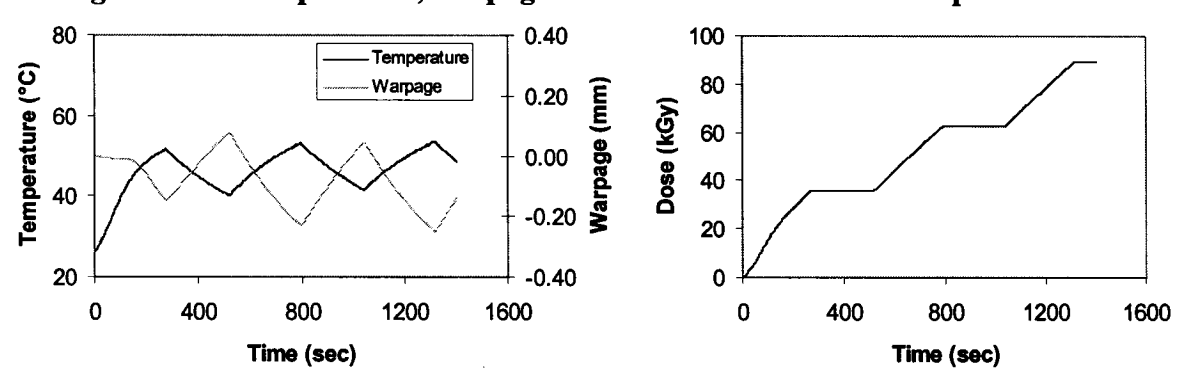


Figure C. 2: Temperature, warpage and dose vs time results for specimen RS14

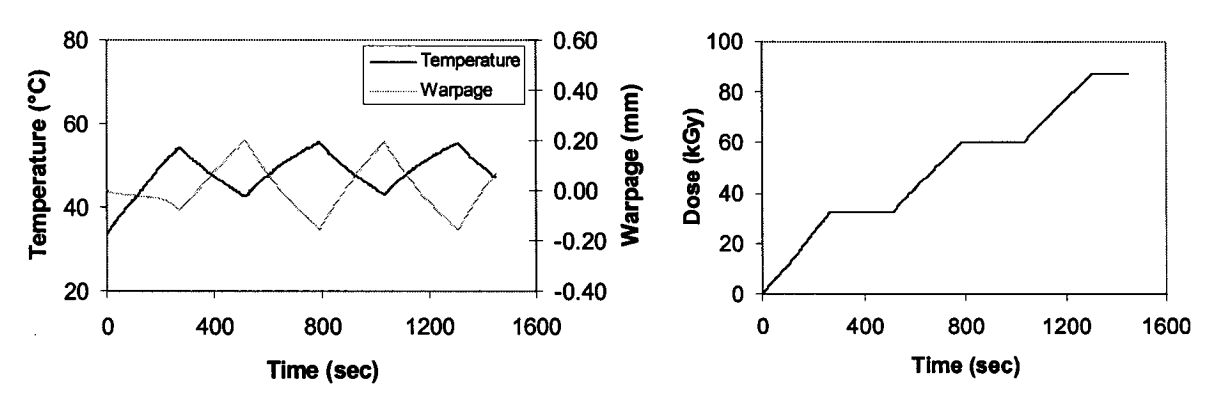


Figure C. 3: Temperature, warpage and dose vs time results for specimen RS15

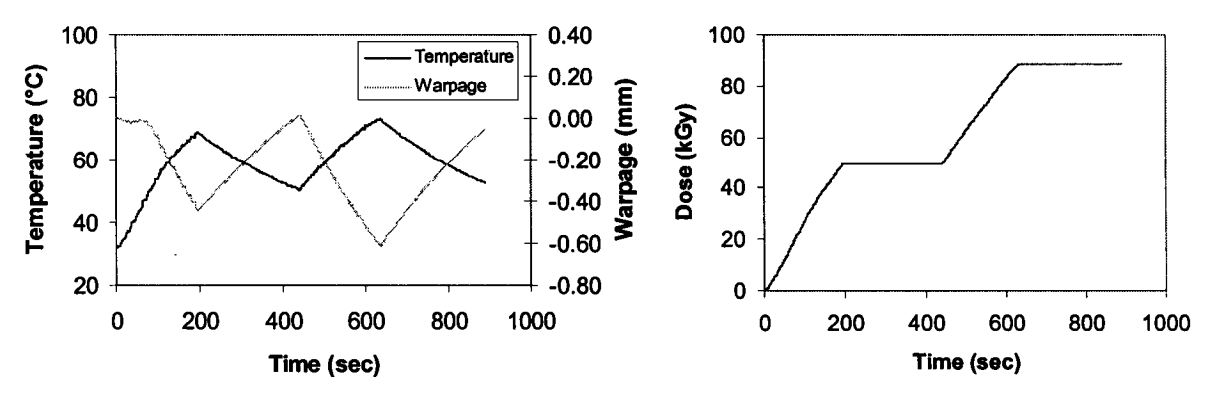


Figure C. 4: Temperature, warpage and dose vs time results for specimen RS16

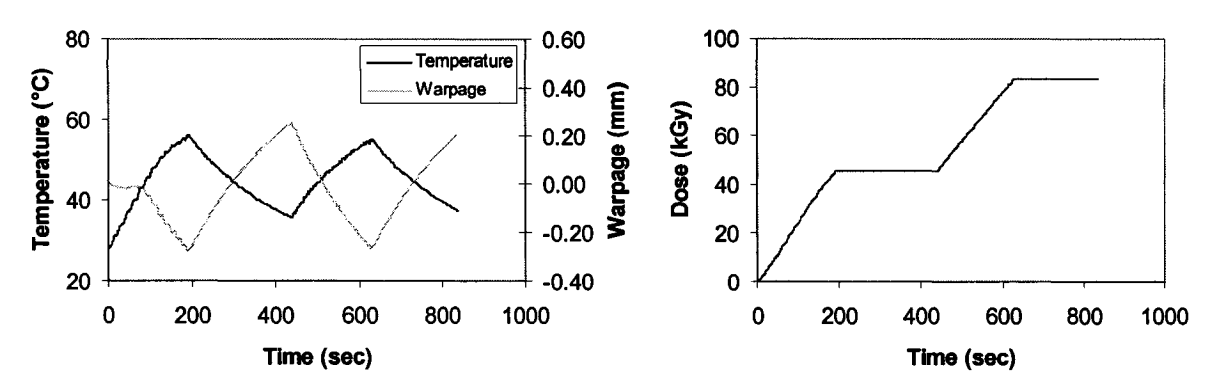


Figure C. 5: Temperature, warpage and dose vs time results for specimen RS17

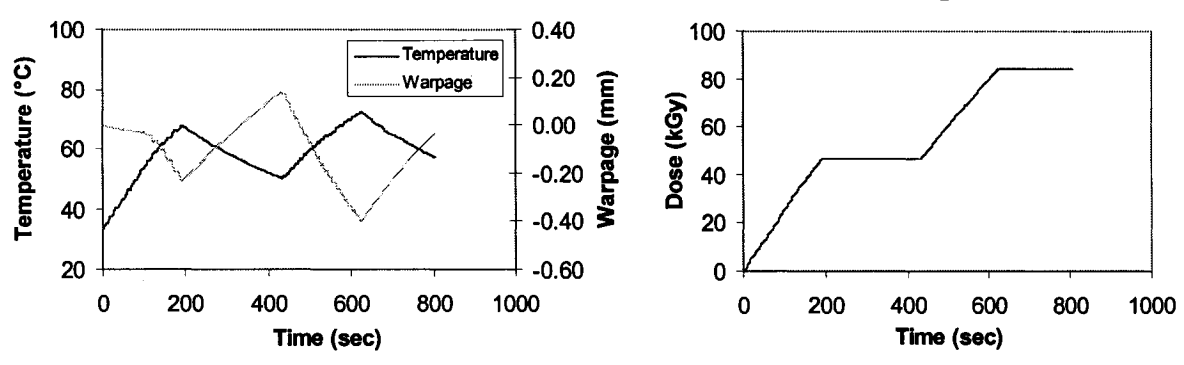


Figure C. 6: Temperature, warpage and dose vs time results for specimen RS18

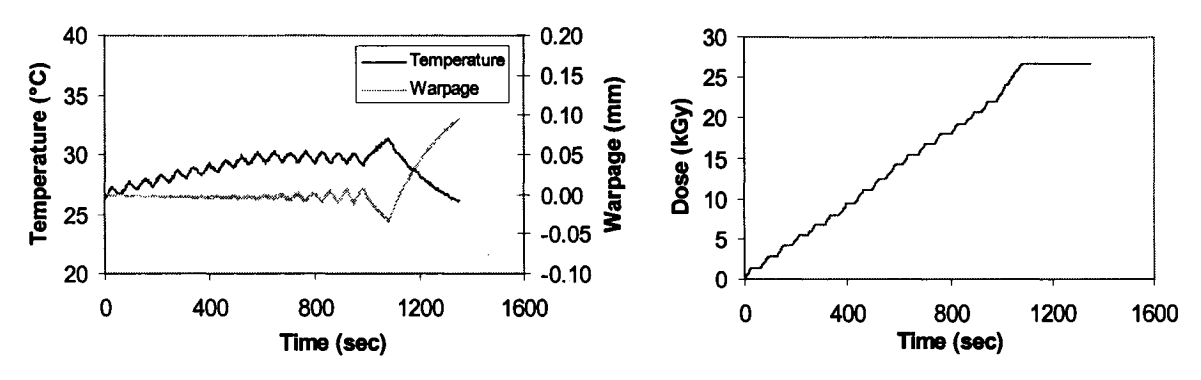


Figure C. 7: Temperature, warpage and dose vs time results for specimen RS19

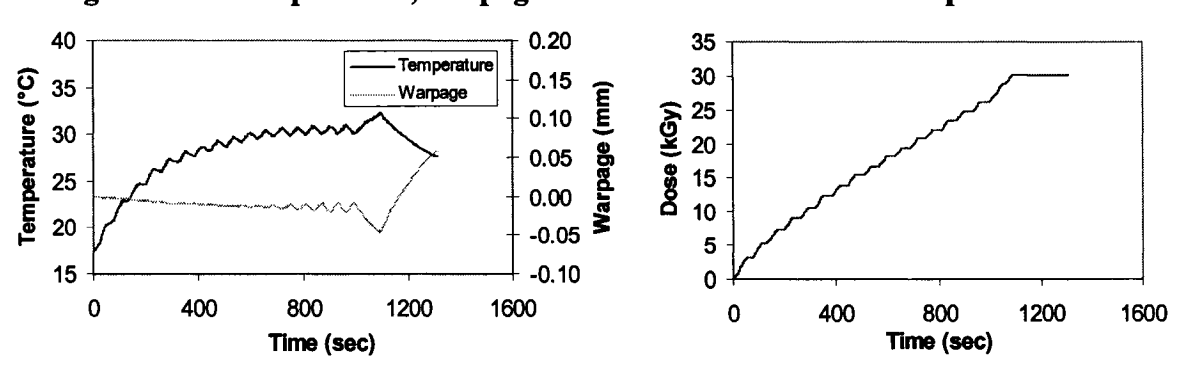


Figure C. 8: Temperature, warpage and dose vs time results for specimen RS20

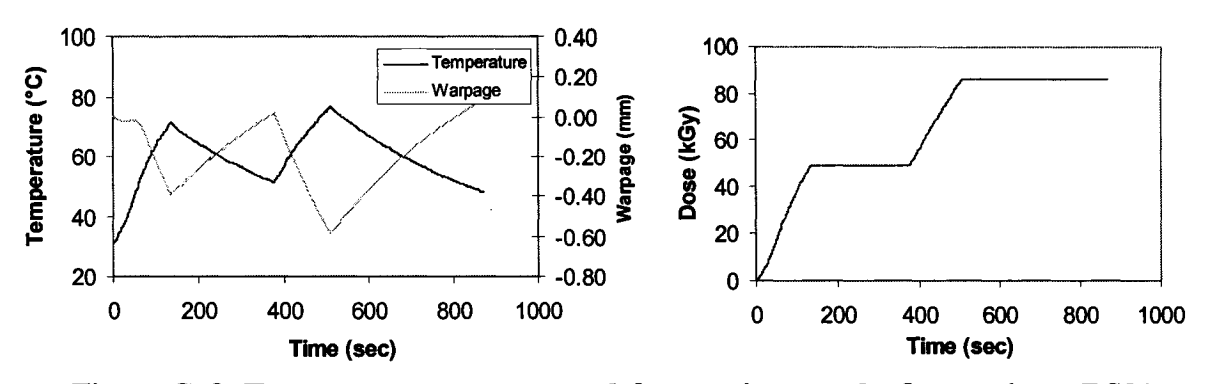


Figure C. 9: Temperature, warpage and dose vs time results for specimen RS21

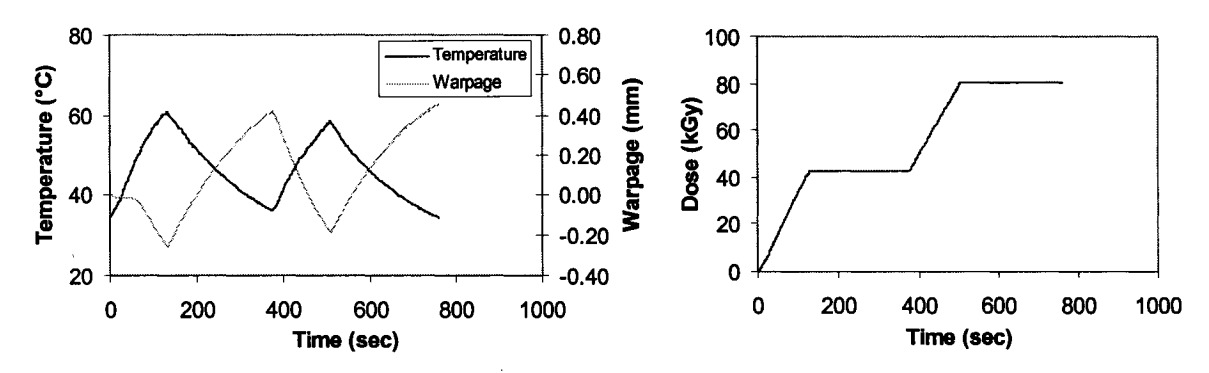


Figure C. 10: Temperature, warpage and dose vs time results for specimen RS22

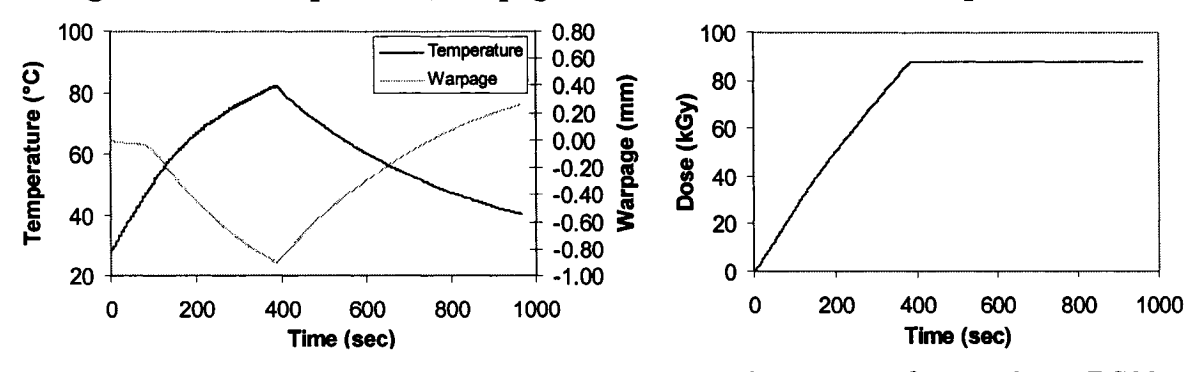


Figure C. 11: Temperature, warpage and dose vs time results for specimen RS23

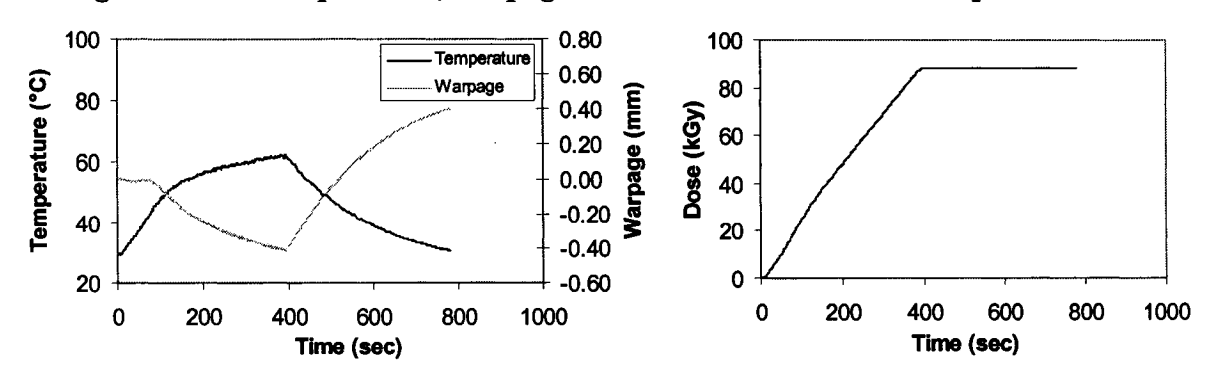


Figure C. 12: Temperature, warpage and dose vs time results for specimen RS24

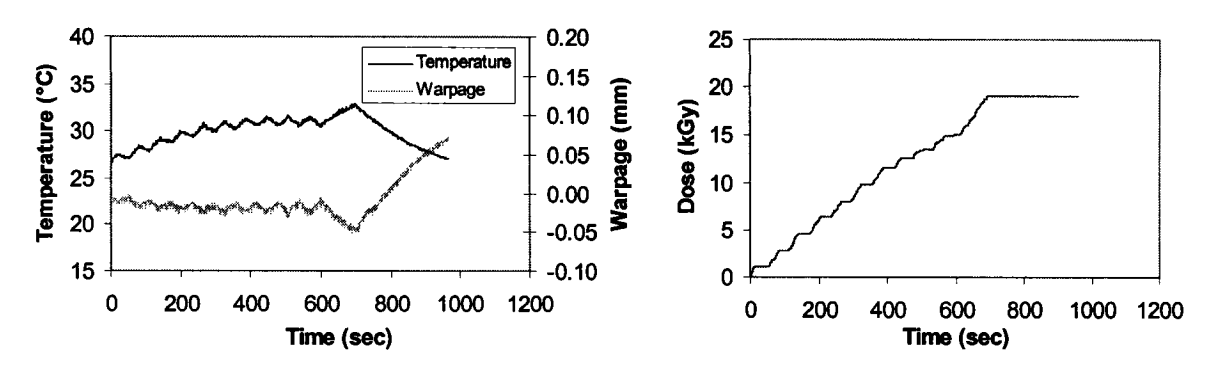


Figure C. 13: Temperature, warpage and dose vs time results for specimen RS25

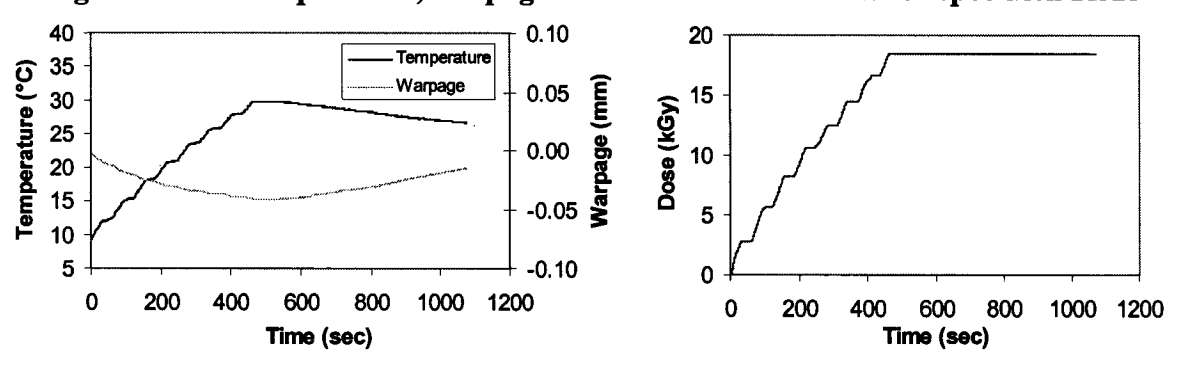


Figure C. 14: Temperature, warpage and dose vs time results for specimen RS26

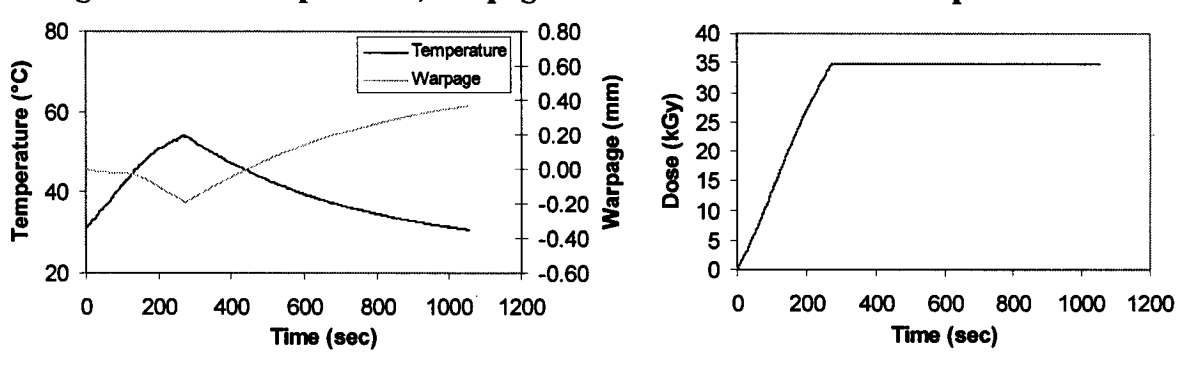


Figure C. 15: Temperature, warpage and dose vs time results for specimen RS27

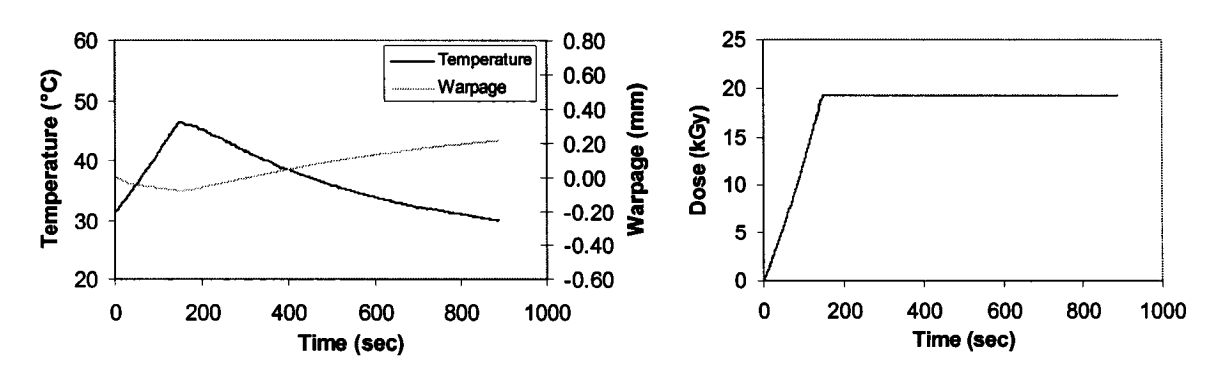


Figure C. 16: Temperature, warpage and dose vs time results for specimen RS28